EXPLORING AND UNDERSTANDING THE MECHANICAL RESPONSES OF POLYMERIC GLASSES USING EXPERIMENT AND SIMULATION

A Dissertation

Presented to

The Graduate Faculty of the University of Akron

In Partial Fulfillment

of the Requirements for the Degree

Doctor of Philosophy

Xiaoxiao Li

Dec, 2017

EXPLORING AND UNDERSTANDING THE MECHANICAL

RESPONSES OF POLYMERIC GLASSES USING EXPERIMENT

AND SIMULATION

Xiaoxiao Li

Dissertation

Approved:	Accepted:
_____	_____
Advisor Dr. Shi-Qing Wang	Department Chair Dr. Coleen Pugh
_____	_____
Co-advisor Dr. Mesfin Tsige	Dean of the College Dr. Eric Amis
_____	_____
Committee Member Dr. Toshikazu Miyoshi	Dean of the Graduate School Dr. Chand Midha
_____	_____
Committee Member Dr. Hunter King	Date
_____	
Committee Member Dr. Jie Zheng	

ABSTRACT

Polymeric glasses are important engineering materials in industry application and they are also of great academic interest. Unlike non-polymeric glasses rarely yielding during the external deformation, polymeric glasses with high molecular weight can undergo various mechanical response, such as shear yielding, necking, crazing, strain hardening, and brittle failure. Although enormous efforts, dating back to 70 years ago, have been made to understand the physics behind, the nature of the various mechanical response is still unclear and under debate. In this dissertation, we combine mechanical tests with computer simulation to investigate the mechanical response of polymeric glasses. With the help of our recently proposed hybrid structure model, we are able to understand the brittle-ductile transition, origin of stress, relaxation and elastic yielding. It is found that chain network is essential for polymeric glass system to avoid brittle failure. However, the failure of specimen with high molecular weight can also be achieved by dynamically chain pull-out through crazing. In the case that failure is avoided and large deformation is achieved, chain network is essential for building high level of stress, no matter in tensile or compression mode. When specimen relaxes after large deformation, relaxation of chain network is independent of alpha process, therefore is able to hold stress at temperature near T_g. Otherwise, if the specimen is released after large deformation, it is found that the imbedded stress coming from strained chain network, which is able to show up after increasing temperature.

ACKNOWLEDGEMENTS

Firstly, I would like to express my sincere thanks to my advisor Prof. Shi-Qing Wang. I can still remember the first time I met him at University of Science and Technology of China when I was in undergraduate. Prof. Wang gave us a presentation of his work. I was amazed by his passion for science and innovative way of thinking. That encouraged me to Akron and to join his group. From then on, I continued benefiting from his everlasting passion and sharp critical thinking. He is like a mirror, showing me the way to be a noble person. This will benefit me for my whole life.

Secondly, I would like to express my great thanks to my co-advisor Prof. Mesfin Tsige. He is knowledgeable, wise and kind. Under his mentor, I stepped into to the amazing new world of computer simulation. He guided me to look into and analyze physical questions at molecular level, which refreshed my understanding on polymer dynamics.

I would also like to thank my dissertation committee: Prof. Toshikazu Miyoshi, Prof. Hunter King and Prof. Jie Zheng for their valuable suggestions and insightful comments on my work. I would like to thank Prof. Jutta Luettmer-Strathmann who attended in my research presentation and Prof. Gary R. Hamed who attended in my formal seminar. They gave me a lot of helpful instructions.

I appreciate all the help from my former and current group: Dr. Shiwang Cheng, Dr. Hao Sun, Dr. Gengxin Liu, Dr. Panpan Lin, Jianning Liu, Mengchen Wang, Yexin Zheng, Yue Zhao, Zhichen Zhao, Masoud Aghjeh, Yi Feng, Yue Lu, Mingyu Yuan and all the group members from Prof. Mesfin Tsige's group. I really enjoy the happy moments we

spent together.

I would like to thank Ed Laughlin, the best machinist in the world. Only with his incredible talent can we move forward with our research.

Last but not least, I would like to thank my family and friends for their love and support during this journey.

TABLE OF CONTENTS

Page

LIST OF TABLES.....ix

LIST OF FIGURES x

CHAPTER

I. INTRODUCTION……..1

II. CHARACTERISTICS OF DEFORMATION…….6

2.1 Polymer and Glass transition 6

2.2 Deformation Modes of Polymer Glasses 7

2.3 Characterization of Deformation 9

2.5 Characteristics in Tensile Deformation..... 10

2.5.1 Shear Yielding and Necking..... 10

2.5.2 Brittle Failure 11

III. THE EMERGENCE OF HYBRID MOLECULAR PICTURE 13

3.1 Introduction……..13

3.2 Discussion……15

IV. MAPPING THE BRITTLE AND DUCTILE BEHAVIOR OF POLYMER GLASSES 17

4.1 Brittle-Ductile Transitions (BDT) 17

4.2. Our Hybrid Structure Model 21

4.3 Experiments 22

4.3.1 Materials and Specimen Preparation 22

4.3.2 Apparatus and Methods 24

4.3.3 Results and Discussion 24

4.3.4 Temperature Effect 24

4.3.5 Rate Effect 26

4.3.6 Mapping the Brittle and Ductile Behavior of Polymer Glasses 32

4.4.5 Investigation into Dynamical/Ductile Failure (DF) 36

4.4.6 Our Proposal of Understanding Based on the Molecular Picture 55

V. THE ORIGIN OF STRESS 58

5.1 Introduction into Molecular Dynamic simulation 58

5.2 Decomposition of Stress 59

5.4 Simulation 61

5.4.1 Coarse-Grained Model of Polystyrene 61

5.4.2 Simulation Protocol 65

5.4.3 the Origin of Stress in Tensile Mode 68

5.4.4 the Origin of Stress in Compression Mode 76

VI. STRESS RELAXATION 85

6.1 Introduction 85

6.2 Mechanical Experiment: Relaxation Near T_g 87

6.2.1 Introduction of Alpha time 87

6.2.2 Materials, Apparatus and Methods 89

6.2.3 Result and Discussion 90

6.3 Simulation 96

6.3.1 Simulation Protocol 96

6.3.2 Stress Decomposition during Relaxation 97

6.3.3 the Role of Chain Network during Relaxation 100

VII. ELASTIC YIELDING 107

7.1 Introduction 107

7.2 Simulation Protocol 108

7.3 Result and discussion 109

VIII. SUMMARY 115

BIBLIOGRAPHY 119

LIST OF TABLES

Table Page

4.1 Stress levels at different temperatures and rates (PS) 31

6.1 Sample Information of the Polymer Glasses 89

LIST OF FIGURES

Figure Page

2.1 Three basic deformation modes in terms of the specimen shape change. Arrow represents the direction of applied deformation..... 8

2.2 Two basic deformation modes in terms of applied deformation. Tensile deformation is used as example 8

2.3 Specimen dimension before (left) and after deformation (right) 9

2.4 Typical stress-strain curves of polymeric glasses undergoing start-up tensile deformation. Black curve shows a ductile response and red one shows a brittle response. Inset are the photos of specimen after brittle failure (red frame) and undergoing necking front propagation (black frame).....10

3.1 Hybrid structure of polymer glasses upon large deformation along z-direction with load-bearing chain network already emerged. Dots and short bars represent polymer segments connected by Van der Waals network. A load-bearing strand (thin rings) forms chain network with the assistance of two adjacent chains (thick rings) through two hairpin structures. (replot of Figure 12.1 Roth, C. B., Polymer Glasses. CRC Press: 2016.)..... 14

4.1 Typical stress-strain curves (left) of brittle (red) and ductile (black) and a snapshot of polymer specimen (right) after brittle failure (red framed) and snapshot of polymer undergoing ductile necking propagation (back framed)..... 19

4.2 Demonstration of BDT in the LDWO hypothesis, which is represented by plotting critical brittle stress σ_B and critical yield stress σ_Y vs. temperature..... 20

4.2 Engineering stress vs. the draw ratio from various tensile extension tests at the different temperature for PMMA at 35 °C, showing brittle fracture (circles), ductile drawing (triangles) and premature failure (squares)..... 25

4.3 Engineering stress vs. the draw ratio from various tensile extension tests at the different initial rates defined by V/L0 for PMMA at 35 °C, showing brittle fracture (circles), ductile drawing (triangles) and premature failure (squares and diamonds)..27

4.4 Engineering stress vs. the draw ratio from various tensile extension tests at the different initial rates defined by V/L_0 for PS at 70 ^oC, showing brittle fracture (circles), ductile drawing (triangles) and premature failure (squares). At 0.02 min^{-1}, there is shear yielding leading to necking with multiple neck fronts, visible from the top photo. The diameter of specimen shrinks to 0.66 mm, whereas the original diameter is 1.16 mm, amounting to a large local draw ratio of 3.1. At 0.001 min^{-1}, the drawing is uniform as shown in the second photo in the inset until breaking at $L/L_0 = 1.2$. Clear opaqueness due to intensive crazing can be seen from the bottom photo. 28

4.5 Toughness at different rates for extruded PS at 70 °C, extruded PMMA at three temperatures (35, 40, and 50 °C) and polished dogbone-shaped PMMA at 80 °C, evaluated from data such as those in Figure 4.3 and 4.4 according to $\mathbf{1}\boldsymbol{\lambda break}\boldsymbol{\sigma engr}(\boldsymbol{\lambda})\boldsymbol{d\lambda}$ 29

4.6 Engineering stress vs. the draw ratio from various tensile extension tests on PS at three temperatures, showing plastic flow at 90 °C, premature failure at 80 °C and typical brittle failure at 60 °C. 31

4.7 Diagram depicting the various mechanical responses at different temperatures T and rates V/L_0 for PMMA, showing the brittle fracture (dark blue color online) at low temperatures, the ductile failure at intermediate temperatures (violet color online) and the ductile yielding (pink color online) at high temperatures. With varying rate or temperature, PMMA shows BDT and passed through DF 33

4.8 Either brittle stress or peak stress of tensile extension of PMMA as a function of temperature for different applied rates of 18 (squares), 2 (circles), 0.2 (diamonds), 0.02 (upward triangles) and 0.002 (downward triangles) min^{-1}. Inside the U-shaped region resides the ductile yielding. Above the near-horizontal line there is brittle fracture. Ductile failure occurs in the rest of the space 34

4.9 Photo of the dog-bone shaped specimen cutting from the hot-pressed film (left) and the side surface from microscope (right) perpendicular to the paper, with cutting direction from top to bottom. The specimen in the left is put under Carl Zeiss microscope with 10X eyepiece and 10X objective lens 38

4.10 Photo of the extruded cylindrical specimen of PMMA under microscope showing the smoothness of side surface of cylindrical specimen. The specimen is put under Carl Zeiss microscope with 10X eyepiece and 2X objective lens 38

4.11 Engineering stress vs. draw ratio of polished PMMA dog-bone specimens at different initial rates (defined by V/L_0) at 70 °C, showing the brittle fracture (circles), the ductile drawing (squares) and the premature failure (triangles and diamonds) 39

4.12 Photos of crazes in the PS specimen (left) and it side view (right). Injection molding PS specimens were drawn at constant rate (V/L_0=0.1/min) at room temperature. The specimens are drawn to a few percent of deformation before fracture……. 42

4.13 The relationship between density and weight concentration of the KBr aqueous solution. Dots were plotted from the chemist handbook[81] and the curve is fitted from dots. Inserted table is the polynomial fitting parameter of the curve. R = 1 stands for an ideal fitting. 45

4.14 Photos of stems suspended in the KBr aqueous solutions. The suspend condition indicates the stems have the same density as the solutions. Density of the samples increases from left to right 45

4.15 Engineering stress vs. time curve during tensile deformation up to failure (open circles) and the corresponding temperature vs. time curves at various positions on the sample (filled symbols). Positions are marked in Figure 4.16 47

4.16 IR camera image showing the position of 4 temperature detector cursors (left) and snapshot at 1.5s when the sample is ready to break (right)..... 47

4.17 Engineering stress vs. the draw ratio from various tensile extension tests at the different initial rates defined by V/L_0 for PMMA at 70 ^oC. It shows the brittle fracture (circles), the ductile drawing (squares) and the ductile failure (triangles and diamonds). Corresponding sample images under microscope with 10X eyepiece. Magnification of objective lens are marked in each photo. 52

4.18 Photo of polished dog-bone shaped sample of PMMA after tensile deformation at rate V/L_0 0.002/min (top left), microscope photo of the crack marked in red frame of the top left photo, taken under 10X eyepiece and 2X objective lens (bottom left), microscope photo of the crack marked in red frame of the bottom left photo, jointed by 8 microcopy photos taken 10X eyepiece and 10X objective lens (right)..... 53

5.1 Alteration of inter- and intra-segmental interaction during deformation of a polymeric system. Light blue cuboid represents a piece of glassy polymer, and red and blue curves represent two adjacent chains in the piece 60

5.2 Extension stress-strain curves of three specimens with different chain length. A total deformation of lambda $\boldsymbol{L/L0}$ = 1.8 is applied to the 3 specimens respectively, at the same deformation rate $\boldsymbol{V/L0}$ = 0.5 /ns. Retractive stress value is defined as positive 68

5.3 The stress decomposition of stress during the tensile deformation of 500-mer specimen. Retractive stress is defined as positive..... 69

5.4 The stress decomposition of stress during the tensile deformation of 500-mer specimen. Retractive stress is defined as positive..... 70

5.5 Intra-segmental stress decomposition during the deformation of 500-mer specimen. The intra-segmental stress is divided into the contribution from bond stretching, angle opening and dihedral distortion. Retractive stress value is defined as positive 71

5.6 The orientation (calculated as P2 function) and average bond length of 500-mer specimen during the tensile deformation..... 72

5.7 (left snapshot) Visualization of a typical chain (red) in 500-mer specimen after deformed to $\boldsymbol{L/L0 = 3.0}$ along z-direction. The white, blue and green chain segments form “hooks” structure which hooks the red chain. (right plot) Bond length of each backbone bond along the chain (circles) and opened angle (diamonds) along the chain. Retractive stress is defined as positive 74

5.8 Stress decomposition of stress in z-direction during compression deformation of 500-mer polystyrene at 300 K. Repulsive stress value is defined as positive 77

5.9 Stress decomposition of stress in z-direction during compression deformation of 21-mer polystyrene at 300 K. Repulsive stress value is defined as positive 77

5.10 Orientation calculated from P2 function of 500-mer and 21-mer specimen during compression. Reference direction z-direction 80

5.10 Average bond length of backbone bonds of 500-mer and 21-mer specimen during compression 80

5.11 Visualization of a typical chain in 500-mer specimen before deformation (left) after compressed to $H_0/H=1.8$. Compression is along z-direction..... 81

5.12 Stress decomposition of lateral direction during compression of 500-mer specimen. 82

5.13 Stress decomposition of lateral direction during compression of 21-mer specimen..83

6.1 A scheme of typical stress-time curves of relaxation in deep glassy state starting from post-yield regime (red) and pre-yield regime (blue)..... 88

6.2 Tensile (engineering) stress during and after uniaxial extension of PC. The stress produced by pre-yield extension decays slowly while the stress from post-yield extension decreases fast initially before approaching a similar relaxation rate to pre-yield relaxation. Draw ratios: L/L_0 = 1.02 (pre-yield), 1.03 (pre-yield) and 1.8 (post-yield), crosshead speed V = 6 mm/min, initial specimen length L_0 = 39 mm 91

6.3 Tensile (engineering) stress during and after drawing PC at temperature from 98 to 155 ^oC. Draw ratios L/L_0 = 1.0175 (pre-yield), cross head speed V/L_0 = 0.15 mm/min. (Experiment by Jianning Liu)..... 92

6.4 Tensile (engineering) stress during and after drawing PC. The pre-yield curve is moved horizontally to share the same relaxation starting time. Draw ratios L/L_0 = 1.03 (pre-yield) and 1.7 (post-yield, at the beginning of strain hardening regime), at a crosshead speed V/L_0 = 0.15mm/min..... 93

6.5 Engineering stress during and after drawing of PS to draw ratios L/L_0 = 1.02 (pre-yield) and 1.92 (post-yield) at a crosshead speed V/L_0 =0.02 /min. Similar to Figure.6.4, stress from post-yield drawing survives at long times. The stress relaxation in the inset shows contrasting characteristic time scales: the stress relaxation is much slower from post- yield deformation. (Experiment by Jianning Liu)..... 94

6.6 Different components of stress and bond lengthening (right-hand-side Y axis) during drawing of PS at 370 K..... 97

6.7 Relaxation of different stress components after pre-yield deformation of L/L_0 = 1.03. 98

6.8 Relaxation of different stress components from post-yield drawing to L/L_0 = 1.8 100

6.9 Bond length decrease and bond disorientation in terms of P_2 as a function of time during relaxation from post-yield drawing to $L/L_0 = 1.8$. 101

6.10 Bond orientation auto-correlation against relaxation time in post-yield relaxation and pre-yield relaxation. Starting time for correlation: t = 0 ns (left set), t = 8 ns (center set), t = 16 ns (right set) 103

6.11 Visualization of sample mobility at post-yield relaxation. (left) whole piece of sample, (right) stretched part of the sample 103

6.12 States of bond stretching after stress relaxation 4 (left) and 24 ns (right) respectively, after tensile extension to a draw ratio of $L/L_0 = 1.8$. All bonds longer than 2.6 Å are displayed with colors (online) representing different strands. At 4 ns, more load-bearing strands are observed than at 24 ns. These strands stem from one to the other end of the system. The equilibrium bond length is 2.574-2.575 Å..... 105

7.1 Stress-strain curve during the drawing of coarse-grained PS to a draw ratio L/L_0=2.2. Retractive stress value is defined as positive 109

7.2 Stress decomposition during the unload of sample. Contribution of the stress is divided into intra-segmental, inter-segmental and kinetic components. Constant repulsive kinetic stress is not shown to clarify the relationship. Retractive stress value is defined as positive 111

7.3. Emergent retractive stress (diamonds) during the annealing process at $T_{el\text{-}yield}$ (360 K) < T_g (380 K) of a pre-deformed PS. The result is based on MD simulation of a coarse-grained model, and the decomposition of the total stress is separated into intra-segmental (retractive-circles) and inter-segmental (compressive-squares) components 111

7.4 Orientation function (P_2) and average bond length of the backbone bond against time during the deformation at 300 K (regime (1)), upon releasing at 300 K (regime (2)) and during elastic yielding upon annealing at 360 K (regime (3)) 112

7.5 Orientational autocorrelation function against time in the pre-deformed and non-deformed systems at 360 K 114

CHAPTER I

INTRODUCTION

According to PlasticsEurope (PEMRG), the world produced 322 million metric tons of plastic in 2015. In modern world, plastic or glassy polymers are one type of the most widely used materials in everyone's daily life. When comes to practical application, the mechanical property of materials, defined as the response of material to external deformation or load, is always firstly evaluated. The most important properties are strength, ductility, hardness, impact resistance, and fracture toughness. It is of great importance to achieve good properties in application and people are always pursuing better properties for industry purpose.

Mechanical properties of glassy polymers[1-5] are also of central academic interest due to their unique chain connectivity and chain uncrossability[6]. These unique properties not only allow polymer glass to have larger ductility and higher impact resistance than small molecular glasses, but also lead to rich and unique mechanical response. Upon deformation, polymeric glasses are able to show various response such as brittle failure, yielding, necking, strain-hardening and crazing, etc.

Over the decades, a lot of efforts have been made to understand the physics behind the rich phenomenology of mechanical responses in polymeric glass system. Several models developed based on rubber elasticity tried to explain the nature of

mechanical stress upon deformation in glassy state. For example, eight-chain model from Haward[7] and Boyce[8, 9] describes the chain geometry as 8 chains of which one ends joint together at the center of a cube and the other 8 ends are placed at each vertex of the cube. And the stress upon deformation comes from the restriction of segmental rotation and configurational entropy of molecular alignment which means the stress is dominated by intra-segmental. Later on, Kramer[10] brought out the opposite idea mechanical stress at large deformation is mainly inter-segmental. The reason was that the modulus at large deformation in glassy state is 2 orders higher than the rubber elasticity and entropic force decreases linearly as the temperature cools down and extrapolates to zero when temperature is close to $T_{g.}$ More recently, molecular-level microscopic constitutive theory from Schweizer[11-14] have similar spirit as Eyring[15] that when external force is applied to the segment, the energy barrier is lowered. When the external force is large enough and the barrier is sufficiently low, plastic flow of the specimen is enabled. In this theory chain connectivity is included by heightening the barrier of connected segments but this model only count inter-segmental interaction contribution to mechanical response. Besides these efforts to pursue the origin of stress, a large number of other theories have also been developed to account for other aspects of mechanical response. For example, Ludwik[16]−Davidenov-Wittman[17]−Orowan[18] (LDWO) hypothesis tries to explain brittle-ductile transition. It treats yielding and brittle fracture as independent and competing events in a continuum. It describes two different dependence on temperature for critical brittle stress and critical yield stress, both of which decreases with increasing temperature. The yield stress has stronger dependence and at high temperature, the yield stress σ_Y is lower than the brittle stress $\sigma_{B,}$ so that plastic flow

would occur instead of fracture. Below T_{BD}, σ_Y would be higher than σ_B because σ_Y has been observed to increase significantly with decreasing temperature.

Each of those efforts can successfully explain one aspect of the model, but none of previous theories can explain all the rich phenomenon in a coherent way. Therefore, a coherent model to reveal all aspects of mechanical response of polymeric glass is still in need. Based on our study on polymer melt rheology[19-25], we extend our understanding of chain network into glassy state[26]. A model of hybrid structure that values the role of network and intra-chain interaction is built to approach the rich phenomena such as brittle-ductile transition, the nature of stress. The model will be described briefly in the following.

It is nature to consider that under deformation, not all strands are equally stretched or load-bearing. The load bearing ones participate as units and form load bearing network. We consider the polymeric glass as a hybrid of this network and the rest redundant part (called primary structure). When deformation is applied to the system, network holds the integrity of the specimen, contributes dominantly to the mechanical stress, and most importantly, acts like a proactive role to "push" surrounding primary structure to climb over their energy barrier. This "pushing" process is also named as "activation", because the mobility of primary structure segments is increased in orders during this process. In the meantime, the load or tension in load bearing strands increasing with increasing deformation. When all the primary structure segments are fully activated, the system will yield and undergo plastic deformation. However, if the tension in load bearing strands is so large that excesses the threshold before the primary structure fully activated, chain pull-out takes place leading to the failure of load-bearing network

and failure of the sample.

In this work, both experimental and computer simulation study are performed to test the hybrid model and understand the mechanical response of polymeric glasses.

In Chapter II, sufficient information related to background is introduced and reviewed. The definitions of polymer and glassy state are reviewed, followed by the deformation modes used and the quantification of deformation result. The terminology is then used to introduce the characteristics in tensile mode which is the frequently used in this work.

In Chapter III, we review our recent proposed model about the hybrid structure of (intramolecular) chain network and vitreous (intermolecular) primitive structure.[26] The brittle-ductile transition and origin of stress are interpreted briefly based on this model.

In Chapter IV, we carry out a series of tensile extension tests on two most common polymer glasses and describe their generic mechanical responses as a function of deformation rate at various temperatures. We find that PMMA and PS are brittle at the highest applied rate, ductile at intermediate rates and but become much less ductile as the rate further decreases. We draw phase diagrams and summarize the relationship between brittle-like and yield-like states in terms of temperature, rate and stress. Based on finding, a coherent understanding of the rich phenomenology is built with our hybrid structure model.[26]

In Chapter V, we further test our hybrid model by computer simulation and study the origin of stress in both tensile and compression modes. Coarse-grained model for polystyrene is used for molecular dynamics simulation. Specimens with different

chain length are built, equilibrated and cooled down to their glassy states. Tensile and compression deformations are then applied to these specimens respectively. In our study, he arising stress is decomposed into inter- and intra-segmental contribution based on force field, and the origin of emerging stress can be analyzed at molecular level. Coherent understanding is built based on the molecular level information and has been proven to support our proposed hybrid structure model.

In Chapter VI and Chapter VII, we further discussed our experimental phenomena on polymer glasses stress relaxation and elastic yielding use our understanding built from previous chapter. In Chapter VI, we conduct relaxation experiment at near-T_g temperature. It is found that tensile stress vanishes shortly after pre-yield deformation of polymer glasses while tensile stress from post-yield stays high and relaxes on much longer time scales. The experimental observation in this chapter is consistent with our simulation discovery of the nature of stress in Chapter V. Molecular dynamics simulation based on the same coarse-grained PS is conducted and near-T_g stress relaxation of both post-yield and pre-yield are analyzed at molecular level. In Chapter VII, we study the phenomenon of elastic yielding. After ductile drawing at room temperature to a sufficient extension ratio and unloading to permit stress relaxation in an unconstrained manner, stress is still embedded in glassy state. When annealed at temperature above the storage temperature yet still substantially below T_g, considerable retractive stress may emerge. Molecular dynamics simulation is again conducted with the same coarse-grained model to investigate the emerging stress during elastic yielding.

In Chapter VIII, a summary of the work is presented in a coherent manner.

CHAPTER II

CHARACTERISTICS OF DEFORMATION

2.1 Polymer and Glass transition

Polymers, referred as synthetic plastics,other than biomolecules are long chain molecules composed of repeating units.[27, 28] When temperature is high enough, polymer is liquid-like, because the mobility of the polymer segments are high enough to allow fast relaxation. However, polymer “liquid”, called melt[29-32], has the viscosity that is much higher than other common liquids. It can be honey-like sticky or even solid-like, as long as the molecular chain is sufficiently long and the temperature sufficiently low. This special property comes from its connectivity and resulting uncrossability, which means that the polymers are long chains and cannot go across each other. As a result, entanglement becomes the most important factor of polymer. Like a bowl of noodle, polymers with long chains will form knots when mixed. These knots tie the whole piece of polymer together and make it impossible to move one chain without disturbing others. Therefore, polymer can present unique mechanical properties such as viscoelasticity in melt state[33] as well as the ability to plastically flow in glassy state.

When polymers cooled down from melt state, thermal motion will be lowered

down. If the cooling takes place fast enough, at a point, the mobility from thermal motion will be insufficient to allow the system to explore all the possible configurations. In other words, the polymer system cannot reach equilibrium.[33] Consequently, the polymer system will be trapped in a non-equilibrium state, called glassy state.[1-3] This featured temperature is referred as glass transition temperature.

Not only polymer system, small molecule system has also been observed with thus transition process. In fact, all the systems in glassy state share many same properties such as physical aging and non-Arrhenius temperature-dependent α-relaxation time. However, because of the low mobility of long chain system, polymer systems show their advantage to illustrate such phenomenon. The entanglements in polymer system increase the melt viscosity and lower the chain mobility, making the system trapped in non-equilibrium state much easier as the temperature decreasing.

Fundamentally, polymeric glass system is a super-cooled liquid trapped in a non-equilibrium state but behave more similar to a solid.

2.2 Deformation Modes of Polymer Glasses

There are three basic deformation modes in terms of how the shape of specimens would change after deformation. They are tensile (stretching) mode, compression and shear, as shown in Figure 2.1. Only tensile and compression mode are going to be used in this work, so they will be discussed further.

These two modes are different in their sample handling. For a tensile test, the usual way is to fix two ends of the specimen and force them to apart from each other; whereas for a compression test, the sample is usually placed between two plates and

compressed by forcing the two plates approach to each other. The two modes will induce different mechanical responses of the polymeric glasses, which will be investigated in detail in Chapter V. But briefly, one important reason is that the segments are forced to be separated in tensile mode while getting closer in compression mode. This also leads to their disparity in poison ratio.

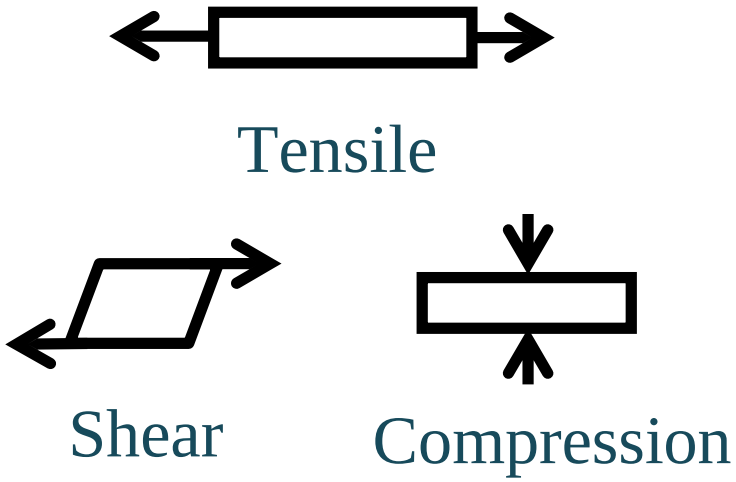

Figure 2.1 Three basic deformation modes in terms of the specimen shape change. Arrow represents the direction of applied deformation.

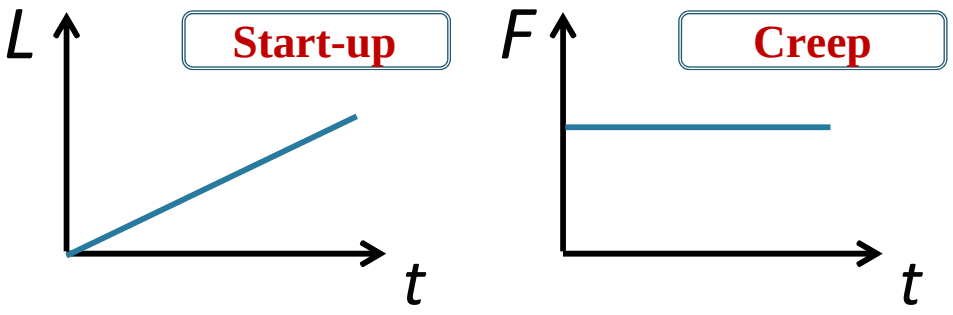

Figure 2.2 Two basic deformation modes in terms of applied deformation. Tensile deformation is used as example.

There is another way to define a deformation based on how is deformation is performed. Generally, the deformation can be divided into two types in this way. Taking the tensile deformation as an example, deformation can be applied to the specimen at constant rate (left in Figure 2.2), showing as the specimen length growing linearly with time. This is called start-up mode. In another way, it can also be applied with a constant force (right in Figure 2.2), which is called creep mode. In this work, all the deformation is applied with start-up (constant rate) mode.

2.3 Characterization of Deformation

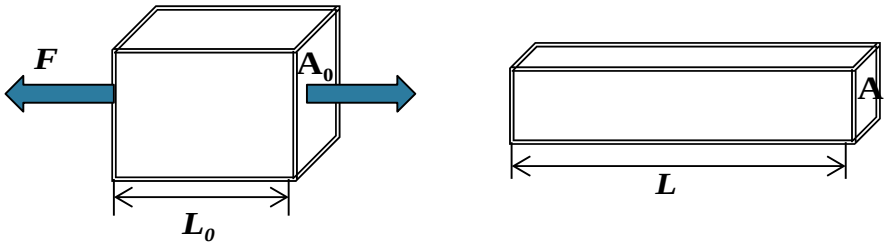

Figure 2.3 Specimen dimension before (left) and after deformation (right).

After classifying the types of deformation, we introduce the commonly-used method to quantify the deformation and corresponding response. Taking start-up tensile as an example: when external tensile deformation is applied to the specimen, stress that shows up during the deformation can be used to define the mechanical response. A piece of material with L_0 in initial length becomes L after applying deformation. The deformation of the material, therefore, can be defined by strain $\lambda = \frac{L}{L_0}$, and the response of material can be defined by stress $\sigma = \frac{F}{A}$, where F is the force response at the

deformation direction and A is the cross-section area of material at the same direction. When A is real time cross-section area that keeps shrinking with deformation, the stress is referred as true stress; and when A is the initial cross-section area before deformation A_0, stress is referred as engineering stress. Stress responses to the increasing strain during the deformation in most cases are described by stress-strain curves.

2.5 Characteristics in Tensile Deformation

2.5.1 Shear Yielding and Necking

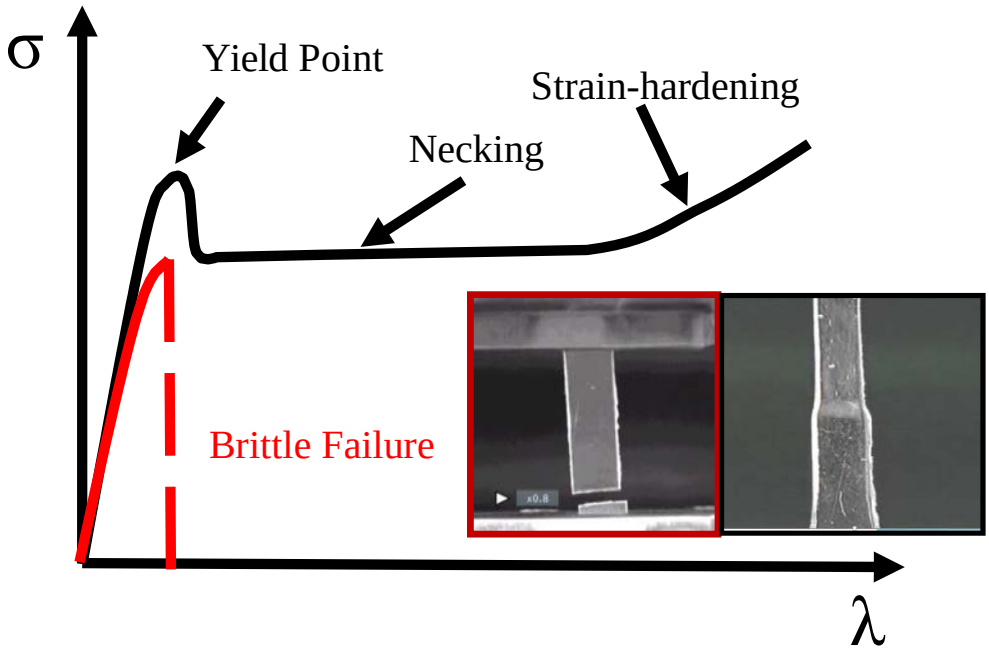

Figure 2.4 Typical stress-strain curves of polymeric glasses undergoing start-up tensile deformation. Black curve shows a ductile response and red one shows a brittle response. Inset are the photos of specimen after brittle failure (red frame) and undergoing necking front propagation (black frame).

Black curve in Figure 2.4 shows a typical stress-strain curve of glassy polymer upon constant rate extension deformation. At the beginning of the deformation, stress grows linearly with increasing strain, which is called linear regime or elastic regime. The deformation at this strain is recoverable, which means if the constraint is released at this regime, the specimen can recover to its initial shape.

After elastic regime, stress response deviates from the linear relationship and reaches the maximum of the curve which called the yield point. For a glassy polymer, it is well accepted that shear yielding occurs at this point. A strain localized regime called necking regime would show up on the specimen and it is highly stretched than the rest part of the specimen. With the deformation continues, the two fronts of necking propagate towards the two ends of the specimen, shown by the inset photo (black framed) in Figure 2.4 that one of the necking front which propagates from top to bottom. The stress response keeps constant until the two necking fronts reach the ends. As a result, it shows the plateau in stress-strain curve. After that, the stress will increase again with deformation if necking finishes, and this is called strain-hardening. If strain localization does not occur after yielding, strain-hardening will show up after a small amount of deformation.

Before the yield point is reached, the regime is defined as pre-yield regime. And the regime after yielding is defined as post-yield regime.

2.5.2 Brittle Failure

As a comparison shown in Figure 2.4, a ductile response of polymeric glasses includes linear regime, shear yielding, necking (if it occurs) and strain-hardening, while a

brittle response stops before yielding. Typically, a brittle failure is defined when specimen breaks at the stress maximum just after the elastic regime. For common polymer, this occurs within strain λ=1.1. In contrast, if polymeric glass can be drawn ductile, it can usually reach more than 170% of its initial length.

Brittle-ductile response will be discussed detail in the following Chapters III and IV.

CHAPTER III

THE EMERGENCE OF HYBRID MOLECULAR PICTURE

3.1 Introduction

We treat polymeric glasses with high molecular weight as a structural hybrid.[26, 33] This hybrid is made of network at two levels. Between segments, there is short-ranged Van der Waals interaction which constructs a Van der Waals network as primary structure. This network also exists in small molecule system. The other one is the network peculiar to high molecular weight polymeric system, which is constructed by chain connectivity and uncrossability. As discussed above in chapter 2.1, polymeric system is an entirety connected by chain entanglements. In this chain network, interaction is dominated by bonded interaction, such as bond stretching, angle opening and dihedral distortion.

However, we need to emphasize that this chain network is not exactly the same as "entanglement network". It is reasonable to believe that when deformation is applied to the system in different direction, the tightened (load-bearing) entanglements are not necessary to be the same each time. Therefore, it is also reasonable to believe that not all the entanglements participate efficiently upon a certain deformation. We believe that

chain network is an idea of dynamic network that only constructed from load-bearing strands under deformation. This difference between entanglement network and our load-bearing strands chain network also shows up when network density is estimated. Calculation shows the length of a load-bearing strand is proportional to Kuhn length l_K [26]and that of an entanglement strand is proportional to the packing length p[34, 35]. The ratio of planar network density between these two chain networks is $(p/l_K)^2$ and the density of load-bearing strand network is lower since p is smaller than l_K. These results fit our speculation that not all entanglements are participating.

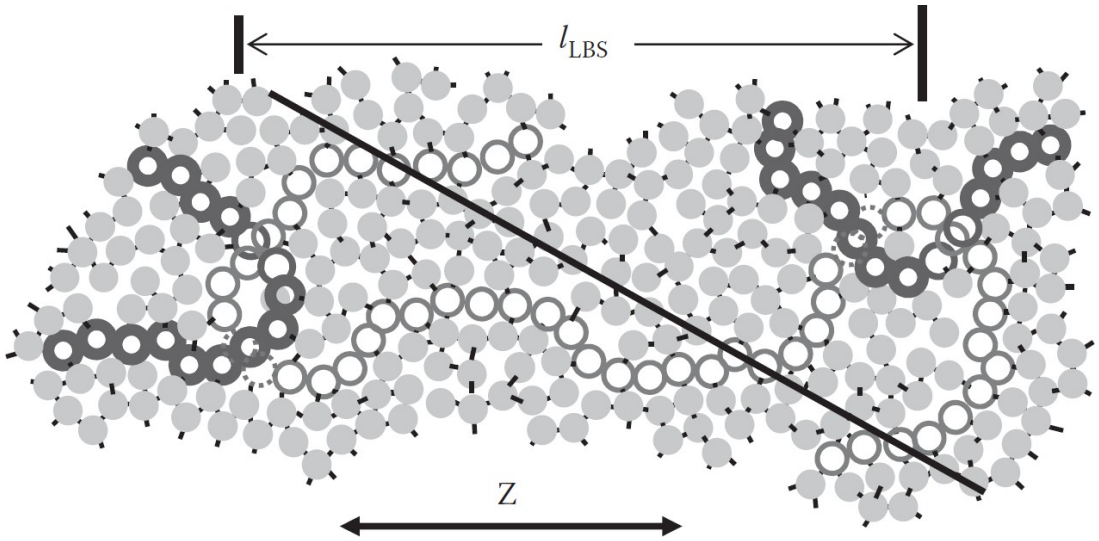

Figure 3.1 Hybrid structure of polymer glasses upon large deformation along z-direction with load-bearing chain network already emerged. Dots and short bars represent polymer segments connected by Van der Waals network. A load-bearing strand (thin rings) forms chain network with the assistance of two adjacent chains (thick rings) through two hairpin structures. (replot of Figure 12.1 Roth, C. B., Polymer Glasses. CRC Press: 2016.)

3.2 Discussion

At the beginning of deformation, in pre-yield regime, the deformation is limited and the molecular level displacement is still within the limit of Van der Waals interaction. In this stage, deformation is still affine, elastic and recoverable. In addition, the stress is dominated by inter-segmental Van der Waals interaction. The reason is obvious, as shown in Figure 3.1, the Van der Waals network density overwhelms the density of the intra-chain network. As the deformation increases, short-ranged Van der Waals interaction reaches its range limitation. If the polymer chains are not long enough to build chain network, the specimen will break at this point. However, in the case where molecular weight of the polymers is sufficiently high, chain network emerges as load-bearing strands emerge due to chain connectivity and uncrossability. The role of chain network is not only to keep the integrity of the system, but also to mobilize the primary structure with its own displacement.

At the point reaching global yielding, the entire primary structure connected by the Van der Waals network should be mobilized sufficiently and be ready to undergo plastic deformation. During this process, we will observe the stress deviates from linear relationship as Van der Waals network “melting down”, and reaches the maximum as the primary structure is fully mobilized. At this point, if no stain localization (such as necking) occurs, stress decreases as the primary structure starts to plastically deform. However, as the deformation continues, the stress increases again with increasing strain, which is mentioned above as strain-hardening. In this regime, with the primary structure “melt-down”, stress is contributed by the load-bearing strain chain network, which is deformed more and more with increasing deformation.

During this process chain network keeps building more tension with increasing deformation. And if the primary structure is not fully mobilized before the chain tension reaching its threshold, chain pull-out would occur. This will lead to the collapse of chain network and eventually the brittle failure of the specimen. Detail information will be discussed in the following chapter.

CHAPTER IV

MAPPING THE BRITTLE AND DUCTILE BEHAVIOR OF POLYMER GLASSES

4.1 Brittle-Ductile Transitions (BDT)

The brittle-ductile property is one of the key properties of the application material. However, structural failure of matter under mechanical deformation is among the most difficult phenomena to depict in physics. Earthquake is a leading example of breakdown of a continuum. [36] Modern engineering materials including metals, ceramics and polymers (below their glass transition temperature T_g) frequently undergo brittle fracture after elastic deformation at small strains. Contrary to organic low molar-mass glasses that are always brittle, polymer glasses of high molecular weight can be highly ductile, drawn to double their initial length during uniaxial extension. Just as shown in the Figure 4.1, the red curve represents the mechanical response of the brittle polymers which the brittle failure typically happens at linear region before reaching yield point, while the black one represents the mechanical response of the ductile ones. A ductile response, especially in this work, is typically defined when deformation lasts beyond yield point and reach the stress plateau ofnecking or the strain hardening region. For the polymer used in this work, this means the tensile deformation $\lambda = {}^{L}/_{L_0}$ should be at least large than 1.3. At the right part of Figure 4.1 the snapshot with red border is a

piece of brittle polymer after continues tensile deformation and a sharp brittle failure can be seen on this piece of polystyrene specimen. And the snapshot with the red border shows a piece of polycarbonate specimen under the same continues deformation and a clear border of necking front can be seen meaning the specimen is current in the stress plateau region of the stress-strain curve.

The mechanical response of glassy polymer can switch from being ductile to being brittle when the temperature T is sufficiently reduced. Despite decades of continuous investigations,[2, 37, 38] it has remained an elusive task to propose a coherent molecular mechanism for the brittle-to-ductile transition (BDT) in most glassy polymers, located in a rather narrow range indicated by T_{BD} (brittle-ductile transition temperature). To explain the BDT phenomenon in extension, different accounts have been put forward, including the Ludwik[16]−Davidenov-Wittman[17]−Orowan[18] (LDWO) hypothesis, the correlation between primary[39] or secondary relaxation[40, 41] and BDT, the relationship between entanglement density and crazing behavior,[42-47] considerations that relate the degree of strain hardening vs. softening to the ductility of polymer glasses,[48-54] as well as fracture mechanical considerations.[55-57] These efforts, summarized in several monographs,[2, 37, 38, 55] have formed a vast background for the subject of mechanical behavior of polymer glasses.

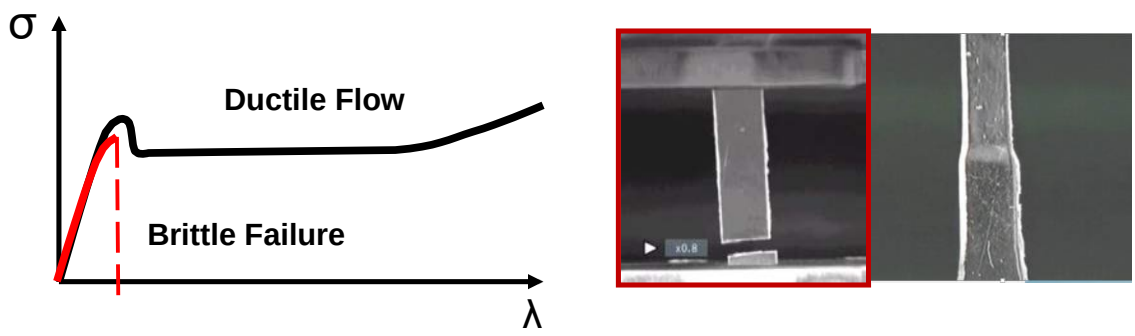

Figure 4.1 Typical stress-strain curves (left) of brittle (red) and ductile (black) and a snapshot of polymer specimen (right) after brittle failure (red framed) and snapshot of polymer undergoing ductile necking propagation (back framed).

4.2.1 The LDWO Hypothesis and Other Understandings

The textbook explanation for BDT is phenomenological, based on the Ludwik-Davidenov-Wittman-Orowan (LDWO) hypothesis,[16-18, 38] which treats yielding and brittle fracture as independent and competing events in a continuum. It describes two different dependence on temperature for critical brittle stress and critical yield stress, both of which decreases with increasing temperature. The yield stress has stronger dependence and at high temperature, the yield stress σ_Y is lower than the brittle stress $\sigma_{B,}$ so that plastic flow would occur instead of fracture. Below T_{BD}, σ_Y would be higher than σ_B because σ_Y has been observed to increase significantly with decreasing temperature. This explanation does not attempt to answer how and why polymer glasses can yield well below T_g. Consistent with the prevailing idea from Eyring[15], LDWO hypothesis anticipates the BDT at a lower temperature, i.e., the glass being more ductile at lower rates because σ_Y decreases gradually with lowering rate whereas σ_B is nearly independent

of rate. In addition, it is commonly argued that plastic flow in polymer glasses takes place when the deformation rate is comparable to the internal material relaxation rate.[15, 58] Therefore, a lower extensional rate is always believed to favor a more ductile response.

Another way to think of brittle-ductile response is through fracture mechanism. [55-57] The key of this idea is that brittle failure is caused by the defects and flaws on the surface of or inside the specimen. The stress concentrates at the tip of the flaw, where the tip stress depends greatly on the shape and size of the flaw, as well as the stress applied to the specimen. The tip propagation cannot result in the catastrophic failure until the tip reaches its critical stress. No matter whether it is the major factor for breaking polymer specimens or not, the flaws are unavoidable because of the existence of duct, air bubbles or surface scratches in real polymer specimens. However, discussion related to these topics does not help to understand physics of polymer as it is unable to answer the question why different polymers can be brittle or ductile in present of same sized notches.

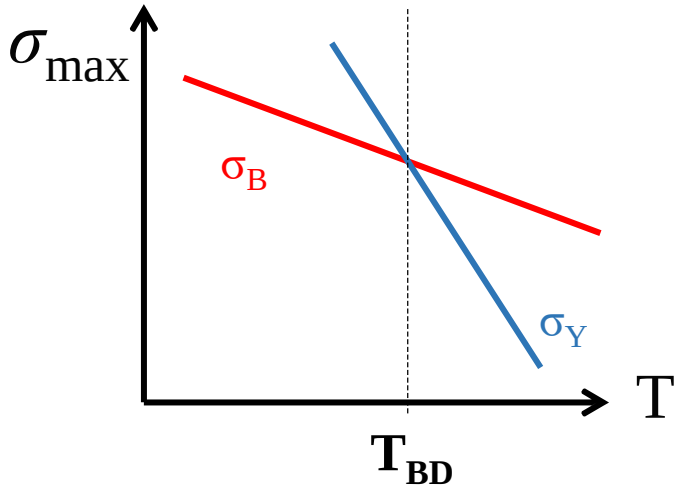

Figure 4.2 Demonstration of BDT in the LDWO hypothesis, which is represented by plotting critical brittle stress σ_B and critical yield stress σ_Y vs. temperature.

Others like the primary[39] or secondary relaxation[40, 41] theory finds that there's a direct link between the microscale relaxation of segments and brittle-ductile response. Polymers with fast primary or secondary relaxation are more flexible with higher mobility, hence have higher chance to undergo ductile deformation. Besides, the crazing theory[42-47] believes that brittle facture is caused by the failure of crazes, which will be described in detail in section 4.4.5.

4.2.2 Our Hybrid Structure Model

Frequently, the BDT phenomenon is examined by tensile extension of glassy polymers at a constant rate over a temperature range that covers T_{BD}. There are several known characteristics associated with the extreme mechanical behavior of polymers glasses, which all needed to be property addressed for eligible theories. (a) A most ductile glassy polymer, i.e., bisphenol A polycarbonate (PC), loses its ductility upon reduction of its molecular weight below a critical value. (b) Mechanical "rejuvenation", i.e., certain types of large-magnitude mechanical deformation at $T < T_g$, can make a brittle glass behave in a ductile manner. (c) Upon physical aging, even the ductile PC turns brittle. (d) Brittle polystyrene (PS) and poly (methyl methacrylate) (PMMA) become ductile at room temperature after melt extension to a sufficient degree.[59, 60] (e) PS can be as ductile as PC under sufficiently high hydrostatic pressure.[61] (f) Upon incorporation of some plasticizing small-molecule additives into polystyrene, its BDT shifts to a higher temperature.[62] To provide a coherent account for all these six factors, we need a molecular picture that recognizes the role of a global network formed by sufficiently long chains.

In a zeroth order picture, a polymer glass should be regarded as a structural hybrid,[26] made of a chain network embedded in a vitreous continuum that we call "primary structure", which is bonded by short-ranged van der Waals intersegmental interactions. Here the chain network in a ductile polymer glass is the driver for yielding of the primary structure. In other words, polymer glasses are able to yield thanks to the activation of the primary structure by the displacing chain network.**Error! Bookmark not defined.** With this molecular model, we are able to provide a sensible explanation for why PS is the most brittle and PC the most ductile respectively among all known polymer glasses:[63] Since the areal density ψ of load-bearing strands (LBSs) in the chain network is much higher in PC than in PS, at a comparable distance from T_g it is much easier for activation zones in PC, produced around the LBSs by the LBSs, to permeate throughout the primary structure, leading to global plasticity during large deformation. Moreover, T_{BD} is a Goldilocks temperature where the chain network is on the verge of a structural breakdown while barely able to produce global plasticity in the primary structure. However, the model does not predict how the BDT may shift with the deformation rate although it certainly anticipates the following: If a polymer glass is ductile at one rate, it could turn brittle at a higher rate where chain tension could build up to reach the condition for chain pullout before the primary structure has enough time to get activated.

4.3 Experiments

4.3.1 Materials and Specimen Preparation

The polymer glasses under study are PMMA from Plaskolite West Inc. (item number CA-86), having a molecular weight of M_w = 125 kg/mol and polydispersity PDI = 1.43, and PS from Dow (Styron 663) with M_w = 319 kg/mol and polydispersity PDI = 1.44. The glass transition temperatures of PMMA and PS are ca. 113 and 103 ^oC respectively.

There are three types of specimen used in this study: extruded cylindrical specimens, dog-bone shape specimens and polished dog-bone specimens.

Most data produced in this work is with cylindrical specimens, made by capillary extrusion using a Monsanto Capillary Rheometer. For PS, the pellet-like resin was heated up to 150 ^oC in the barrel and a pressure of 123 bar was applied to compress the resin in the barrel, squeezing out air trapped between pellets. After 30 min resting at 190 ^oC, the PS melt was extruded using a capillary die of length L=15D and diameter D = 1 mm, at a wall stress of σ_w = 0.078 MPa. To make the specimen thicker at the two ends of such a cylindrical specimen, a higher stress of 0.114 MPa was applied to achieve a higher die swell ratio. For PMMA, the pellet-like resin was firstly heated up to 210 ^oC in the rheometer and after 10 min resting without compressing, it was cooled down to 165 ^oC. Then a similar procedure was taken, compressing at 165 ^oC at 123 bar and extruding at 210 ^oC. The capillary wall stresses were 0.139 and 0.180 MPa respectively. For both PS and PMMA, the specimens have an effective length of 50 mm and diameter equal to 1.15 and 1.18 respectively.

The dog-bone specimens were cut from hot compressed sheet. For PMMA, the pellets resin was put into square spacer between two layers of non-stick thin film and heated up to 200 ^oC. Then pressure was applied to the resin for 5 min. The pressure was

then released for another 5 min. These two steps were repeated for another 2 times to complete the degas process followed by a 60min relaxation process with applied pressure. Then the resin together with the mold was cooled down to room temperature and cut into dog-bone shape specimens with dumbbell shape cutter D412D. The PS specimens were produced in the same way.

The polished dog-bone specimens were produced by polishing the dog-bone specimens from the procedure above. The two cutting side surfaces were polished with sand paper first until smooth and then were polished with NOVUS 7136 Plastic Polish Kit step by step until transparent.

4.3.2 Apparatus and Methods

An Instron 5567 with an environmental chamber was used for the tensile extension tests. The tensile tests started after the specimens were loaded onto the Instron 5567 at a prescribed temperature for 10 min. The available crosshead speed ranges from 0.05mm/min to 900mm/min. During tests, the temperature was maintained within ± 0.5 ^{o}C.

4.4 Results and Discussion

4.4.1 Temperature Effect

Firstly, we demonstrate the classic temperature effect on brittle-ductile behavior of glassy polymer in Figure 4.2. Deformation is applied to the extruded cylindrical

specimens at constant rate $^{V}/_{L_0} = 2\ \text{min}^{-1}$, where V is the crosshead speed and L_0 is the length of the specimen between two fat ends.

In Figure 4.2 we demonstrate the brittle-ductile transition with the stress-strain curves of PMMA specimens being deformed at varies temperature. As temperature decreases, the response of the specimen turns from ductile to brittle. At high enough temperature which is 35 °C in the figure, the specimen undergoes ductile response. It is drawn far beyond yield point and reaches more than 150% of its initial length. As contrast, at lowest temperature of 17 °C, the specimen shows a shape brittle failure by breaking at the maximum of stress-strain curve and unable to be deformed to more than within 10% of its initial length.

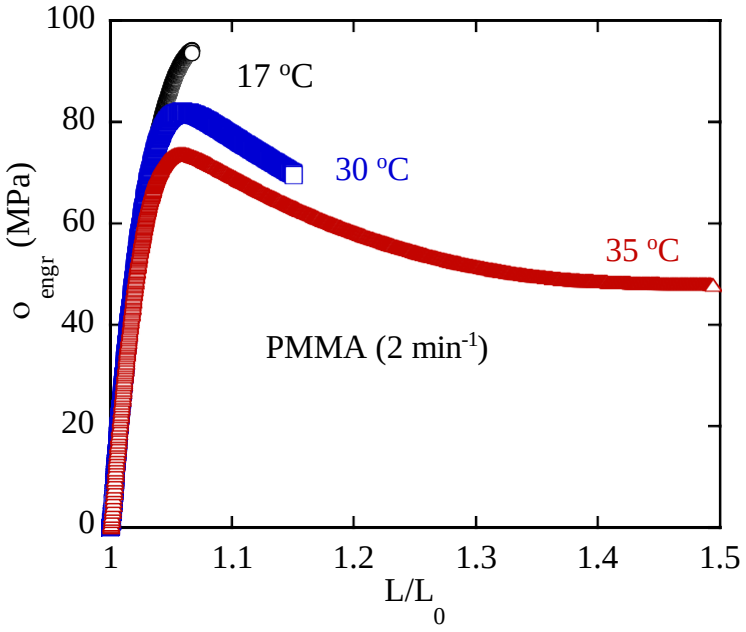

Figure 4.2 Engineering stress vs. the draw ratio from various tensile extension tests at the different temperature for PMMA at 35 °C, showing brittle fracture (circles), ductile drawing (triangles) and premature failure (squares).

In our perception based on hybrid structure of polymeric glass, the chain network constructed by load-bearing stands (LBSs) emerging during deformation will try to drive the rest redundant part (primary structure) in order to enable yielding and plastic flow. When temperature is sufficient warm, the mobility of primary structure is high enough to be driven or be activated to undergo plastic deformation, since the mobility of primary structure is controlled by alpha process before any external deformation. Upon deformation, the activation zone spread from close to far from the LBSs, when all the segments are activated the specimen yields and stress drops from the maximum due to less vitreous state. Otherwise, when the temperature is low, the specimen is too vitreous. Upon deformation, the activation of the LBSs network propagates slow, meanwhile the tension in the LBSs grows with elongation and reaches the tension of pull-out before activation enable the whole specimen to flow. Then brittle failure takes place due to the chain network breaking down.

4.4.2 Rate Effect

Effects of deformational rate on the yielding behavior of polymer glasses are well established.[2, 38] The Eyring model[15] has been applied to explain the logarithmic dependence of σ_Y on rate although the activation idea of Eyring is far from adequate to describe other effects including temperature. More sophisticated microscopic theory has been developed to provide a better description.[11-13]. Moreover, the available literature data[64-66] indicate that polymer glasses are usually more brittle at higher rates. Our experiments confirm this common knowledge as shown in Figure 4.3 by the comparison between circles at 18 min^{-1} and triangles at either 2 or 0.2 min^{-1}. However, when the

extensional rate is further reduced to 0.02 or 0.002 min^{-1}, PMMA appears brittle-like again, unable to draw.

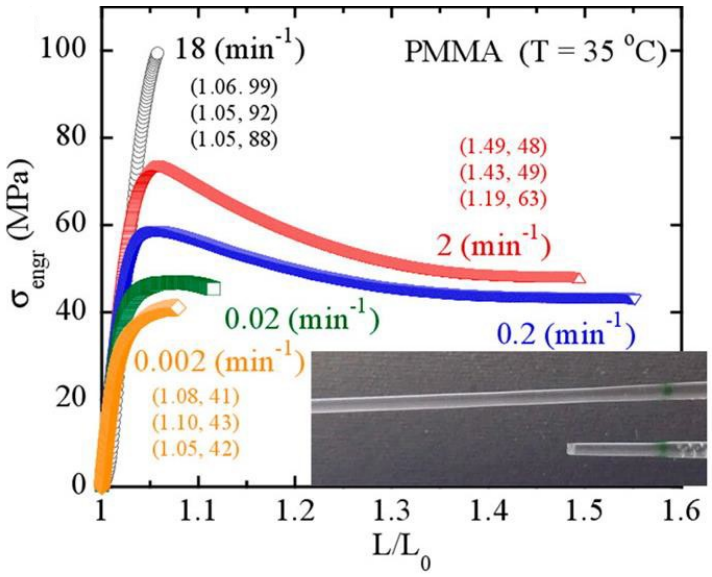

Figure 4.3 Engineering stress vs. the draw ratio from various tensile extension tests at the different initial rates defined by V/L0 for PMMA at 35 °C, showing brittle fracture (circles), ductile drawing (triangles) and premature failure (squares and diamonds). The numbers in the brackets are (L/L_0, σ_{engr}) in the units of mm and MPa, respectively, at breaking, for three runs, with the top numbers corresponding to the data presented in the figures. Here, L_0 = 50 mm is the original effective length of specimen that is undergoing extension, and ($L - L_0$) measures the lengthening of the specimen of initial length L_0. At 0.2 and 2 min^{-1} in (a), the ductile drawing was nearly uniform: no visible neck front, and there was only a small smooth variation in the specimen diameter of 5% or so from the thinnest section to the thickest section, as shown by the photo (0.2 min^{-1}) in the inset.

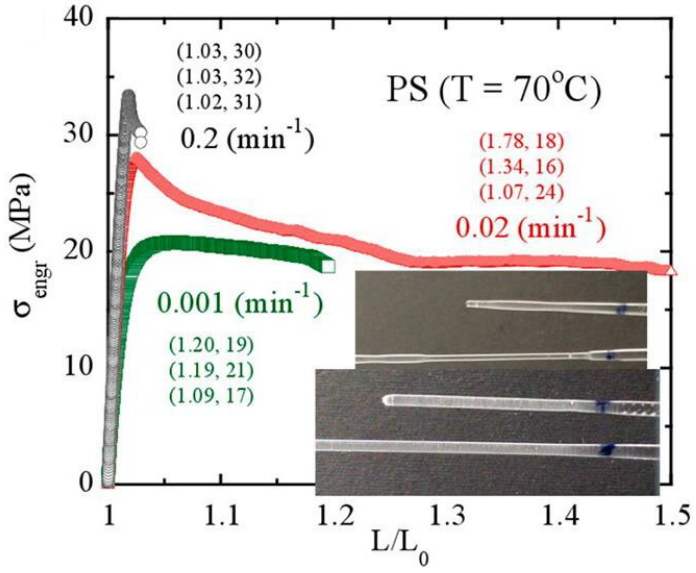

Figure 4.4 Engineering stress vs. the draw ratio from various tensile extension tests at the different initial rates defined by V/L_0 for PS at 70 ºC, showing brittle fracture (circles), ductile drawing (triangles) and premature failure (squares). At 0.02 min^{-1}, there is shear yielding leading to necking with multiple neck fronts, visible from the top photo. The diameter of specimen shrinks to 0.66 mm, whereas the original diameter is 1.16 mm, amounting to a large local draw ratio of 3.1. At 0.001 min^{-1}, the drawing is uniform as shown in the second photo in the inset until breaking at $L/L_0 = 1.2$. Clear opaqueness due to intensive crazing can be seen from the bottom photo.

To examine the universality of this surprising result, we carried out a comparable set of extensional tests on PS. Figure 4.4 shows similar behavior to that in Figure 4.3: PS is completely ductile at 0.02 min^{-1} but suffers a mechanical failure at 0.001 min^{-1}. Both PMMA and PS lost its ability to draw when the deformation rate is sufficiently lowered. Such a reversal of BDT as a function of extensional rate has broadened the scope of the phenomenology associated with BDT. We can evaluate the overall toughness at different rates and indicate that it is strongly non-monotonic, as shown in Figure 4.5, at several temperatures for PMMA and at 70 °C for PS. To the best of our knowledge, such a dramatic and unexpected loss of toughness with lowering rate has not previously been reported in the literature and challenges the conventional wisdom.

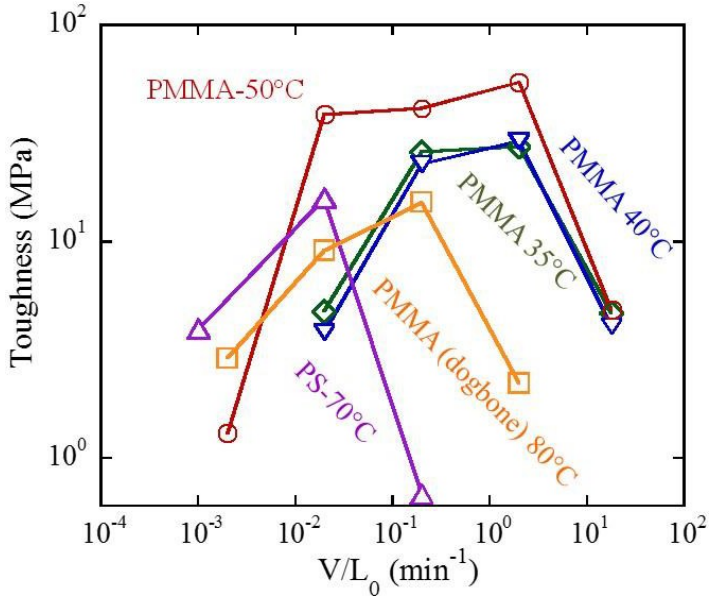

Figure 4.5 Toughness at different rates for extruded PS at 70 °C, extruded PMMA at three temperatures (35, 40, and 50 °C) and polished dogbone-shaped PMMA at 80 °C, evaluated from data such as those in Figure 4.3 and 4.4 according to $\int_1^{\lambda_{break}} \sigma_{engr}(\lambda) d\lambda$.

To thoroughly explore the extraordinary behavior, we also probe PS at different temperatures within the range of applicable extensional rate. Table 4.1 summarizes the results, where the data in the boxed row are from Figure 4.4 and the different colors (available online) designate the different responses, indicating respectively brittle fracture (BF) at the high rates – blue, ductile yielding (DY) at the intermediate rates – red, and dynamical or ductile failure (DF) at the low rates – violet. Reading "vertically", e.g., at V/L_0 = 0.2 or 0.02 min^{-1}, we see in Table 4.1 that as the temperature rises, the brittle PS first turns DF before becoming ductile. Figure 4.6 presents the actual stress vs. strain curves at three temperatures, corresponding to the data in the boxed column in Table 4.1. The phenomenon in Figure 4.6 refines the recently proposed depiction**Error! Bookmark not defined.** of the BDT in polymer glasses: At 90 ^oC PS can undergo plastic flow, i.e., showing DY. As the temperature is lowered, e.g., to 80 ^oC, the activation of the primary structure is accompanied by the increased chain tension. To the first order, we may regard the responses at 0.02, 0.002 s^{-1} in Figure 4.3 and at 0.001 s^{-1} in Figure 4.4 as well as at 80 ^oC in Figure 4.6 to be in the same category of DF. As the test temperature is lowered, the emergence of DF on the way from DY to BF is perhaps unsurprising. On the other hand, as the deformation rate decreases, how can polymer glasses turn from DY to DF, and what is the nature of DF?

Table 4.1 Stress levels at different temperatures and rates (PS)

T (°C)/ Rate (min^{-1})	0.001	0.02	0.2	2
90			24	
80	15	21	30	35
70	21	28	33	
60	24	34	37	
50	29	36		
17	40		42	42

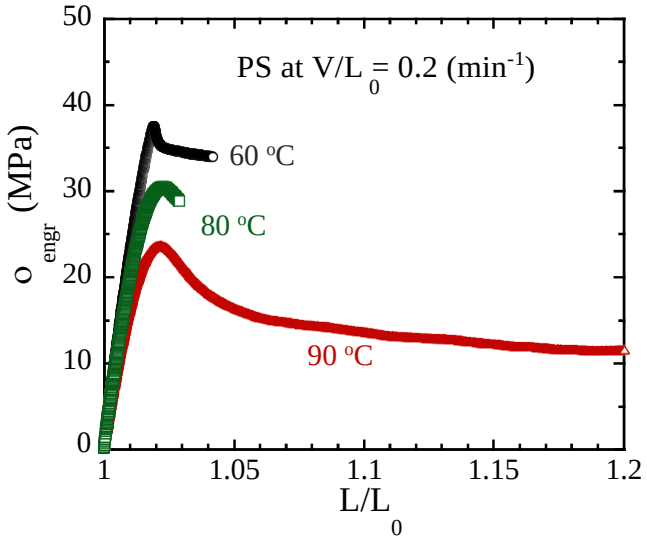

Figure 4.6 Engineering stress vs. the draw ratio from various tensile extension tests on PS at three temperatures, showing plastic flow at 90 °C, premature failure at 80 °C and typical brittle failure at 60 °C.

4.4.3 Mapping the Brittle and Ductile Behavior of Polymer Glasses

Before proceeding further, it is necessary to discuss the mechanism of ductile failure (DF). At certain temperature, e.g., 70 ^{o}C for PS or 35 ^{o}C for PMMA, as shown in Figures 4.3 and 4.4 respectively, when their extensional rate is sufficiently low, the polymer glasses lost their ability to undergo shear yielding or necking. During the apparent homogeneous extension, the tensile stress shows a leveling-off to a significantly low value. A close examination has revealed the appearance of crazes beyond the initial elastic deformation. These crazes randomly and uniformly populated within the extended specimen and grow in width as a function of the draw ratio L/L_0. In the zeroth order account,[26] brittle fracture (BF) occurs when the chain network breaks down as a result of a critical chain tension value f_{cp}. The fracture is perceived to occur spontaneously unlike an activated process that requires a hopping time. The DF seems to illustrate second scenario that the chain network can break down over time even if the chain tension stays lower than f_{cp}. In other words, at low enough rate, chain pullout could "nucleate" to cause a macroscopic breakdown of the chain network. Such a process is possible, leading to a sharp breakup of the specimen, coexisting with ongoing macroscopic plastic deformation.

We summarized the two methods to access DF, either by varying applied rate or changing temperature. The data in the row of 80 ^{o}C in Table 4.1 illustrates one method. As the applied rate V/L_0 increases, the response changes from DF to DY and then back to DF before reaching BF. In other words, DF is accessible at both low and relatively high rates, sandwiching a regime of DY. To understand such behavior, we pointed out that polymer glasses also encounter the state of DF as a function of temperature, as shown in

Figure 4.6. In short, at either very low temperature or high rate, where the polymer glass is brittle, it undergoes DF as the temperature rises or the rate lowers. There is insufficient buildup of chain tension and chain pullout could "nucleate" independent of the occurrence of global plasticity. Thus, as a function of temperature, it goes from BF to DF and finally to DY. In contrast, as a function of the applied rate, DF could re-enter. This re-entry is hard to predict and thus rather remarkable. Its occurrence implies that the ductile yielding (DY) behavior within an intermediate rate range is more special at the relatively low temperatures, e.g., 70 ^{o}C for PS and 35 ^{o}C for PMMA.

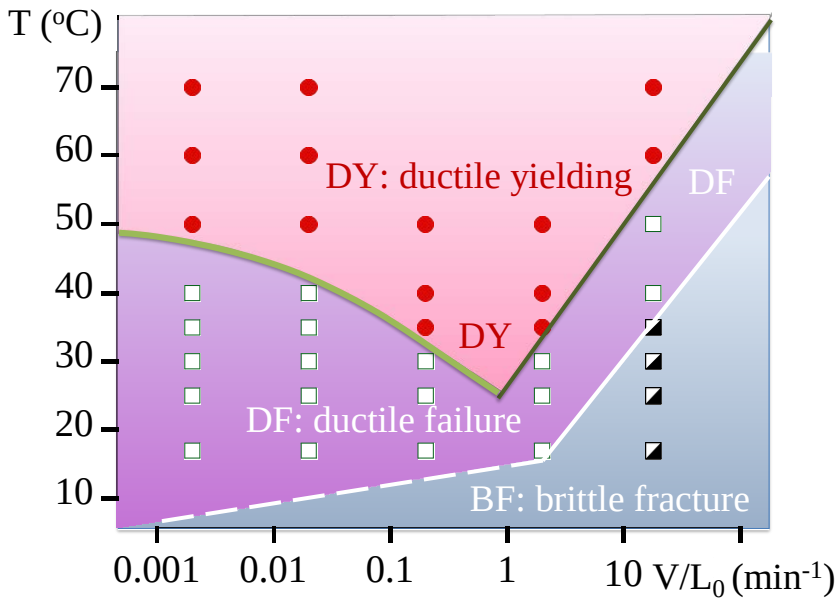

Figure 4.7 Diagram depicting the various mechanical responses at different temperatures T and rates V/L_0 for PMMA, showing the brittle fracture (dark blue color online) at low temperatures, the ductile failure at intermediate temperatures (violet color online) and the ductile yielding (pink color online) at high temperatures. With varying rate or temperature, PMMA shows BDT and passed through DF.

Finally, the rich phenomenology, extracted from the numerous experiments, as shown in Figure 4.7 can be represented in another insightful way. Plotting the peak tensile stress at different temperatures and various applied rates, we showed the transitions between DF and DY and between DF and BF in Figure 4.8, respectively.

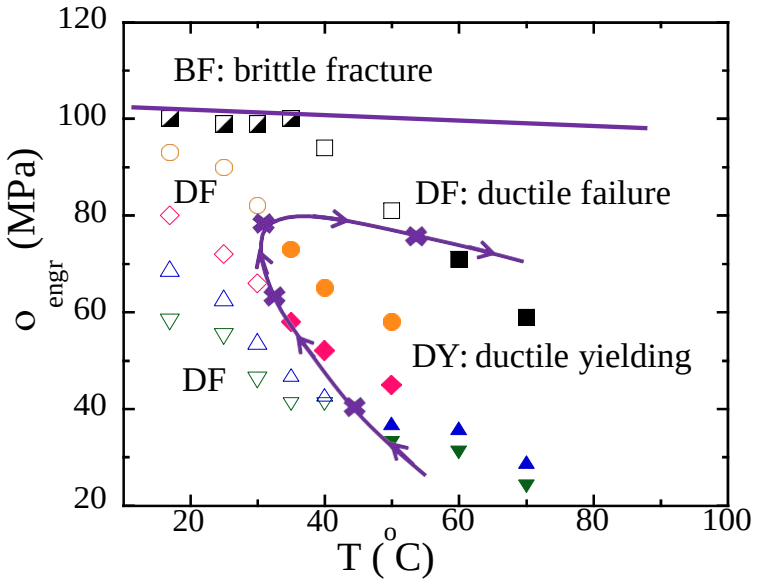

Figure 4.8 Either brittle stress or peak stress of tensile extension of PMMA as a function of temperature for different applied rates of 18 (squares), 2 (circles), 0.2 (diamonds), 0.02 (upward triangles) and 0.002 (downward triangles) min^{-1}. Inside the U-shaped region resides the ductile yielding. Above the near-horizontal line there is brittle fracture. Ductile failure occurs in the rest of the space.

The U-shaped purple (color online) curve is a BDT borderline dividing DF from DY, with the arrows in the curve indicating the direction of increasing rate. The transition between DY and DF first shifts to lower temperatures with increasing rate before switching the sense of directionality, going to higher temperatures with increasing rate.

The first part where T_{BD} shifts to lower T with increasing rate comes as a surprise and has not been explored previously to our knowledge.

In summary of sections 4.4.1 to 4.4.3, we have identified a remarkable phenomenon regarding the mechanical behavior of polymer glasses at large deformation: the mechanical response is ductile but turns brittle-like at a lower rate. Such unexpected behavior requires and inspires a new theoretical understanding. Clearly, beyond the recent zeroth order picture,[26] we must include the rate effect when depicting the BDT in polymer glasses. At lower rates, the chain network in polymer glasses can undergo structural breakdown over time even though the chain tension is not high to reach the threshold for spontaneous chain pullout. Therefore, at relatively low temperatures, there is only a fairly small window of rate where the primary structure can be fully activated to exhibit ductile drawing. Based on the extensive experiments at different temperatures and extensional rates, we have constructed two phase diagrams in Figures 4.7 and 4.8 to depict the borderlines between the various "phases" that are either ductile yielding (DY), dynamical/ductile failure (DF) or brittle fracture (BF). Although the diagrams are filled with quantitative information based on the behavior of PMMA, the general characteristics may hold qualitatively for all polymer glasses of high molecular weight. The phenomenon of re-entrant failure with respect to decreasing rate and the corresponding molecular-level explanation may have far reaching implications and consequences. For example, the idea that enhanced mobility always leads to improved toughness cannot be a universal principle[62], although a recent MD simulation study[67] identified the high mobility of nanofillers as a toughening mechanism for polymer nanocomposites.

4.4.5 Investigation into Dynamical/Ductile Failure (DF)

To further investigate the nature of dynamical/ductile failure, more experiments are carried out to test the hypothesis stated above. Before that, comparison between the 3 types of specimens will be demonstrated to answer a question related to the dynamical/ductile failure: why no dynamical/ductile failure has been reported before?

As reported in the literature[66, 68, 69] and our own experience, the specimens cut from film will show much higher brittle-ductile transition temperature. Cut dog-bone shape specimens of PMMA will experience brittle failure until the temperature is higher than 80 ^{o}C, whereas PS specimens are too brittle to show any ductile yielding in glassy state. In Figure 4.7, ductile failure can only be observed at a very shallow temperature range as narrow as around 20 ^{o}C. When the brittle-ductile temperature is high, it means the window of ductile failure will be covered by the normal brittle failure and then fail to be observed.

The brittle-ductile behavior is obviously different between extruded cylindrical specimens in the previous sections and the cut dog-bone specimen here. We believe the reason could be 1) the orientation of polymers at the surface of the extruded specimen; 2) cracks from cutting at glassy state; 3) the geometry. Further discussion is listed below.

Firstly, during capillary extrusion, the at-wall shear stress is highest around the extruding die cross-section and may cause the polymer at the surface to orient to the extruding direction, namely, the drawing direction. This enhancement and anisotropy may lead to more ductile behavior and may also be account for the arising of ductile failure. To eliminate this possibility, extrusion pressure was controlled in the linear at-wall stress regime, so there is no severe orientation effect.

Secondly, we conduct some microscopic study on the surface of these two specimens. Shown in the left photo of Figure 4.9, dog-bone shaped specimen cut from hot-pressed film showed uneven cutting surfaces, even can be observed with bare eyes. The right photo is the cutting surface (one of the two surfaces perpendicular to the paper at the side of the specimen) under microscope. After 100X magnification, cracks can be seen on the surface. Based on the fracture mechanism[55-57], the fracture stress is determined by the largest crack on the specimen. Therefore, the larger size of the dominating crack, the lower stress needed for fracture of the specimen. So the crack is considered as the main reason that why the cut dog-bone shaped specimen has a brittle-ductile transition temperature much higher than the cylinder specimen. Along with the effect that fracture stress is distinctly lowered, the tensile deformation at constant rate is poorly repeated with dog-bone specimen because of the uncontrollable cracks during the cutting process. On the contrary, cylinder specimen (Figure 4.10) can be prepared with clearly smooth surface.

To test the first two speculations, we make third type of specimens by polishing the cut dog-bone shape specimen with NOVUS 7136 Plastic Polish Kit until the side surfaces were smooth and transparent. The polished specimens, like the dog-bone specimens, are isotropic and free of surface orientation. After that, the polished dog-bone shaped specimens are tested by measuring the constant rate tensile deformation at different rates and temperatures, demonstrating their brittle-ductile behavior.

Figure 4.9 Photo of the dog-bone shaped specimen cutting from the hot-pressed film (left) and the side surface from microscope (right) perpendicular to the paper, with cutting direction from top to bottom. The specimen in the left is put under Carl Zeiss microscope with 10X eyepiece and 10X objective lens.

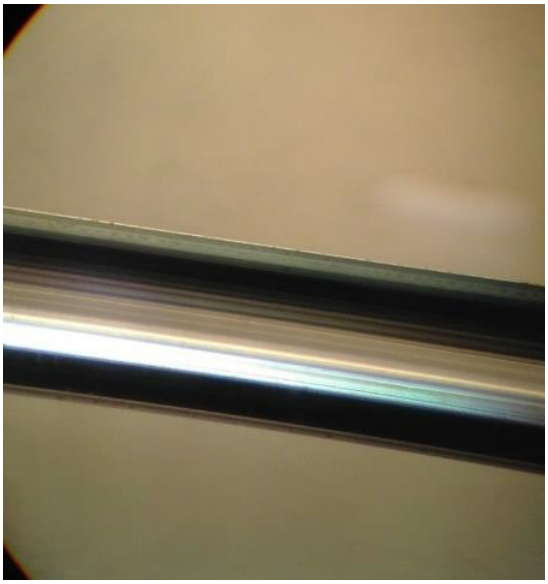

Figure 4.10 Photo of the extruded cylindrical specimen of PMMA under microscope

showing the smoothness of side surface of cylindrical specimen. The specimen is put under Carl Zeiss microscope with 10X eyepiece and 2X objective lens.

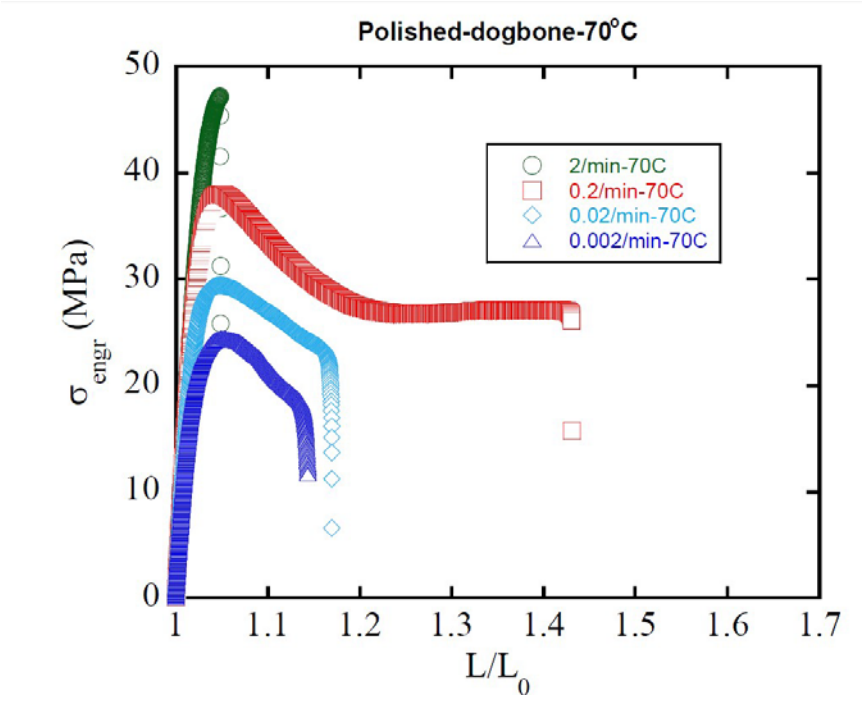

Figure 4.11 Engineering stress vs. draw ratio of polished PMMA dog-bone specimens at different initial rates (defined by V/L_0) at 70 ^oC, showing the brittle fracture (circles), the ductile drawing (squares) and the premature failure (triangles and diamonds).

The result in the Figure 4.11 demonstrates result of the polished specimens. At 70 ^oC, when deformed at high rate, such as 2/min, the specimen suffers a sharp brittle failure within a few percent of elongation compared to its original length. With deformation rate decreasing, ductile response occurs with the sign of the necking propagation after the yielding showing by the plateau of the stress from L/L_0=1.2 to L/L_0=1.4. This marks the brittle-to-ductile transition of the materials. When the applied rate further decreases to

0.02/min or 0.002/min, we see elongation decreases. This non-monotonic dependence of elongation on the deformation rate is similar to the result of extruded cylindrical specimens shown in Figure 4.3. The constant rate deformation is also applied to the polished dog-bone specimen at 80 ^{o}C. The toughness in this condition is plotted against rates along with the result from cylindrical specimens of PS and PMMA in Figure 4.5. The curve of polished specimen shows the same trend with the toughness increasing and then decreasing as the increasing applied rate.

We have shown that not only cylindrical specimens can undergo ductile failure. The arising of ductile failure with polished dog-bone shaped specimens ruled out the possibility that the ductile failure is caused by the anisotropy of extruded specimen. It also demonstrates that it is a universal behavior as long as the surface is smooth enough. This also proved Speculation **2** that the cracks from cutting on the side surface would make the specimen more brittle and show a lower BDT temperature. The regime of ductile failure and part of the ductile yield will be replaced by brittle failure if large cracks present. The results are the miss of ductile failure and a higher brittle-ductile transition temperature.

Finally, under the same condition, we still find that the brittle-ductile transition temperature of cylindrical specimen is dozens of degrees lower than the other one. The reason might come from the surface of extruded specimen, naturally free of scratches and surface imperfections, which is even smoother than the polished one. Besides, we think the difference in brittle-ductile transition temperature is also contributed from their geometry, where cylindrical specimen could be more resistant to failure than the dog-bone shaped specimen. No matter what is the molecular picture behind the brittle failure,

we believed fracture favors the “weak” places in specimen grow and propagate. Moreover, as it is often believed, the surface is always “weaker” than the interior of the specimen, because of the scratches and defects on the surface: at each point on the surface, only half of its surrounding is filled with material and the other half is void, while in the case of interior, it is all surrounded by the material. Therefore, when comes to the case of dog-bone shaped specimen, its middle part is a stripe, and the four edges of the stripe are even much “weaker” because only one fourth is surrounded by the material. However, in the case of cylindrical specimen, all the points on the surface is half filled by the material. In conclusion, by applying cylindrical geometry, the specimen will not suffer four fragile edges, which is expected to lower the brittle-ductile transition significantly.

After excluding the effect of anisotropy of cylindrical specimens and demonstrating the universality of the ductile fracture, we make hypothesis related to the nature of ductile fracture. However, before that, an important concept in the mechanical response of glassy polymer needs to be introduced, which has already been briefly mentioned in section 4.2.1.

The crazing behavior was first recognized more than 30 year ago. The first and continuing used methods to investigate crazes were optical interferometry[70-72]. From the research based on the optical microscopy, the principles of crazes were revealed: 1) crazes can grow all over even across the specimen and the specimen remains the ability to undergo ductile deformation; 2) crazes grow perpendicular to the principle stress during tensile deformation. As shown in Figure 4.12, crazes can be centimeters in length 3) Crazes show different refractive index from bulk part of specimen, which is also the

origin of whiteness of craze. Those studies indicated the crazes are load bearing and have different density compared to the bulk.

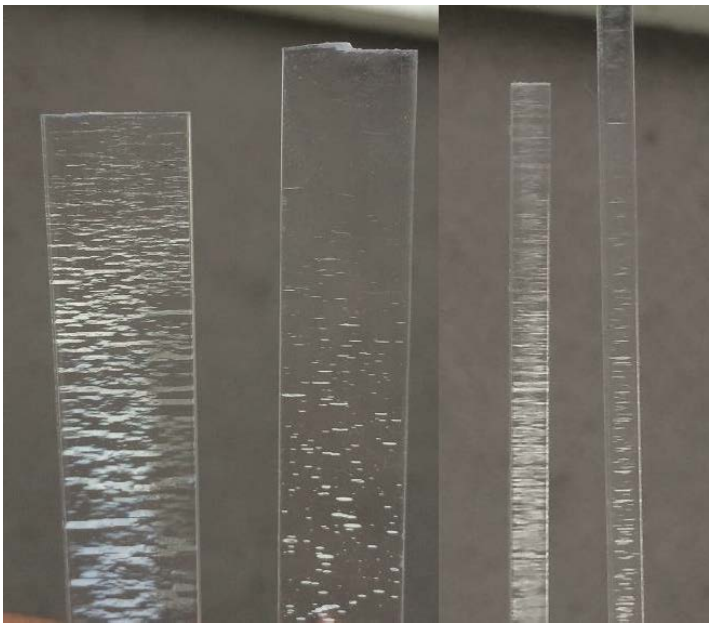

Figure 4.12 Photos of crazes in the PS specimen (left) and it side view (right). Injection molding PS specimens were drawn at constant rate (V/L_0=0.1/min) at room temperature. The specimens are drawn to a few percent of deformation before fracture.

Later on, a detailed internal structure of crazes was discovered by the work of Kambour[73-75]. Crazes are special micro cracks that have fibrils inside. The fibrils are oriented perpendicular to the craze-bulk interface and aligned with principle stress. They are extended to maximum length, hold the structure of craze and play the role of load-bearing. The space between adjacent fibrils is filled with voids, so the crazes are lower in density than the bulk and optically opaque in color.

More recent work from Kramer[44, 76-78] made deeper investigation into the

mechanism of craze. Briefly, crazes are always initialed at the site of defect through local plastic deformation. Then the void arises to release the stress. At the stable stage of craze propagation, the growth of craze will only occur at the tips of craze, which means the width of craze would remain constant during this stage. The widening of craze occurs when the fibrils inside the crazes fail due to entanglement lose and lead to the failure of craze.

After addressing the concept, we introduce our speculation that, the nature of ductile failure is through the failure of crazing. Reasons are listed below:

1) PMMA and PS are polymers known to favors crazes. As shown in the insert in the Figures 4.3 and 4.4, whiteness due to crazing can be seen in specimens.

2) Crazing, as an activation process in nature, are demonstrated to be favored at high temperature[79]. However it fails in the competition with shear yielding[77]. When temperature is high enough, crazing response turns into shear yielding. It fits the trend in Figure 4.7, where the region of ductile yielding always stays above the ductile failure region as increasing temperature.

3) Shown by the work of Plummer and Donald[80], the onset deformation strain of crazing decreases with decreasing rate. This is to be expected, because of the activation nature of crazing. This also fits the trend in Figures 4.3 and 4.4, where ductile yielding turns to ductile failure with decreasing rate, if ductile failure is caused by crazing.

Based on the low density, plastic deformation and other features of crazing, several experiments are conducted to test our speculation. Firstly, the density of several specimens after deformation is measured by KBr aqueous solution. Three cylindrical specimens of PMMA were selected specimens as representatives. They were firstly

deformed at 40 ^{o}C at deformation rate 0.002/min, 2/min, 20/min, respectively. These three specimens showed mechanical response of ductile failure, ductile yield, and brittle failure during the deformation. Then a density against weight concentration curve is plotted and fitted based on the chemistry handbook[81], as shown in Figure 4.13. 15 mL of KBr-water solution is prepared, whose density calculating from the fitting curve is 1.2 g/cm^3. The solution is divided into three 20 mL vials. The weight of the vials and solution were carefully measured. A one-centimeter-long piece of stem was cut from the center of each specimen and weight. Starting with the stem from ductile yielding sample, it was put into one of the vial. The stem would float if its density is lower than the solution. If so, water would be added into the vial drop by drop and the solution would be shacked well after each drop. The procedure continued until the stem suspended in the solution (Figure 4.14). In this condition, the stem was considered to have the same density as the solution. Then weight of the diluted solution was measured, and its density was calculated according to Figure 4.13. Densities of the other two deformed specimens were measured in the same way.

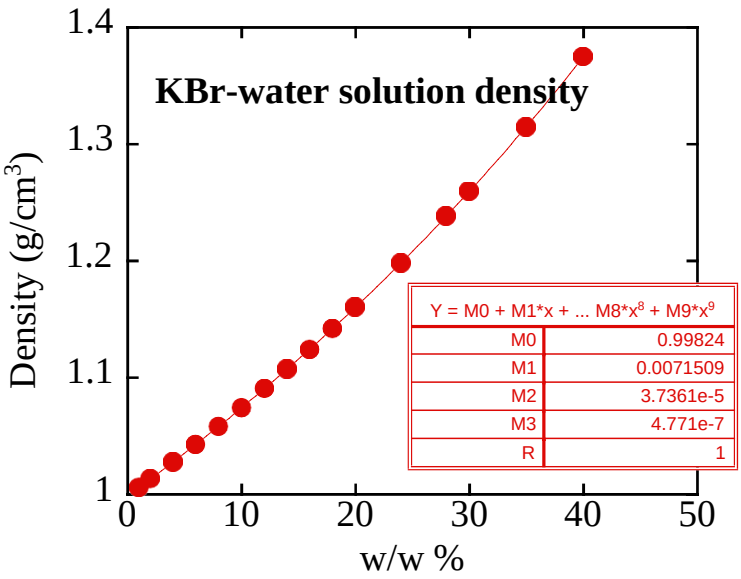

Figure 4.13 The relationship between density and weight concentration of the KBr aqueous solution. Dots were plotted from the chemist handbook[81] and the curve is fitted from dots. Inserted table is the polynomial fitting parameter of the curve. R = 1 stands for an ideal fitting.

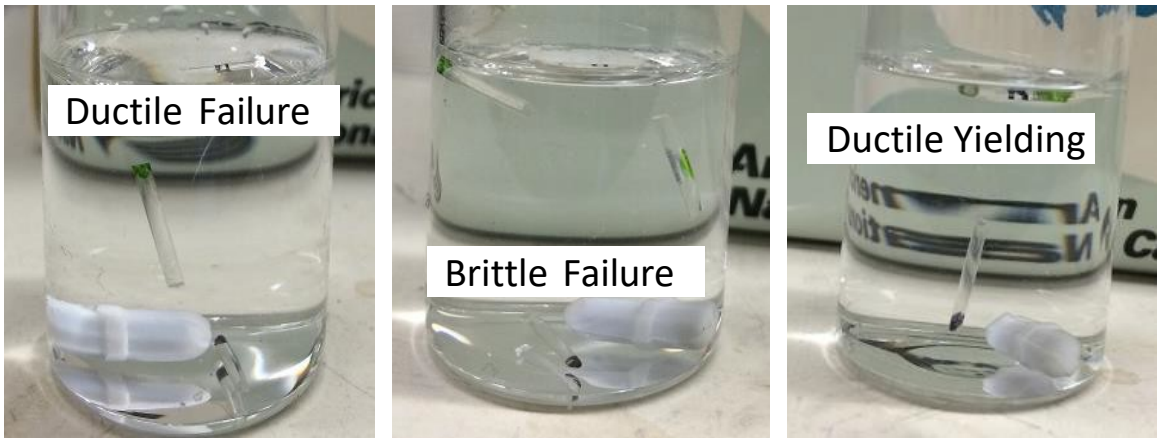

Figure 4.14 Photos of stems suspended in the KBr aqueous solutions. The suspend condition indicates the stems have the same density as the solutions. Density of the samples increases from left to right.

The result shows the ductile failure specimen has the lowest density (1.1802 g/cm^3) in three deformed specimens, followed by brittle failure one with density of 1.1805 g/cm^3 and ductile yielding one with density of 1.1827 g/cm^3. The lowest density of ductile failure sample is consistent with the observation that many crazes are seen over the sample undergoing ductile failure, because as mentioned above, crazes are lower in density than the bulk.

The objective of second experiment is to verify whether there is plastic deformation associating with crazes. Unlike the elastic deformation storing energy, during plastic deformation, the work done is transferred into heat and elevates the temperature of sample. Therefore, the temperature increment can be considered as the sign of plastic deformation. The condition for test is cylindrical PS specimen draw at rate of 2/min at room temperature. Stress behavior against time is shown in Figure 4.15. Similar figure of "tailing" of stress curve (plateau after stress maximum) before ductile failure can also be seen at Figure 4.4. Although this "tailing" can be easily mistaken as the normal stress plateau during necking fronts propagation, there are enough reasons to believe it is not. Firstly, the turning points before "tailing" in Figures 4.15 and 4.4 (square) have different curvature from the curve of ductile yielding (triangles) in Figure 4.4. Secondly, during the "tailing", the sample does not show any visible strain localization or necking fronts; on the contrary, the sample is uniformly deformed accompanied by decreasing density.

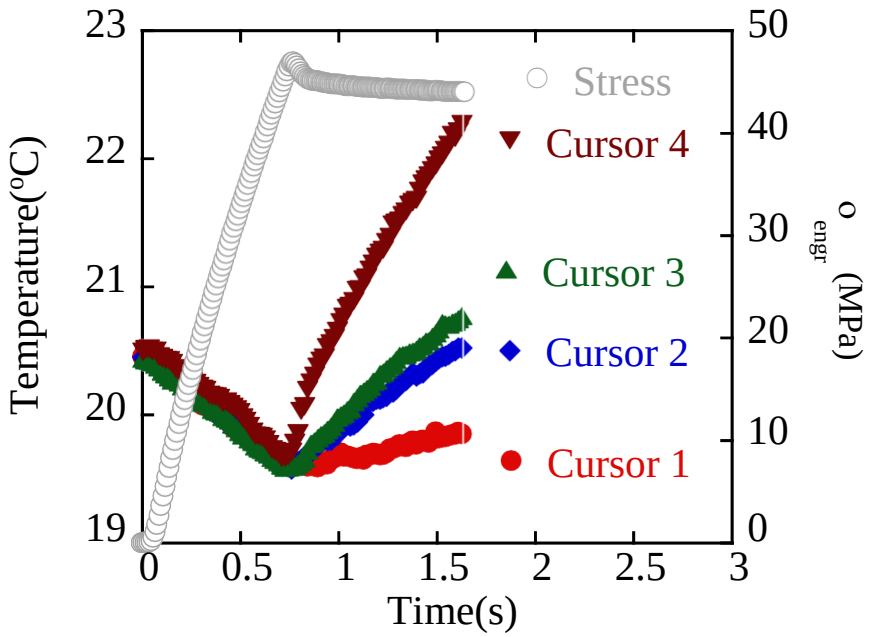

Figure 4.15 Engineering stress vs. time curve during tensile deformation up to failure (open circles) and the corresponding temperature vs. time curves at various positions on the sample (filled symbols). Positions are marked in Figure 4.16.

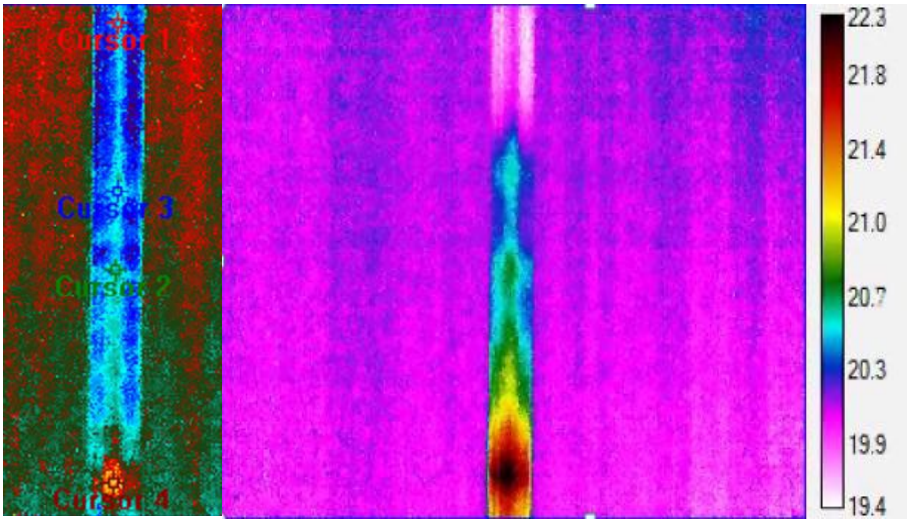

Figure 4.16 IR camera image showing the position of 4 temperature detector cursors (left) and snapshot at 1.5s when the sample is ready to break (right).

Everfocus EQ250 IR temperature camera is used to record the sample during its deformation. The data is analyzed with FLIR ExaminIR PRO. 4 cursors are put in the image to track temperature at different positions during the tensile deformation (Figure 4.16, left). Cursor 4 is put at the position where failure eventually takes place. Cursor 1 is put farthest from the failure site. Cursor 2 and 3 are put in between. The corresponding temperature of these 4 positions is plotted against time together with stress curve in Figure 4.15. From the result, we notice that before the turning point, the temperature of the sample decreases with increasing elongation. This can be explained by the work from Lin[82]. In the regime of linear response (the first few percent of deformation), the response is elastic, which means the work done is stored in the sample. However, the work done to the sample is less than the energy build-up in the sample, so based on the first law of thermodynamics, heat is transferred and leads to the decreased temperature of the sample. After stress reaches maximum, shown from Figure 4.15, the temperatures at 4 positions all increase. As contrast, in the case of shear yielding which is macro-scale plastic deformation, the IR image would show a sharp transition between necking front and the rest, where the necking front show a significant higher temperature than the surrounding. This higher temperature region moves along the sample as the necking front propagates. In the “tailing” process, as shown in the right photo in Figure 4.16, no figure of necking front can be found. The heating region (colored in deep red) does not move during the deformation, which further proves the physics behind the “tailing”: something other than shear yielding. In this “tailing” process, as shown in Figure 4.15, the temperature of the whole sample increases but not uniformly. This indicates the energy

dissipative plastic process occurs on whole sample but concentrates more on some area. At the end of “tailing” process, ductile failure takes place at the site of highest heating region, where should be crazes most concentrate at. In addition, during the deformation, no macro-scale strain localization can be observed.

The observation from IR camera fits the speculation that crazes play important role in the ductile failure process, further indicating the concentrated crazes may facilitate ductile failure. When deformation of the sample reaches the limit of linear regime, crazes arise leading to the release of stress, which will show up as the turning point and following stress plateau on the stress-time curve. Since crazing propagates through plastic deformation at craze tips, the process would release energy and result in temperature increase of the sample. Unlike shear yielding which is macro-scale plastic process, craze propagation as a micro-scale plastic deformation taking place all over the sample, result in temperature of the whole sample increased. However, temperature may not increase uniformly along the sample. Just like brittle failure, crazes will localize at “weak” sites of the sample, aggregate and eventually lead to ductile failure.

The last experiment provides direct proof of aggregation of failed crazes leading to the ductile failure. Polished dog-bone shape specimens of PMMA were deformed at 70 ^{o}C at different rates, stress-strain behavior of the samples has been discussed at the beginning of this section. As shown in Figure 4.17, when the specimen is deformed at high rate such as 2/min, the specimen suffers a sharp brittle failure. With deformation rate decreasing, the response turns from brittle failure to ductile yield at rate 0.2/min When the applied rate further decreases to 0.02/min and 0.002/min, samples break though ductile failure. The samples deformed at 2/min, 0.2/min and 0.02/min are investigated

with Carl Zeiss microscope on the condition of 10X eyepiece and 10X objective lens after ultima failure. The sample deformed at 0.002/min is investigated with 3.2X objective lens for the best result.

Except for the sample deformed at lowest rate, the microscope photos show the edge of the failure site. Photos are taken from the view as Figure 4.9, which means the surface shown in the photos are part of length-width plane. The left part of each photo is void, and the right part is one of the two broken halves of the sample after failure. With the draw direction marked in the photo, we notice, as expected, direction of crazes shown in the middle two photos grew perpendicularly to the draw direction. When the rate is as high as 2/min, the sample suffers brittle failure and leaves a sharp brittle site but no crazes on the sample. When deformed at 0.2/min, the sample yields and is stretched to more than 1.4 time of its original length before any fracture, as shown in the photo. Shallow and thin crazes can be observed all over the sample, except for crazes at the edge which are clearly deeper. This proves the speculation we mentioned at the beginning of chapter 4.4.5: edges of stripe sample are “weaker” than the surfaces. In this case, sample undergoes ductile yielding in presence of crazes, demonstrating that crazes will not necessarily lead into failure. As the applied deformation further decreases to 0.02/min, the sample goes through ductile failure. Shallow and thin crazes similar as the ones on the ductile yield sample can be observed along with large cavities. There are also crazes with half-open cavities, indicating the large cavities are failed crazes with the internal structure broken down. In the structure of integrated craze, fibrils link the two craze-bulk interfaces, bear the stress, hold the structure and prevent the craze from widening. When the fibrils fail, crazes are forced to open by external deformation and form the large

cavities. Unlike crazes, cavities are unstable cracks that trigger failure. As shown in the photo, at the edge of the sample or in the middle, there is a large cavity, half of which is missing, indicating the fracture of the sample take place though the cavity.

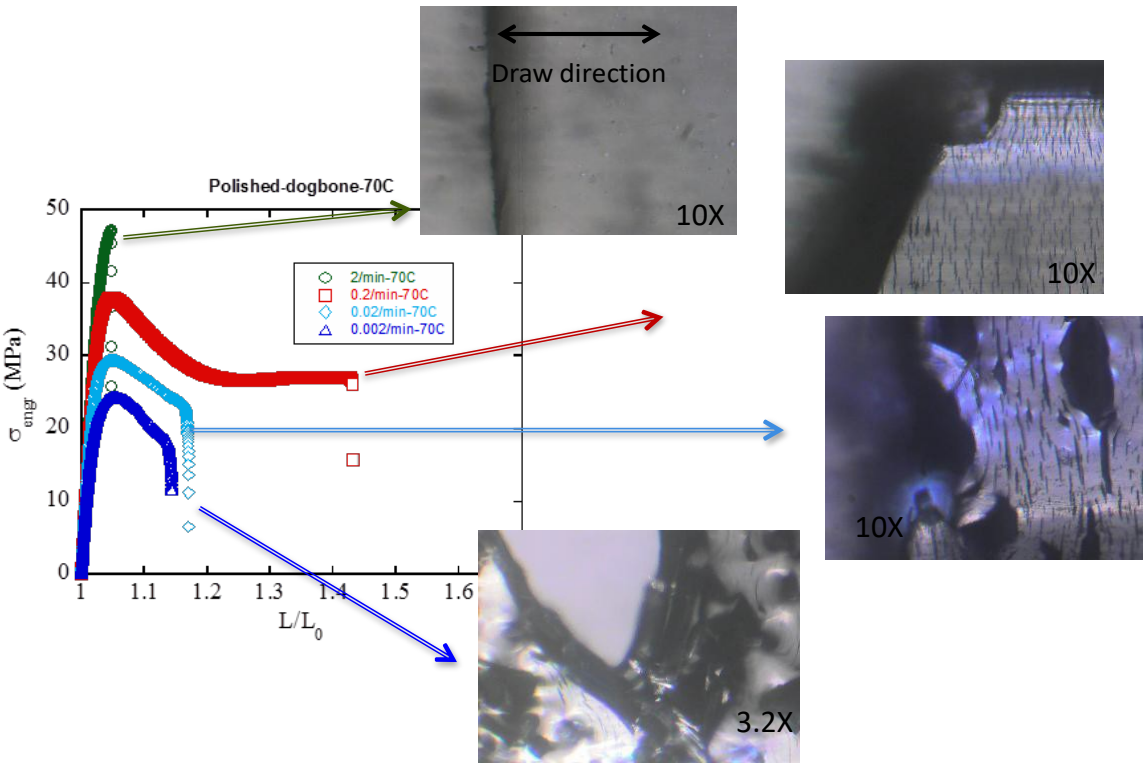

Figure 4.17 Engineering stress vs. the draw ratio from various tensile extension tests at the different initial rates defined by V/L_0 for PMMA at 70 ^oC. It shows the brittle fracture (circles), the ductile drawing (squares) and the ductile failure (triangles and diamonds). Corresponding sample images under microscope with 10X eyepiece. Magnification of objective lens are marked in each photo.

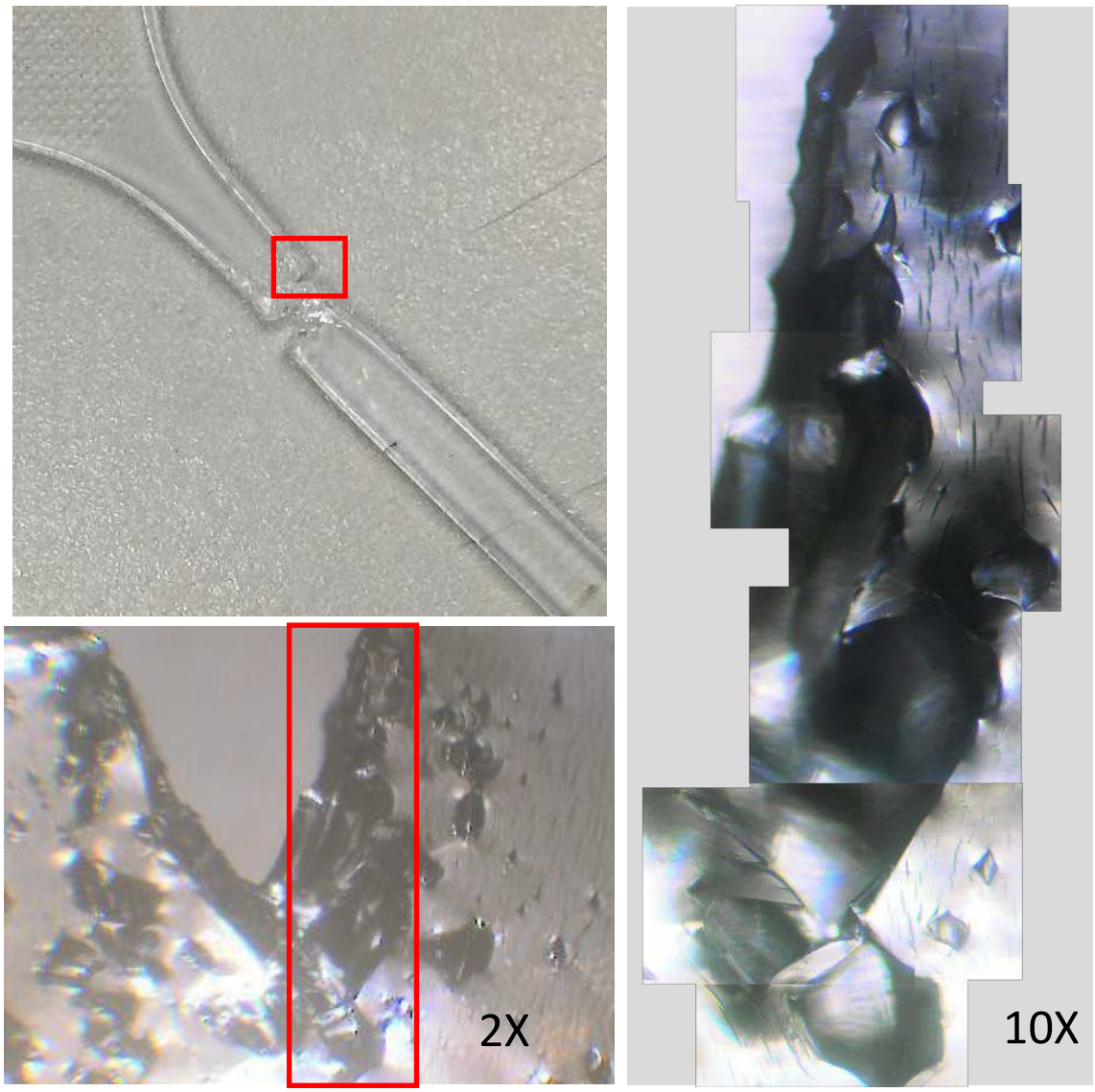

Figure 4.18 Photo of polished dog-bone shaped sample of PMMA after tensile deformation at rate V/L_0 0.002/min (top left), microscope photo of the crack marked in red frame of the top left photo, taken under 10X eyepiece and 2X objective lens (bottom left), microscope photo of the crack marked in red frame of the bottom left photo, jointed by 8 microcopy photos taken 10X eyepiece and 10X objective lens (right).

The sample drawn at the lowest rate 0.002/min fails at similar elongation as the one deformed at 0.02/min. This means, even the stress response between the two samples is in the same order, the sample drawn at the lowest rate is deformed for a period of time that is ten times longer. Therefore, it is to be expected that there would be more craze on the sample drawn at the lowest rate. The top left photo in Figure 4.18 shows the sample after deformation. Contrast to the sharp failure surface of the sample deformed at 2/min, the failure site of this sample is rough even by bare eyes. The crack region framed by red rectangle in top left photo of Figure 4.18 is investigated with Carl Zeiss microscope with 10X eyepiece and 2X objective lens (Figure 4.18 bottom left), 3.2X objective lens (Figure 4.17) and 10X objective lens (Figure 4.18 right), respectively. From the microscope photos taken with 2X and 3.2X objective lens, large cavities can be found, which excess the ones in the sample drawn at higher rate in terms of number and size. These large cavities are also failure crazes. On the right and left side to the framed region of photo taken with 2X objective lens, series of cavities jointed together can be found and form larger cavities. The direction of these jointed cavities is perpendicular to the drawn direction and parallel to the macroscale crack (red framed, in the middle of the photo). Based on the roughness and discontinues curvature of the macroscale crack, it is to be expected that the failure also forms by jointed cavities. With 10X objective lens, the detailed structure of the red framed area can be observed (Figure 4.17, left). On the right side and bottom of the photo, several cavities can be seen. Compared to the olive-shape cavities in Figure 4.17, these cavities are widened and have rhombus shape. In this microscope photo, it is clear that the rough and discontinues curvature of the edge is formed by connected cavities and some craze tips can still be found on the edge. This

confirms that ductile failure is caused by aggregation of failed crazes.

To briefly summarize this section, the microscope phenomenology of three different mechanical responses is distinguish different. Sample will undergo brittle failure when deformed at high rate, and the failure sites are sharp. When sample ductile yields at medium rate, crazes will grow but will not cause the sample broken. Finally, when the applied rate is low enough, time allows the internal fibrils structure to fail and cause crazes to open. These crazes without load-bearing fibrils structure are pulled open by principle stress and form cavities. As cavities grow bigger with deformation, they merge and connect together and at last form crack which will lead to failure of the whole sample. This process of crazes-caused ductile failure is proved by the density of samples and IR tests.

4.4.6 Our Proposal of Understanding Based on the Molecular Picture

As we demonstrate that the mechanical response of polymeric glass is a complicated combination of ductile yielding, brittle failure and ductile failure. The physics behind these three responses are different but related. As mentioned above, a lot of work has been done trying to explain the mechanical response of polymeric glass, like shear transformation zone theory[83] to explain yielding and plastic deformation or Ludwik[16]−Davidenov-Wittman[17]−Orowan[18] (LDWO) theory to explain transition of brittle failure and ductile yield. However, neither of these theories nor the theories we mentioned in section 4.2.1 can fully explain this kind of rich phenomenology. So, based on the new investigation into the nature of ductile failure, we propose our own physical model.

Under deformation, some strands are load bearing and some are not. Naturally, the load bearing strands participate as units of load bearing network. We consider the polymeric glass as a hybrid of this network and the rest redundant part called primary structure. When deformation is applied to the system, network holds the integrity of the specimen and acts like a proactive role to “push” surrounding primary structure to climb over their energy barrier. This “pushing” process is also named as “activation”, because the mobility of primary structure segments is increased in orders during this process. In the meantime, the load or tension in load bearing strands increasing with increasing deformation. When all the primary structure segments are fully activated, the system will yield and undergo plastic deformation. However, if the tension in load bearing strands is so large that excesses the threshold before the primary structure fully activated, chain pull-out takes place leading to the failure of load-bearing network and failure of the sample. This explains the transition of brittle failure and ductile yield. When the temperature is high, the activation process is easier with a shallower energy well. When the rate is low, there will be more time for the activation to take place before the load-bearing strands pull-out. Hence, as confirmed by the experiments, brittle failure will turn to ductile yield when temperature increases or the rate decreases.

When crazes in presence, the fibrils inside are stretched to maximum and hold the structure of crazes. To be expected, the load bearing fibrils are close related to load-bearing network, although the relationship is still needed to be investigated. The most reasonable speculation is fibrils contain at least one of load-bearing strands. Because strain localizes severely in the crazes and the fibrils are extended to its maximum, the fibrils are under higher tension than the rest of load bearing network. When the specimen

is deformed slow enough in the present of crazes, load bearing strands in the fibrils are given sufficient time to be pulled out even though the tension in the rest of network is still low. This would cause the crazes to fail and be pulled open into cavities. As cavities grow bigger with deformation, they merge together and form cracks which will lead to failure of the whole sample. This is the nature of ductile failure. So as experiment shows, the lower the rate the easier ductile failure will arise.

In short, the competition between the activation of primary structure and pull-out of load bearing strands with or without the present of crazes results in the phase diagram that describes the rich phenomenology of mechanic response dependence of rate and temperature.

CHAPTER V

THE ORIGIN OF STRESS

5.1 Introduction into Molecular Dynamic simulation

The computer simulation is a powerful tool because of its ability to show the assembly process, structure of the molecules and the microscopic interaction[84]. It builds a bridge over the 10^6 in scale between the laboratory experiment scale (~millimeter) and the molecular scale (~nanometer) and allows us to explore the link between macroscopic properties and microscopic interactions. It also shows the ability to test a theory directly, due to its access to precise structure of the molecule assemblies and the interactions in the system.

Among all of the molecular dynamics, there are two main categories: Molecular Dynamics (MD) and Monte Carlo (MC). MC technique [85] is a kind of computer algorithms that relies on repeated random sampling to obtain the assembly possibilities of the system. Basically, it uses repeat random moves whose possibility is controlled by the energy state. MC is mainly used in three distinct problem classes: optimization, numerical integration, and generating draws from a probability distribution. Unlike MC, MD[86-88] is a kind of computer simulation technique used to study the physical

movement of atoms and molecules. The atoms and molecules in MD will interact with each other at a fixed period of time, and this interaction is calculated by a given force field. Therefore, it can show the dynamic evolution of the system. Generally, the force field is designed based on the interatomic potentials or the molecular mechanics. The movement of atom or molecule during a finite short time step will be calculated numerically by solving Newton's equations of motion and the position will be updated for this atoms or molecules. New movement during the next finite time step will be calculated by the updated coordinates just obtained. This process will be repeated to and thus an evolution of the physical movement of the system can be obtained.

In this work, MD simulation, rather than MC, will be used. Because MD can show the dynamic evolution, time-dependent responses and rheological properties. And these three advantages are the keys to reveal the microscopic interaction generating macroscopic mechanical responses, which is essential in this work. More specifically, the aim in this chapter is using MD simulation to investigate the microscopic interactions in polymeric system that responses to the deformation-induced mechanical stress.

5.2 Decomposition of Stress

When deformation is applied to a piece of polymeric glass, stress arises. There are two types of interactions related to this responsive stress in polymeric glass system: the interaction between atoms that bonded by chemical bonds, angles or dihedrals and the interaction between the atoms of different segments (Figure 5.1). During the deformation, chains in the polymer specimen will be deformed and not keep the same configuration as their original state. The relative position change of bonded atoms causing interactions

within a segment changes. In a polymeric glass, bonded interaction includes bond stretching, angle opening, distortion of the dihedral, configuration altering of chain, etc. The arising stress due to these interactions is defined as intra-segmental stress. On the other hand, the relative positions between non-bonded atoms shift, which will cause the interaction between non-bonded atoms changes and produces an arising stress as well. This kind of stress is defined as inter-segment stress. Inter-segment stress mainly due to Van der Waals force exists between segments that belongs to different chains or the same but not directed bonded. It may also come from H-bonding, electrostatic force or other interaction if they are present. However, in this work, among all the inter-segmental interactions, only Van der Waals interaction is considered due to the chosen model described in the following section 5.4.1.

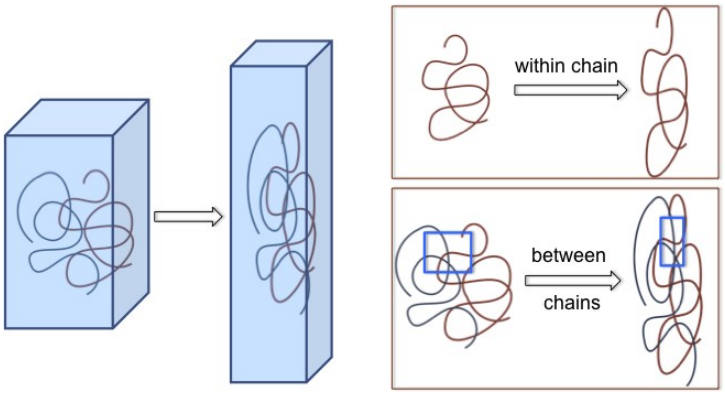

Figure 5.1 Alteration of inter- and intra-segmental interaction during deformation of a polymeric system. Light blue cuboid represents a piece of glassy polymer, and red and blue curves represent two adjacent chains in the piece.

Inter- and intra-stress contribute together to the total stress that is shown in the stress-strain curve. However, the debate about the dominating contribution is still going.

The classic Eyring model[15] and new theory from Schweizer[11-14] share the same assumption that stress is only from inter-segment. 8-chain model claims stress comes from the restriction of segmental rotation and configurational entropy of molecular alignment, which means only intra-segmental interaction contributes to the total stress. Although all the models can predict the stress-strain behavior in a certain range, they are, in fact, built based on different understanding of the origin of stress.

Identification of the origin of stress is not only valuable in academic study, but also shed light on industry application. The intra-segmental and inter-segmental interaction is expected to response to deformation and temperature differently. In addition, they have different dependence on molecular weight. A deep understanding of such mechanism should be achieved to design new material and improve the prosperities of existing materials.

Experiment is not a great solution to answer this question. There's no obvious feature can be used in experiment to directly and simply distinguish the contribution from intra-segmental and inter-segment to the stress. However, it is rather easy to obtain such information from MD Simulation. The stress contribution from inter-segmental and inter-segment can be calculated directly based on the force field and coordinates of the atoms. For example, in this work, based on the model, stress contributed from bonds, angles and dihedrals are calculated as inter-segmental stress, while the stress contribution calculated from non-bonded interaction (Van der Waals) is defined as inter-segment stress.

5.4 Simulation

5.4.1 Coarse-Grained Model of Polystyrene

Although the method to distinguish the intra-segmental and inter-segment contribution to stress is relatively clear using MD simulation, the choice of model is crucial to obtain correct and precise result.

In MD simulation, a model is a digital prototype of a physical system to predict its performance in the real world, usually including molecular structures and a force field defining bonded interaction and non-bonded interaction between atoms and beads. The model can only mimic the real system to certain degree. The lower degree of freedom in simulation or any missing details would always cause a deviation from the real system. More detailed the model is, the more accurately it would simulate the real physics system. At a given computational resource, this accuracy can only be achieved at the cost of efficiency. Three categories of the models are mostly used in polymer simulation: atomistic models, coarse-grained models and bead-spring models, with the trend of increasing efficiency but decreasing accuracy.

Atomistic models, or called all-atom models, are the most detailed models used in polymer simulation. Molecules are represented with beads where one of each represents a real atom. The atomic beads are connected by chemical bonds. Force field of atomistic simulation can describe bond stretches, bond angle bends, torsional rotations, non-bonded interactions and other detailed interaction like hydrogen bonding. In all-atom models, there is one-to-one correspondence between the real atoms in a molecule and the beads. Therefore, bonds in this system are real chemical bonds. In this way, atom-level accuracy can be achieved in atomistic model, but the computational calculation required to support this accuracy is huge, which makes it suitable for simulating small system in a short time. However, a long chain polymer system like 500-mer PS system used in this work, is

impossible to be simulated with all-atom model limited by the computational resource. Because the relaxation time to equilibrium a polymer system increases with molecular weight, the system size also (chains contained in the simulation box) need to increase with chain size to avoid self-entanglement across the box boundaries. These two reasons make it nearly impossible to equilibrium a long chain polymer system using all-atom system.

Coarse-grained models are simplified all-atom models[89-91]. A group of several atoms is represented by one bead so that the calculation can be greatly simplified, and this method can reach a much higher efficiency. In this method, the structure of molecules and the force field preserve the chemical specificity, where force field can be mapped by matching either atomistic structural features (bottom-up) or directly macroscopic properties (top-down)[92]. Besides, to utilize both advantages from bottom-up and top-down strategies, more and more coarse-grained studies (like the model used in this work) are choosing a hybrid approach, i.e., combining both bottom-up and top-down strategies together[93-96].

Bead-spring model was developed by Kremer and Grest at 1990 year[97]. It is general for all polymer chains. In this model, polymer chains are represented by one single type of beads connected by one single type of springs. Unlike atomistic model or coarse-grained models, bead-spring model has no chemical specificity and use no real units. Also, one bead in bead-spring model does not necessarily represent one atom, and one bond does not represent one chemical bond, either. The way bead-spring model connected to the real physical system is to map chemical species into the model. In this way, bead-spring model can be roughly applied into varies species of polymers, so that

one bead can represent one repeat unit or more. However, overall bead-spring can only be a model to study the rheology behavior of polymer in a general way. One bead can only represent a specific group of atoms or more means that the one bond in this model may represent a mix of several chemical bonds, angle torsions and Van der Waals interaction between atoms. As the aim of this work is to distinguish the intra-segmental and inter-segment contribution to the stress, bead-spring is not the proper choice.

Based on the discussion above, by considering efficiency, accuracy and limitation of each model, coarse-grained type of model is chosen to be used for this study.

In this work, a coarse-grained model of atactic PS developed by Keten's group[98] is used. One repeat unit of PS is represented by two different beads: one bead for backbone and the other one for side group. The backbone bead is located at the backbone carbon directly bonded to the phenyl ring and represents the combination of -CH- group and half of each adjacent methylene -CH_2- group. The side bead represents the phenyl ring and is located at the center of mass of phenyl ring.

In this model, the force field includes both bonded potential and non-bonded potential. The bonded potential parameter is determined by a bottom-up strategy aiming at replicating the local structural characteristics of the atomistic system, and the resulting potential is optimized to match the according atomistic bonded distributions using the Iterative Boltzmann Inversion (IBI) method[90, 99]. Another interaction, the non-bonded interaction, is tuned top-down aiming to match experimental density, experimental T_g and the elastic modulus from uniaxial extension. A parametric full factorial Design of Experiments (DOE)[100] is used to evaluate the major effect of the respective parameters on non-boned force field and optimize their values.

The bonded interaction in this model includes bond stretching, angle opening and dihedral torsion. The stress contributed by these three bonded interactions is summed up as the intra-segmental stress. Although the entropic force coming from the configuration change of the chains should be included, we argue that the this contribution is not important in glassy state for two reasons: a. ergodicity is essential for entropic stress to show up but it cannot be achieved in glassy state; b. even if the entropic stress exists in glassy state, the stress level from entropic contribution (which is rubber elasticity) is sufficient low (several MPa compared to hundreds MPa yield stress) and can be ignored.

Based on the force field, the stress contributed from the non-bonded interaction, in the form of GROMACS style LJ potential with inner cutoff 12 Å and outer cutoff 15 Å, is counted as the inter-segment stress. The inter-segment part of stress is contributed from non-bonded interaction between beads in different chains and beads from the same chain but more than 2 bonds away. The former possibility should be dominating during the process because: a. for beads, the closet packing layer is realized through either covalent bond linkage or from another chain; b. the possibility of non-bonded beads from the same chain interacting with each other is limited because of the cutoff.

5.4.2 Simulation Protocol

All the simulations were performed using the LAMMPS simulation package[101]. A system contains 500 PS chains with each 500-mers (1000 beads per chains) and is generated at 550 K by randomly distributing the PS chains in a periodic box. A C++ code is written to do this job and outputs the coordinates in the format of LAMMPS data file. The initial coordinates are generated chain by chain and bead by bead, following the

steps below:

1. The size of cubic simulation box is calculated based on the density of system at 550 K.[98]

2. The first backbone bead of a chain is randomly put in the simulation box.

3. A second backbone bead of a chain is randomly presented in the simulation box with meeting the requirement of $r_{12} = l_0$, where r_{12} is the distance between first and second bead and l_0 = 2.568 Å is the equilibrium bond length from the backbone bond potential $U(l) = k(l - l_0)^2$. [98]

4. A third backbone bead of a chain is randomly presented in the simulation box with meeting two requirements: a. $r_{23} = l_0$, where r_{23} is the distance between second and third bead; b. θ_{123} is randomly set between 120°to 180°, where θ_{123} is the angle between 1-2-3 beads. According to the force field, there are two stress minimum values in backbone angle potential, corresponding to ~125° and ~170°, respectively. The energy barrier between is low to be easily overcome by thermal motion. [98]

5. A forth backbone bead of a chain is randomly put in the simulation box in the conditions： a. $r_{34} = l_0$, where r_{34} is the distance between the third and forth bead b. θ_{234} is randomly set between 120°to 180°, where θ_{234} is the 2-3-4 angle. c. ϕ_{1234} randomly distributed between 120° to 180°, where ϕ_{1234} is the dihedral angle (define as LAMMPS) between 1-2-3-4. According to the force field, the backbone dihedral can be expressed by $U(\phi) = A \cos \phi$ and the barrier here can be easily overcome by thermal motion.

6. The resting beads are put in the simulation following the same method for the 4th bead.

7. Side beads are attached to the backbone beads randomly in the condition $r_{11'} = l_0'$, where $r_{11'}$ is the distance between backbone bead and the attached side bead and l_0 '= 2.871 Å is the equilibrium bond length calculated from the side bond potential $U'(l) = k(l - l_0')^2$. [98]

After building the initial coordinates with the C++ code, the coordinates are passed to a MC code written by coworker Dr. Zhuonan Liu. The resulting coordinates are passed to LAMMPS simulator. After soft push-off, the system is equilibrated at 550 K for 4.8 ns and then cooled to 300 K at a rate of 10 K/ns. To mimic an actual uniaxial extension experiment, we doubled the system size in the deformation direction (z-direction) and removed the periodicity in this direction by cleaving chains crossing the periodic boundary at both the top and bottom of the simulation box.

One system containing 1000 PS chains (75-mers) and another one containing 2000 PS chains (21-mers) are constructed, relaxed, cooled and chopped following the same procedure, except that the MC simulation is skipped for the relatively fast relaxation of these two systems.

Tensile deformation is performed by pulling 3 layers of beads (about 7.7 Å thick) at top and bottom at a constant rate in opposite directions at 300 K. Periodic boundary conditions are remained at x- and y-direction. Boundaries of these two directions are allowed to adjust freely by applying NPT ensemble with pressure set to 1 atm. A total deformation of L/L_0=1.8 is applied to the system at constant rate of 0.5 ns^{-1}.

Compression deformation is performed similarly by pushing 3 layers of beads at the top and bottom at a constant rate towards each other at 300 K. X- and y-direction boundaries are allowed to adjust freely with 1 atm pressure applied. A total deformation

of H_0/H=1.8 is applied to the system at constant rate of 0.5 ns^{-1}.

Primitive path analysis[102] is applied to 500-mer specimen without chopping at 300 K. The result shows entanglement length is 109 repeat units. This means in all of these three systems, only 500-mer system is well entangled.

5.4.3 the Origin of Stress in Tensile Mode

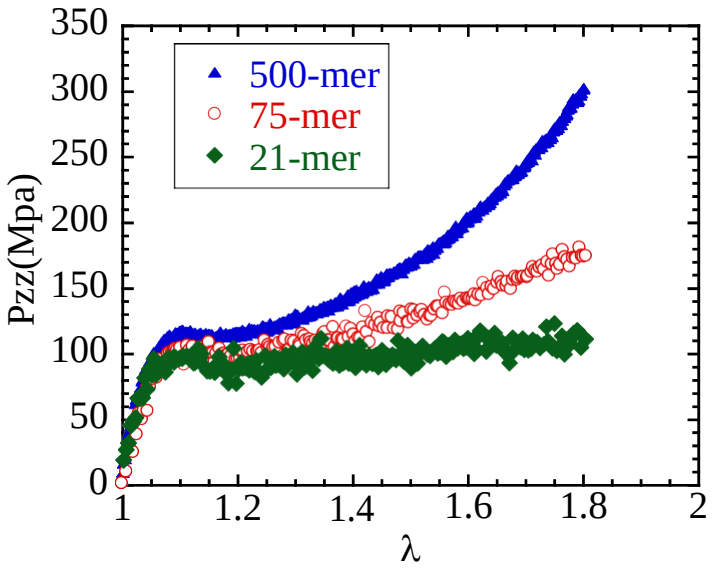

Figure 5.2 Extension stress-strain curves of three specimens with different chain length. A total deformation of lambda L/L_0 = 1.8 is applied to the 3 specimens respectively, at the same deformation rate V/L_0 = 0.5 /ns. Retractive stress value is defined as positive.

To understand the role of chain network and find the evidence of contribution from intra-segmental and inter-segmental stress, we firstly apply extension deformation to the three specimens with different chain length by moving top and bottom 3 layers of beads at Z direction. If the stress is contributed dominantly from inter-segmental part, the

stress response of these three samples should be the same. The reason is that the inter-segmental interaction in these three systems is supposed to be similar because the inter-segmental interaction is based on bead-bead interaction. Therefore, the chain length should be irrelevant.

The result has been shown in Figure 5.2. In the pre-yield regime, stress-strain curves of three specimens overlap, which fits our speculation that stress is dominated by inter-segmental contribution. However, stress level in post-yield regime grows with increasing molecular weight. The well entangled 500-mer specimen is capable of building high stress and strain hardening. But the 21-mer specimen shows a clearly flow-like stress-strain behavior with non-obvious strain hardening after yielding. This indicates that in the post-yield regime, intra-segmental contribution may dominate.

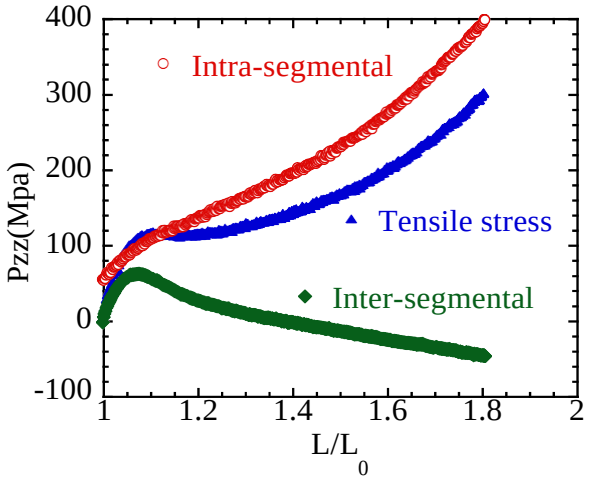

Figure 5.3 The stress decomposition of stress during the tensile deformation of 500-mer specimen. Retractive stress is defined as positive.

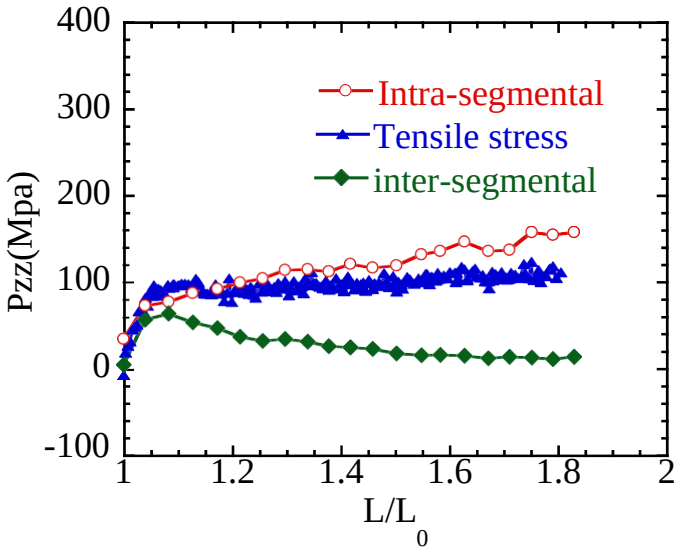

Figure 5.4 The stress decomposition of stress during the tensile deformation of 21-mer specimen. Retractive stress is defined as positive.

To further investigate the mechanical stress built during tensile deformation, we divide tensile stress into three parts using LAMMPS imbedded rerun commands. Stress contributed from inter-segmental (pair) potential, intra-segmental stress (including bond stretching, angle opening and dihedral distortion) and kinetic energy is calculated separately. Inter-segmental, intra-segmental and total stress (replotted from Figure 5.2) in 500-mer specimen system is plotted against elongation in Figure 5.3. Stress coming from kinetic energy describes the thermal motion of all beads. Its components are the same in all 3 directions, depending only on temperature and keeping at the same level during deformation.

The result is shown in Figure 5.3. During the tensile deformation of 500-mer specimen, intra-segmental stress increases monotonically with deformation strain and contributes majorly to the stress in the hardening regime. The inter-segmental stress

increases in the pre-yield regime due to decreasing density of the specimen and begins to decrease in the post-yield regime and even goes to be repulsive at the later stage. This phenomenon can be understood to partly balance the increasing retractive bonded stress. As speculated from comparison of Figure 5.2, the stress response of 500-mer specimen is dominated by inter-segmental contribution in pre-yield regime but intra-segmental contribution in post-yield regime.

Similar feature also shows up in the deformation of 21-mer specimen, as plotted in Figure 5.4. However, the segmental stress remains positive at the end of deformation and the growth of intra-segmental stress is limited. Comparing Figure 5.3 and Figure 5.4, it is clear that when chains are sufficiently long, and entanglements are present, the intra-segmental stress is able to be built up in the presence of chain network.

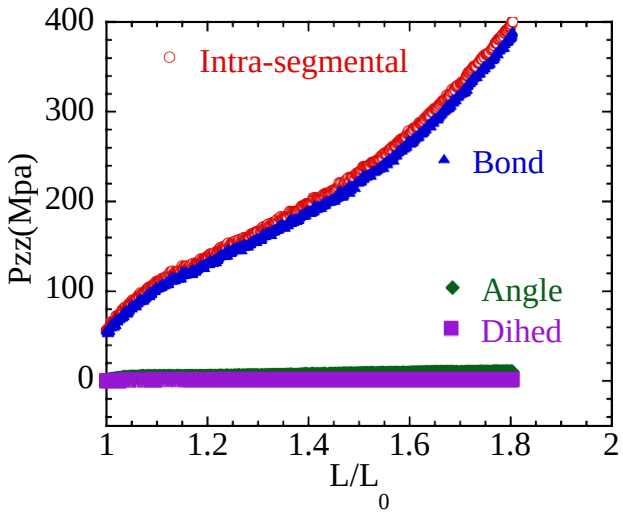

Figure 5.5 Intra-segmental stress decomposition during the deformation of 500-mer specimen. The intra-segmental stress is divided into the contribution from bond stretching, angle opening and dihedral distortion. Retractive stress value is defined as positive.

Intra-segmental stress during tensile deformation of 500-mer is further investigated. Using similar LAMMPS rerun command, the intra-segmental stress is further divided into contribution from bond stretching, angle opening and dihedral distortion. The result is plotted against elongation in Figure 5.5. The result shows that the intra-segmental stress is dominated by the stretch of bond. Stress coming from angle opening or dihedral distortion is negligible in this system. Further investigation shows the stress contributed from bond stretch is mainly from backbone bonds instead of side bonds.

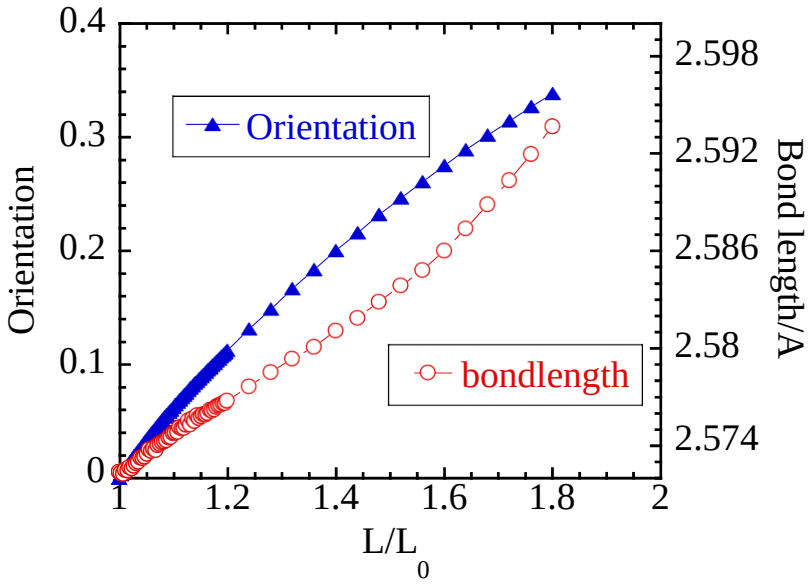

Figure 5.6 The orientation (calculated as P2 function) and average bond length of 500-mer specimen during the tensile deformation.

Then statistic investigation is conducted to the backbone bonds of 500-mer specimen during deformation. Orientation and bond length of backbone bonds are

calculated. The bond orientation function (P2) was calculated based on the 2nd-order Legendre polynomial, $P_2(t) = \frac{1}{2}(3\langle cos^2\theta_i(t)\rangle - 1)$, where $\theta_i(t)$ is the angle between the i^{th} bond and the deformation direction (z- direction) at time t, and the angular bracket indicates an average over all backbone bonds in our sample. The P2 function ranges from -0.5 to 1. And the values of P2 function -0.5, 1 and 0 correspond to the states that orientation perpendicular to, parallel to the selected direction and absolutely random. As shown in Figure 5.6, the backbone bonds are randomly oriented before any deformation and oriented to z-direction with deformation. In the meantime, the average length of backbone bonds also increases with deformation. Besides, the same orientation and bond length investigation is conducted to the 21-mer system. The result shows P2 around 0.32 and bond length is less than 2.58 Å at the end of deformation. These values are lower than that of 500-mer. The comparison emphases the necessity of the presence of well-entangled chain network to build high mechanical stress and show strain hardening in the post-yield region.

Results from Figures 5.2 to 5.6 draw a picture of the origin of stress during tensile deformation of polymeric glass. In pre-yield region, the stress is dominated by inter-segmental contribution. However, the inter-segmental contribution decreases after yield. In post-yield region, the stress is dominated by the intra-segmental contribution which grows monotonically with elongation. And intra-segmental stress majorly comes from the oriented and stretched backbone bonds, instead of from angle opening, dihedral distortion or stretching of side bonds. And this stress buildup cannot be achieved without the presence of chain network.

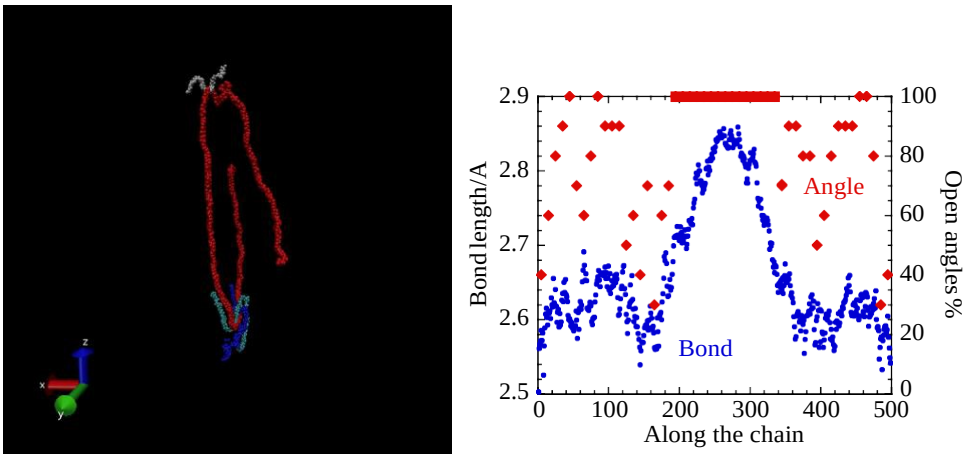

Figure 5.7 (left snapshot) Visualization of a typical chain (red) in 500-mer specimen after deformed to $L/L_0 = 3.0$ along z-direction. The white, blue and green chain segments form "hooks" structure which hooks the red chain. (right plot) Bond length of each backbone bond along the chain (circles) and opened angle (diamonds) along the chain. Retractive stress is defined as positive.

To investigate the procedure behind stress build-up under deformation through the backbone bonds as well as the role of chain network, the 500-mer specimen is further extended to elongation $L/L_0 = 3.0$. Visualization of the specimen is performed with Visual Molecular Dynamics (VMD)[103] tool. Left snapshot in Figure 5.7 shows the morphology of a typical chain (red) in the specimen after deformed to $L/L_0 = 3.0$. This Two "hairpin" structures can be seen along z-direction. The chain is folded and can be treated as 3 strands connected by two bending parts. We also find other chains that forming hooks structure at the two bending ends of the red chain. The parts of chains that hook with the red chain is shown in white, blue and green in the snapshot. During the deformation, these small "hooks" hook the bending ends of the red chain and stretch it

from a coil to a “clip”.

The bond lengths of the back-bone bonds along the red chain is calculated from the coordinates and shown in the right plot in Figure 5.7. Three maximum values can be told in the curve. The maximum positions are corresponding to in the middle of the three strands and the two minimum positions are the two bending parts. This means that the strands instead of the bending parts are stretched most during the tensile deformation and contributes majorly to the stress. This speculation is confirmed by the analysis of the angle along the bonds.

The statistic of the angles on the backbones of the specimen shows the distribution of angles concentrates at around 130° and 170° which corresponding the two minimum values of the angle potential. During deformation, the distribution changes but still concentrates at these two angles. With increasing deformation, the population migrates from around130° to around 170°, so the average angle is more opened. Based on this statistic, we define the angle that larger than 160° as “opened” angle and analyze the angle opening along the red chain in Figure 5.7. The angles along the chain are separated in groups ten by ten. For example, the 1^{st} to 10^{th} angle along the chain are put into one group and the 11^{th} angle to 20^{th} are put into the second group. Then the percentage of opened angles against the total angle number in the group (which is ten) is calculated and plotted along the chain in right plot in Figure 5.7. Similar to the result of bond force, the angles are located on the strands, especially the middle of the strands are mostly opened. This draws the same conclusion as the bond length that the strands instead of the bending part are stretched and provide the mechanical stress.

It is to be expected that the stretching of the strands can only be achieved through

the “hooks” or to be properly called “entanglements”, proven by the lack of orientation and bond stretching of the 21-mer specimen. Based on above results, we are able to derive the nature of stress of polymeric glass during tensile deformation.

At the early stage of elongation, the deformation is affine. It causes the inter-segmental interaction stretched and dominates the mechanical stress. Since this process is inter-segmental dominated, the stress response is not molecular weight dependent. After the deformation reaches yield point, the sample undergoes plastic deformation and inter-segmental stress begins to decrease. In this stage, if chain network is present, the strands in the network are stretched and oriented by the entanglements due to the uncrossability. The stretched and oriented strands contribute to the mechanical stress and build a strong stress response. Molecular weight dependence also shows up in post-yield region. When the chain length is as low as 21-mer, stretching and orientation of backbone bonds is limited due to the absence of chain network. Therefore, the stress of 21-mer specimen in post-yield regime hardly increases with increasing deformation.

5.4.4 the Origin of Stress in Compression Mode

Similar as the investigation conducted to tensile deformation, start-up compression is applied to 500-mer and 21-mer specimen by moving top and bottom 3 layers of atoms. A total deformation of $H_0/H = 1.8$ is applied to each specimen at constant rate 0.5/ns. Similar as the tensile mode, result shows 500-mer specimen (Figure 5.8) is capable of building higher level stress than 21-mer specimen (Figure 5.9). In addition, the 500-mer specimen shows significant strain hardening, while the post-yield stress-strain curve of 21-mer is rather flat. Need to be mentioned that, unlike previous

section, compression stress is defined as positive in this section. This means, in the discussion and figures here, a positive stress or force indicating the interaction is repulsive.

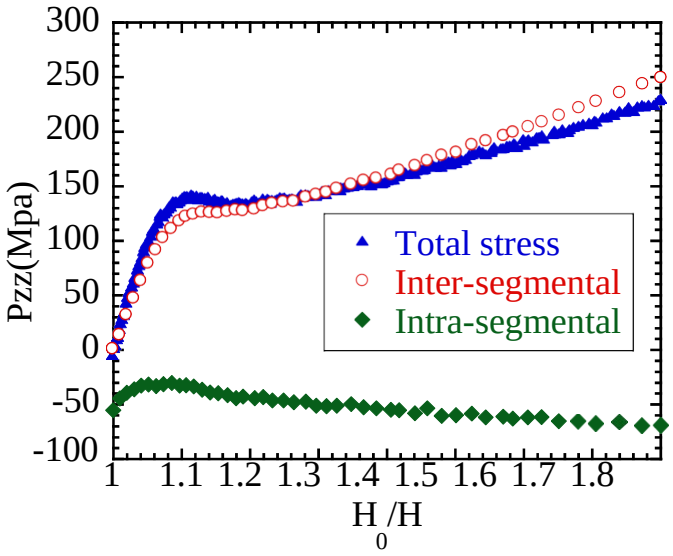

Figure 5.8 Stress decomposition of stress in z-direction during compression deformation of 500-mer polystyrene at 300 K. Repulsive stress value is defined as positive.

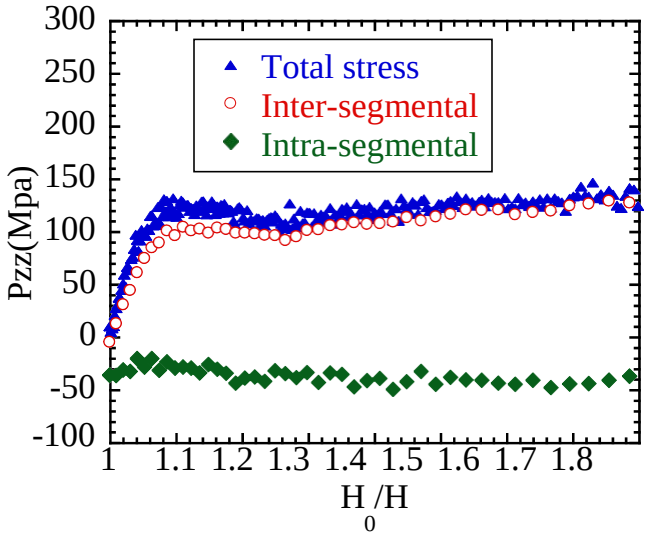

Figure 5.9 Stress decomposition of stress in z-direction during compression deformation

of 21-mer polystyrene at 300 K. Repulsive stress value is defined as positive.

At the early stage of compression deformation, for both 500-mer specimen and 21-mer specimen, stress is dominated by inter-segmental stress, which is similar as in the tensile mode. However, in the post-yield region, the stress is still dominated by inter-segmental contribution. The question arises that why the stress response is molecular weight dependent if it is inter-segmental dominated?

The inter-segmental stress response of 500-mer specimen and 21-mer specimen is basically the same: repulsive inter-segmental stress grows monotonically with deformation. However, the intra-segmental stress of the two specimens is different. Before any deformation, the intra-segmental stress is negative which means retractive. When compression deformation is applied to 500-mer specimen, the intra-segmental stress increases and then decreases before the whole sample yields. Then the intra-segmental stress keeps decreasing with increasing deformation. As mentioned above, negative sign of stress means retractive. This means the retractive intra-segmental stress increases at the later stage of deformation although the sample is compressed. When deformation is applied to 21-mer specimen, the intra-segmental stress is almost constant during the deformation.

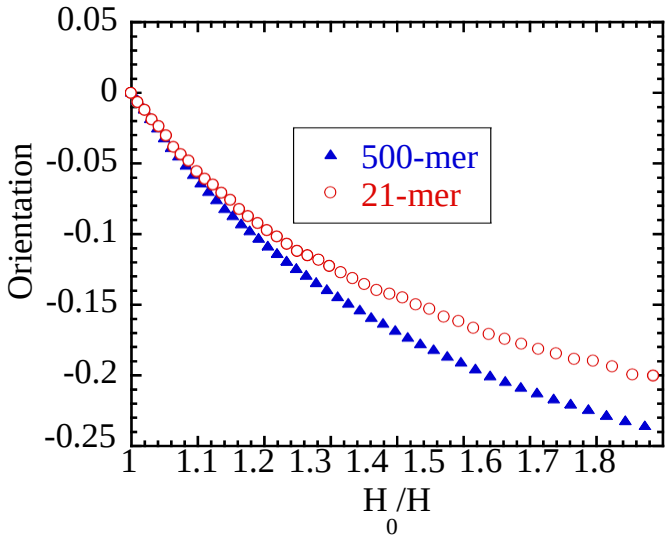

Figure 5.10 Orientation calculated from P2 function of 500-mer and 21-mer specimen during compression. Reference direction z-direction.

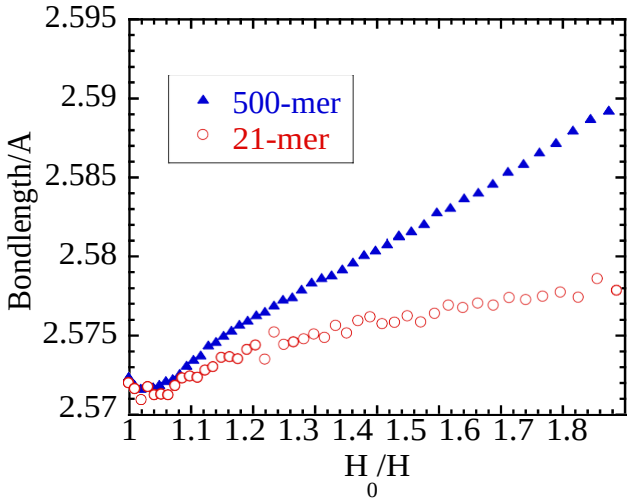

Figure 5.10 Average bond length of backbone bonds of 500-mer and 21-mer specimen during compression.

We further investigate into the intra-segmental stress by analyzing the orientation and average bond length of backbone bonds of 500-mer specimen and 21-mer specimen during compression. As shown in Figures 5.10 and 5.11, when 500-mer specimen undergoes compression deformation, the backbone bonds orient to direction perpendicular to z-direction. At the beginning of compression, the bonds are compressed by the deformation shown as the bond length decreases before H_0/H =1.04. Then the bonds oriented to the lateral direction, and turn from compressed to stretched state, getting stretched more as the deformation continues. This should be to be expected, because during the compression deformation, the dimension of later direction actually expends.

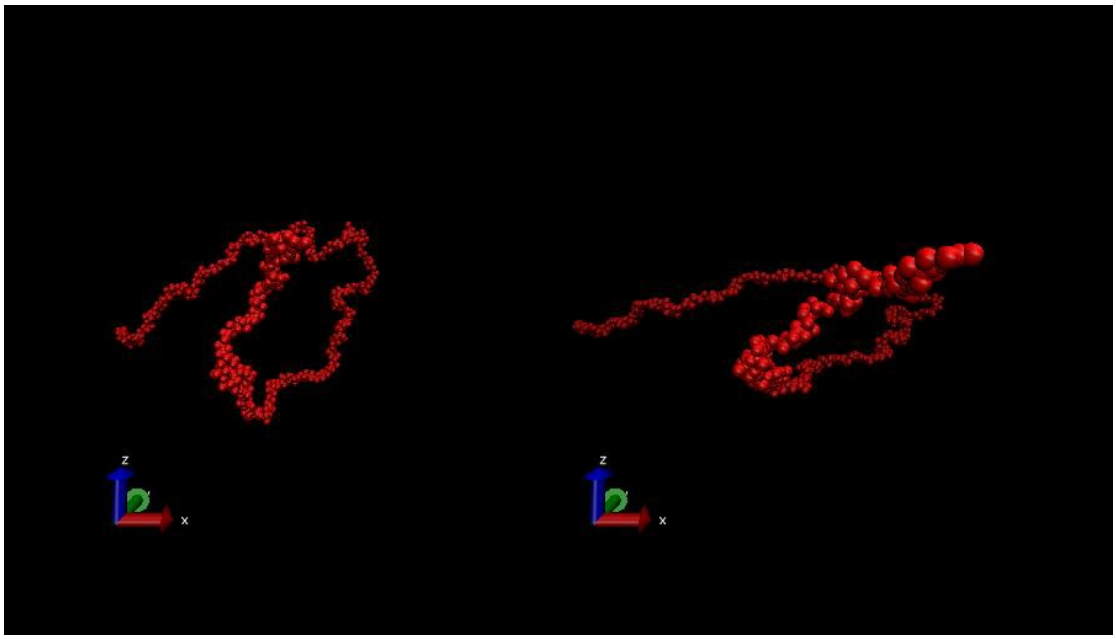

Figure 5.11 Visualization of a typical chain in 500-mer specimen before deformation (left) after compressed to H_0/H=1.8. Compression is along z-direction.

Figure 5.11 shows the visualization of a typical chain before and after

compression, which is the same chain as Figure 5.7. After compression, the strands of the chain are oriented and stretched in the lateral direction. It is to be expected, during compression, the chain network undergoes tensile deformation in later direction. This can also explain the difference between 500-mer specimen and 21-mer specimen. Just like in tensile mode, the bonds of 500-mer specimen are oriented and stretched more than that in 21-mer specimen due to the presence of chain network. This causes a higher (in negative sign) intra-segmental stress in lateral direction of 500-mer specimen than 21-mer specimen, as shown in Figures 5.12 and 5.13. Since the lateral direction is free to adjust, the total stress in lateral direction is zero, shown in Figures 5.12 5.13. A higher inter-segmental stress in 500-mer specimen is required to balance the higher intra-segmental stress coming from stretched chain network. This required higher inter-segmental stress means that the segments will be denser packed than the 21-mer specimen. And this denser packing can result in a higher inter-segmental stress response in the compressing direction, shown by the comparison between Figures 5.8 and 5.9.

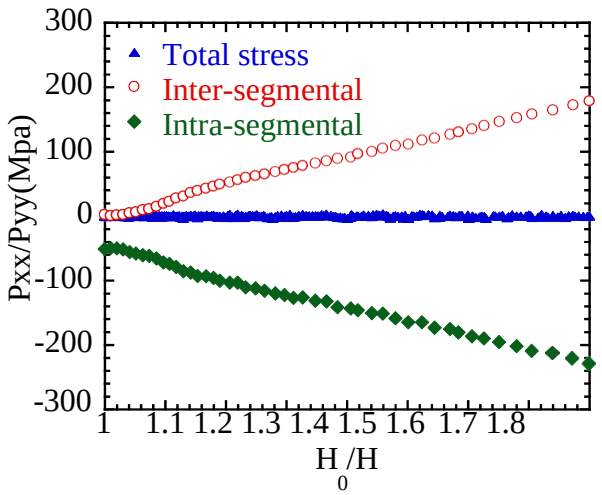

Figure 5.12 Stress decomposition of lateral direction during compression of 500-mer specimen.

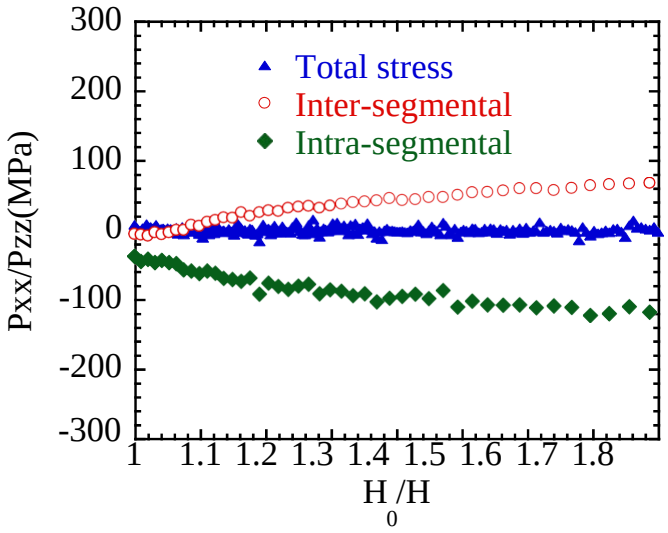

Figure 5.13 Stress decomposition of lateral direction during compression of 21-mer specimen.

This procedure can also be interpreted in another way. When a well entangled polymeric glass under compression, the chain network is forced to be stretched in the lateral direction. This process causes tension to arise in the strands of the network to resist the deformation. The resistance shows up as a higher stress response than the response of low molecular weight specimen because the low molecular weight specimen can adjust more freely in the lateral direction.

As a summary of this chapter, we investigate into the nature of stress for polymeric glass in both tensile and compression modes using molecular dynamics simulation and find that: 1) well-entangled chain network is essential for a specimen to build strong mechanical response and show strain hardening at large deformation regime; 2) in tensile mode, stress is dominated by inter-segmental contribution in pre-yield regime and intra-segmental contribution in post-yield regime; 3) when a well-entangled

polymeric glass undergo tensile deformation, the strands between entanglements are stretched due to uncrossability and contributes majorly to the strain-hardening stress; 4) stress response in compression mode is dominated by inter-segmental interaction in both pre-yield and post-yield region; 5) the resistance of stretching a well-entangled chain network in lateral direction results in a higher stress response in compression direction than that of a low molecular weight specimen.

CHAPTER VI

STRESS RELAXATION

6.1 Introduction

High molar-mass polymers are complicated, strongly correlated many-body systems. Their mechanical responses to large deformation are especially challenging to describe, both in melt state with chain entanglement from intermolecular uncrossability and in glassy state with inter-segmental interaction overwhelming chain network. Unlike other materials such as ceramics or metals, polymeric material is uniquely highly stretchable in liquid state (rubber bands being an example) and drawable in glassy state, e.g., capable of doubling the equilibrium length. Above the glass transition temperature T_g, the high rubbery extensibility of melts is widely understood in terms of a phantom network of Gaussian chains, which can be stretched multiple times of their original size before straightened. However, when temperature below T_g, a sufficiently high molecular weight does not guarantee ductile drawing. Although the concept of chain entanglement has been invoked for decades[48, 104] to acknowledge the prerequisite of high molecular weight for ductility, it was unclear[2, 37, 38] that how polymer entanglement would afford a glassy polymer. For example, bisphenol A polycarbonate (PC) shows

extraordinary ductility: despite its high T_g (145 ^oC), PC can be drawn to a great extent without brittle fracture even at –120 ^oC.

For ductile polymer glasses, Kramer's criticism[10] of a conventional view to regard strain hardening as due to “rubber elasticity” provided the impetus to evaluate intermolecular contributions to the macroscopic stress. By assuming that no chain network would be necessary to achieve yielding and ductile glassy polymers would be able to yield, several recent studies[14, 105-111] asserted that the macroscopic stress in the post-yield regime is largely inter-segmental in origin. More specifically, yielding and stress growth in the post-yield regime (strain hardening) were treated as a different topic from the brittle fracture in glassy polymers. Consequently, they do not aim to answer the long-standing question of how and why ductile polymer glasses turn brittle upon sufficiently lowering the ambient temperature.

Initial stress growth in melt deformation is widely accepted as the result of intra-chain retraction forces of stretched strands in entanglement network. These intra-chain forces can help a melt-stretched polymer undergo complete elastic recoil. For polymeric glasses, it is far less clear that whether or not the intra-segmental forces make a dominant contribution to the tensile stress in the post-yield extension (ductile drawing). New experiments show that tensile stress vanishes shortly after pre-yield deformation of polymer glasses while tensile stress from post-yield stays high and relaxes on much longer time scale. It hints a specific molecular origin of the stress, in ductile cold drawing process: chain tension, rather than inter-segmental attraction. This observation fits our hybrid molecular model nicely[26], where it is believed that chain network contributes dominantly to the stress during tensile deformation. This nature of tensile deformation is

confirmed by the coarse-grained simulation in chapter V. However, the feature of relaxation is still under debate. Although the macro-scale experiment observation indicates the existence of interaction which relaxes slower than the inter-segmental attraction, it is unclear that whether the molecular level analysis will still show the same result? To confirm the essential role of chain network, a molecular dynamics simulation based on a coarse-grained model for polystyrene (PS) is set up and followed by an analysis on the stress decomposition, mobility and visualization based on this simulation.

This work is done with the help from Jianning Liu.

6.2 Mechanical Experiment: Relaxation Near T_g

6.2.1 Introduction of Alpha time

Alpha-process in homo-polymer system is defined as the relaxation process of the segmental motion. Accordingly, alpha-time is defined as the relaxation time of the segmental motion. Alpha process strongly influences the properties of polymer: when alpha-time is sufficiently short, polymer behaves like a liquid; otherwise, it behaves like a solid. It is well accepted that, the alpha-time increases with decreasing temperature, as well, it would also increase tremendously in glassy state: a few dozen degrees lower in temperature could result in alpha-time orders longer. In addition, because of the strong influence of alpha-time on mechanical response of polymeric system, the temperature at which the alpha-time reaches 100 s, is defined as glassy transition temperature.

Resent theory [11] and experiment [112] study reach an agreement that the deformation applied to glassy polymer will accelerate the alpha-process and shorten the

alpha-time by orders after yield point, hence enable the plastic flow. Consequently, at the early stage of relaxation, this accelerated mobility would make a severe difference in the relaxation starting from post-yield region and pre-yield region, shown as Figure 6.1.

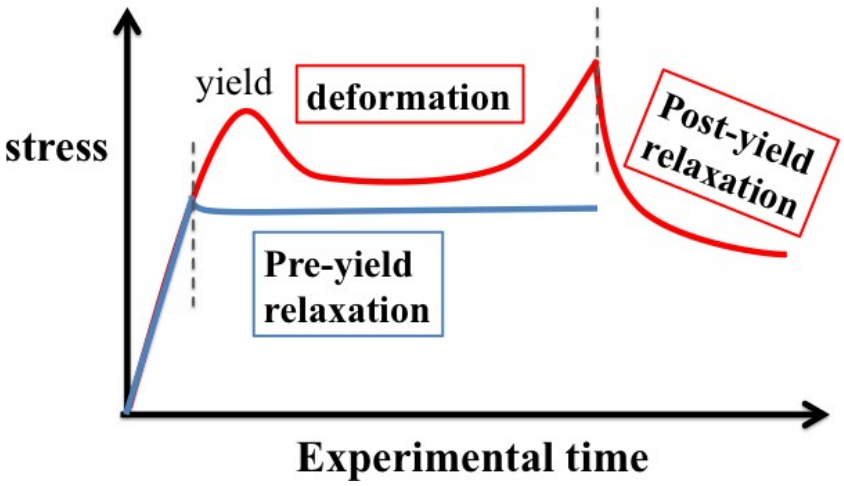

Figure 6.1 A scheme of typical stress-time curves of relaxation in deep glassy state starting from post-yield regime (red) and pre-yield regime (blue).

Figure 6.1 shows the typical pre-yield stress relaxation curve (blue) and post-yield stress relaxation curve (red) in glassy state. In post-yield regime, as mentioned above, the alpha process is accelerated. After yield, the alpha time is shortened and comparable to melt. Therefore, the stress dropped rapidly as the deformation stopped, because of the relaxed stress during high mobility segment rearrangement. Afterwards, segment mobility decreases due to the lack of external deformation, shown by the slow relaxation process. In the case of pre-yield relaxation, because the alpha-process is not accelerated sufficiently, and the alpha-time is still longer than experimental time scale (reasonable time of conducting experiment), stress can be hold and barely drop in the relaxation

process.

6.2.2 Materials, Apparatus and Methods

All the experiments were performed based on two polymers: bisphenol A-Polycarbonate (PC) Lexan TM 141 111 from Sabic (GE Plastic) and Polystyrene (PS) Dow Styron 663. Their properties are listed in Table 6.1.

Table 6.1 Sample Information of the Polymer Glasses

Polymer	Mw (kg/mol)	M_e (kg/mol)	PDI	T_g (°C)	Source
PC	63	1.3	1.58	149	Lexan resin
PS	319	13	1.44	103	Dow Styron

In uniaxial tensile tests, pellet-like resins were compression molded using a Carver press with a 100 × 100 × 0.5 mm^3 mold, sandwiched by two Kapton® polyimide films at 200 °C. Sample was directly cut from such sheets using a dog-bone shaped cutter (ASTM D412D, 39 × 3 × 0.6 mm^3).

Uniaxial tensile extension tests were carried out using an Instron 5567, which was equipped with a custom-made oven with temperature control within ± 0.5 °C. In each test, the specimen was quickly mounted onto the upper and lower clamps at the prescribed temperature and allowed to achieve thermal equilibration in the next 15 min. Then the specimen was drawn at constant cross-head speed till the desired length. At last, the cross-head gap was set at a constant gap to perform the relaxation tests.

The linear viscoelastic properties of PC and PS were evaluated by small-amplitude oscillatory shear (SAOS) measurements, performed on an ARES rheometer at various temperatures. Parallel plates were setup with a gap distance of 1 mm or 8 mm in diameter. Samples with 1 mm in thickness were firstly heated up to sufficiently high temperature above T_g with good adhesion to metal disks. Strain amplitude for SAOS was set 5% for the temperature from T_g + 50 °C to T_g +5 °C and the frequency ranging from 100 to 0.05 rad/s. To access the segmental relaxation (τ_α) dynamics, the frequency sweep amplitude was gradually decreased to 0.01% when temperature near or below T_g in the frequency range between 1 to 0.05 rad/s. Here, τ_α(SAOS) was taken as the reciprocal of the third crossover frequency ω_α: τ_α (SAOS) = $1/\omega_\alpha$.

6.2.3 Result and Discussion

The challenge to explore the molecular origin of stress during ductile deformation well below T_g stems from the inconveniently long alpha relaxation time. Specifically, Figure 6.2 shows that, at room temperature, the stress relaxation of PC after long time after post-yield extension is extremely slow, similar to the pre-yield deformation.

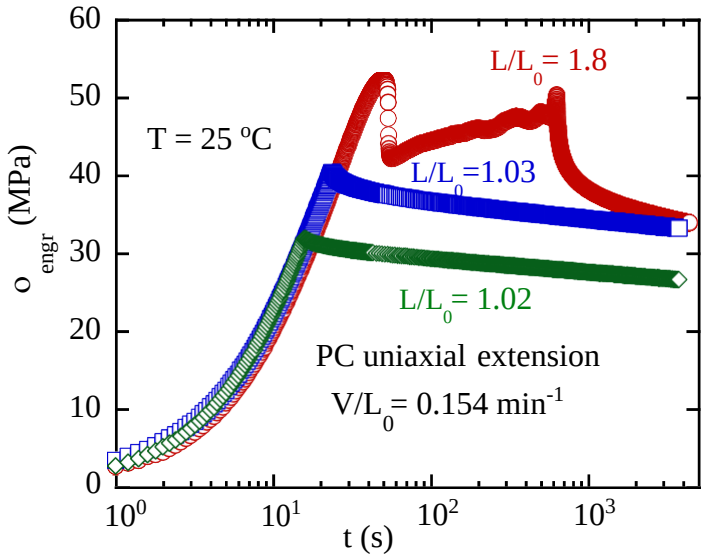

Figure 6.2 Tensile (engineering) stress during and after uniaxial extension of PC. The stress produced by pre-yield extension decays slowly while the stress from post-yield extension decreases fast initially before approaching a similar relaxation rate to pre-yield relaxation. Draw ratios: L/L_0 = 1.02 (pre-yield), 1.03 (pre-yield) and 1.8 (post-yield), crosshead speed V = 6 mm/min, initial specimen length L_0 = 39 mm.

Does the stress in circles have the same molecular origin as those (pre-yield due to stretching of inter-segmental van der Waals bonding) in squares and diamonds at *t* = 1000 s (cf. Figure 6.2)? How do we determine the nature of the stress after the post-yield deformation? Figure 6.3 shows a faster stress decay indicating the faster relaxation dynamics at higher temperature. After fitting the stress relaxation data with KWW function, it was shown that the dominant relaxation time converges to ca. 100 s at temperature around T_g (145 °C), in agreement with the values identified from SAOS data.

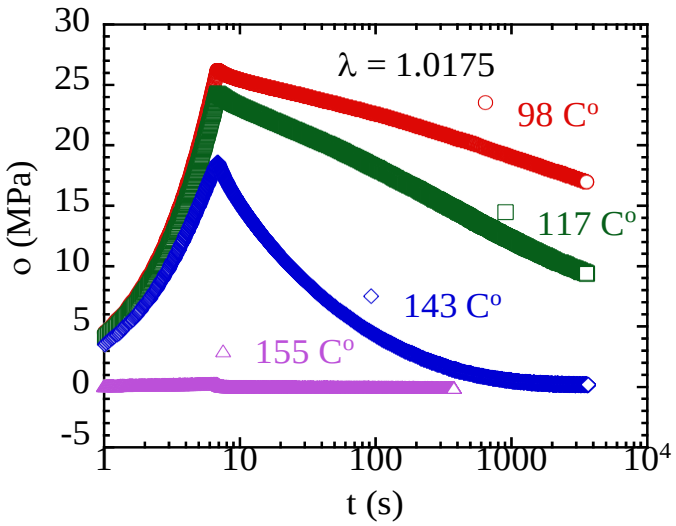

Figure 6.3 Tensile (engineering) stress during and after drawing PC at temperature from 98 to 155 ºC. Draw ratios L/L_0 = 1.0175 (pre-yield), cross head speed V/L_0 = 0.15 mm/min. (Experiment by Jianning Liu).

The information in Figure 6.3 combined with the SAOS results suggests that it may be instructive to perform tensile extension at temperatures not far below T_g where the alpha relaxation time is sufficiently short. In this work we explore the molecular origin of mechanical stress during ductile extension of PC and PS polymer glasses by characterizing the stress relaxation behavior in both pre-yield and post-yield regimes, at 10 to 15 ºC below T_g. The diamonds in Figure 6.4 show that the tensile stress from pre-yield vanishes in 60 min for PC at 133 ºC. This stress decay can conventionally be explained by the segmental alpha relaxation and reveal an alpha relaxation time τ_α less than one hour, as predicted by the SAOS data: τ_α(SAOS) ~ one hour at 135 ºC. During the cold drawing, beyond the elastic pre-yield regime, shear yielding occurs at the peak stress, followed by necking and neck front propagation and the tensile stress remains

constant. The stress relaxation behavior from the post-yield regime is remarkably different (squares in Figure 6.4): the stress relaxation began at the end of necking propagation and the beginning of strain hardening. Specifically, in contrast to the stress relaxation from pre-yield elastic deformation (diamonds), the stress relaxation at the yield point (squares) reveals some residual stress after long time.

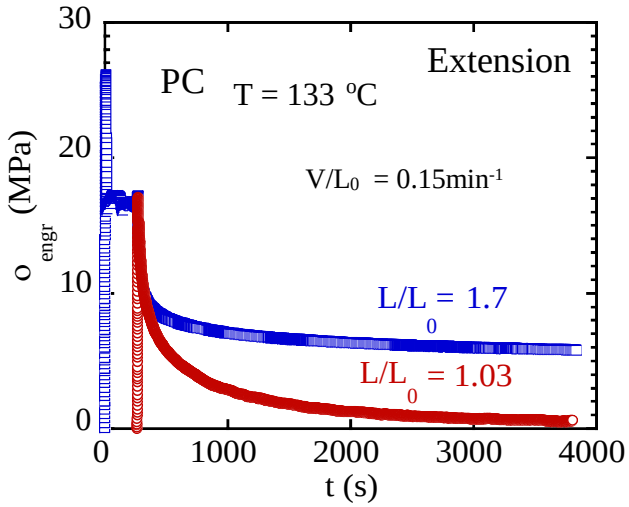

Figure 6.4 Tensile (engineering) stress during and after drawing PC. The pre-yield curve is moved horizontally to share the same relaxation starting time. Draw ratios L/L_0 = 1.03 (pre-yield) and 1.7 (post-yield, at the beginning of strain hardening regime), at a crosshead speed V/L_0 = 0.15mm/min.

Recent consensus suggests[111] that mechanical stress during plastic deformation is dominantly dissipative, leading to an expectation that the square-curve in Figure 6.4 should approach zero as fast as the circle-curve: if coming from the inter-segmental interaction, the stress should vanish in 60 min via the alpha process as it does in pre-yield regime; moreover, much of the initial rapid stress decline should also involve inter-segmental processes. However, unexpectedly, the stress remains high on the pertinent

time scale of 60 min.

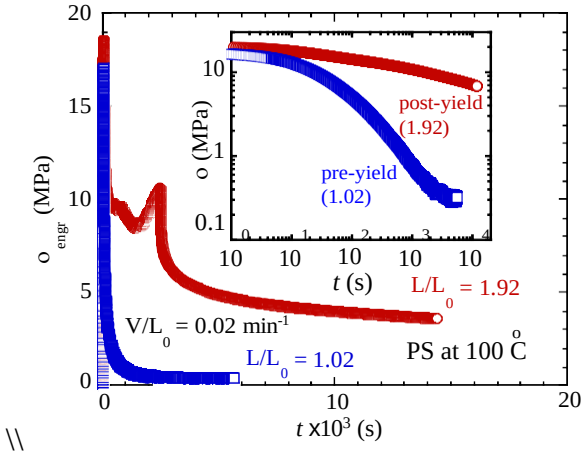

Figure 6.5 Engineering stress during and after drawing of PS to draw ratios L/L_0 = 1.02 (pre-yield) and 1.92 (post-yield) at a crosshead speed V/L_0 =0.02 /min. Similar to Figure.6.4, stress from post-yield drawing survives at long times. The stress relaxation in the inset shows contrasting characteristic time scales: the stress relaxation is much slower from post-yield deformation. (Experiment by Jianning Liu).

To determine whether the observations in Figure 6.4 are universal or not, we carried out similar extensional drawing of glassy polystyrene. PS in the present study has T_g = 105 ^oC and we set the temperature at 100 ^oC for its stress relaxation from pre-yield at L/L_0 = 1.02 and post-yield at L/L_0 = 1.92 beyond the completion of necking. As shown in Figure 6.5, the stress relaxation from pre-yield extension occurs on a time scale of several hundred seconds. In contrast, similar to the behavior in Figure 6.4, the stress remains high after post-yield extension at L/L_0 = 1.92. The inset of Figure 6.5 shows that the pre-yield stress relaxation is rapid in time scales of 10^2 s while the post-yield

relaxation is considerably slower from beginning. Recently experiment [113] showed that the initial stress relaxation from post-yield deformation occurs on the time scales in proportion to the reciprocal of the deformation rate invoked to produce the post-yield deformation. How could the stress relaxation involve a much slower rate than that prescribed by the alpha process? What does this phenomenon of extremely slow initial stress relaxation imply regarding the molecular origin of the tensile stress during post-yield drawing?

This study asserted, consistent with the recent molecular model,[26] that a) the mechanical stress in post-yield has a significant intra-segmental contribution and b) the molecular mobility produced by the post-yield deformation governs how quickly the intra-segmental component of the stress relaxes.

From chapter V we concluded by simulation that in the glassy state, after large tensile deformation, stress is dominated by bond orientation and stretch. Therefore, during relaxation, the chain network constructed by oriented and stretch bonds may keep high retractive stress on longer time scales than the alpha process whose origin is inter-segmental. Two specific experimental features in this chapter prove that. First, the tensile stress from post-yield regime can remain high after long time. Second, the stress decay can be much slower after significant post-yield extension than that from pre-yield deformation. This conclusion drawn from simulation and proven by experiment pertains to many issues in the literature including a) the essence of strain hardening,[14, 105-111] b) the elastic deformation and the energetic storage in post-yield regime,[114] c) "anelasticity" associated with hidden stress in glassy state.

Further, based on our knowledge from Chapter V and the new relaxation

experimental result, we make our speculation about relaxation process at near-Tg temperature. During relaxation, although stress from inter-segmental interaction, i.e., stretching of Van der Waals bonds, can relax through alpha processes, the segmental relaxation is ineffective to fully remove the chain tension produced during the cold drawing. Formation of a chain network in glassy state requires inter-segmental interactions – chain uncrossability is inherently an intermolecular effect. However, for a strained chain network to relax stress, it requires structural adjustment in scales significantly larger than the monomer size, which cannot occur on the alpha time. Therefore, the comparably high pre-yield stress can indeed relax faster.

To test our speculation, simulation of coarse-grained PS undergoing relaxation was performed and will be analyzed and discussed in the next section.

6.3 Simulation

6.3.1 Simulation Protocol

Molecular dynamics simulation was done using the same coarse-grained model of PS[98] in Chapter V. In this model, one repeat unit of PS is represented by 2 beads: one side bead as the phenyl ring and one back-bond bead as the -CH- group and half of the two neighboring -CH_2- group.

All the simulations were performed using the LAMMPS simulation package[101]. A system consisting of 500 PS chains (500-mers, 1000 beads per chains) was generated by randomly distributing the PS chains in a periodic box. This system was initially equilibrated at 550 K for 4.8 ns and then was cooled to 370 K at a rate of 10 K/ns.

The deformation was performed using LAMMPS' fix deform tool. A total deformation of lambda (L/L_0) = 1.8 and 1.03 were applied to the system at the extension direction for the post-yield and pre-yield deformation at a rate of 0.5/ns, respectively. After deformation, the extension direction (z-direction) was fixed to preform relaxation test for an additional 24 ns.

6.3.2 Stress Decomposition during Relaxation

To make better comparation with experimental result, we carry out molecular dynamics simulation of cold drawing (uniaxial extension) and stress relaxation using a coarse-grained model for PS at 370K.

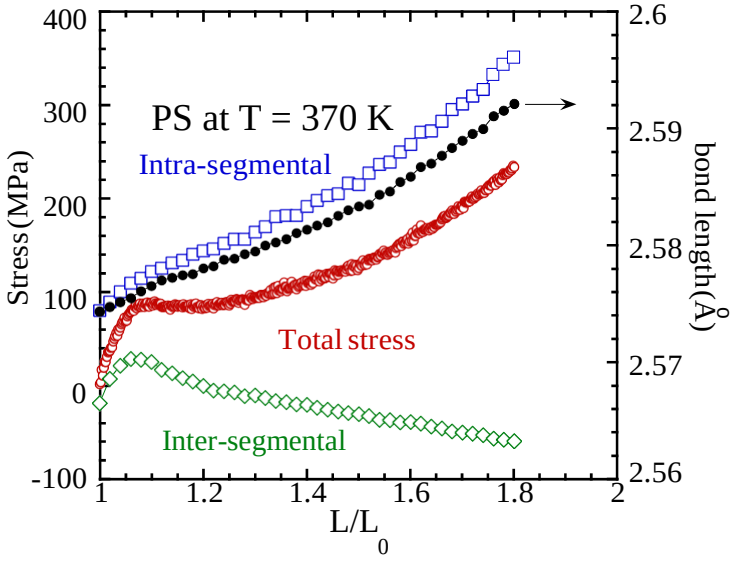

Figure 6.6 Different components of stress and bond lengthening (right-hand-side Y axis) during drawing of PS at 370 K.

Figure 6.6 shows the decomposition of the stress during tensile deformation at

370 K as a function of the draw ratio L/L_0, where appreciable bond stretching accompanies the growing tensile stress. Though temperature is 70 K higher than the temperature used in Chapter V and already close to T_g, we find the nature of stress during deformation is similar as described in Chapter V: before yielding both the covalent bonds and the LJ bonds are stretched, resulting in a retractive stress; in post-yield regime, for PS with Mw ~ 50,000 g/mol, the buildup of the tensile stress comes from the deformed chain network while the inter-segmental interactions turns compressive. Therefore, the simulation result further supports the conclusion derived from the experimental observation in Figures 6.4 to 6.5 that the post-yield extension renders substantial conformational changes associated with stretching of a chain network.

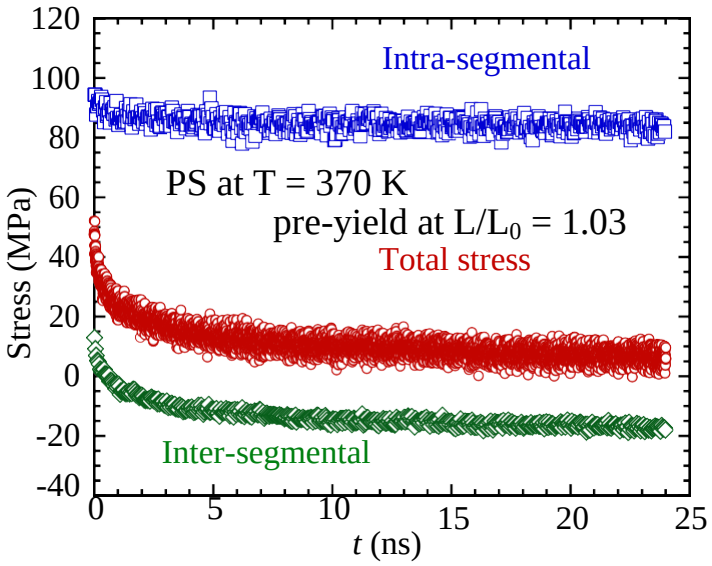

Figure 6.7 Relaxation of different stress components after pre-yield deformation of L/L_0 = 1.03.

The molecular dynamics simulation also supports the interpretation of the

experimental data in Figures 6.4 to 6.5, concerning why stress relaxation from pre-yield deformation could be faster than that from post-yield: The origin of stress is greatly different between pre-yield and post-yield. Specifically, Figure 6.7 shows that the fast stress decay from pre-yield occurs due to the available segmental mobility. As the inter-segmental packing recovers toward its non-deformed state where the inter-segmental stress is compressive, the inter-segmental stress changes from being initially retractive to compressive (negative). In this process, the bonded stress remains unchanged, although the temperature is close to T_g (10 K to 20 K below) and the mobility in the simulation system is high due to the smoother pair potential. Currently, the simulation is still too expensive to approach the state where the overall stress vanishes after pre-yield extension. Nevertheless, the contrast is clear: Figure 6.8 shows that after post-yield drawing, the initial rapid stress decay is dominantly contributed from intra-segmental in origin. And after long time, the retractive stress stays distinctly higher than 0 stress or pre-yield stress due to the slow relaxation of bonded stress. This result confirms the findings and speculation in the experiment section 6.2.3. With the help of simulation, we are able to perform more analysis to explore the origin behind it in the next section.

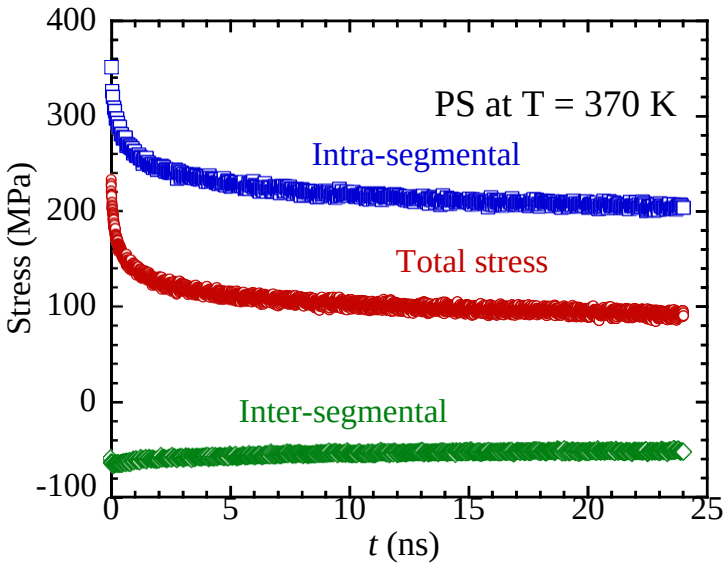

Figure 6.8 Relaxation of different stress components from post-yield drawing to L/L_0 = 1.8.

6.3.3 the Role of Chain Network during Relaxation

In Chapter V, we found that the bonded stress at long tensile deformation is dominated by stretched and oriented backbone bonds. In this chapter, we analyze the bonded stress during post-yield relaxation with similar bond length and orientation calculation on backbone bonds during the relaxation.

Similarly, in Figure 6.9, bond length is calculated by averaging the backbone bonds and the orientation function (P2) was calculated based on the 2nd-order Legendre polynomial:

$$P_2(t) = \frac{1}{2}(3\langle \cos^2 \theta_i(t) \rangle - 1)$$

where $\theta_i(t)$ is the angle between the ith bond and the deformation direction (z-direction) at time t, and the angular brackets indicate an average backbone-bonds in the

sample.

From Figure 6.9, we can see rapid decreases of both bond length and orientation due to accelerated mobility at deformation stage, which is also shown in the Figure 6.10. The decay retards as the mobility decreases with the relaxation time. After the mobility analysis (Figure 6.10), we find out that at the late stage of relaxation, the mobility of post-yield relaxation sample is even lower than the pre-yield sample. This observation confirms our speculation at 6.2.3 that the slow relaxing chain network constructed by stretched bonds holds the stress at the late stage of relaxation of large deformation.

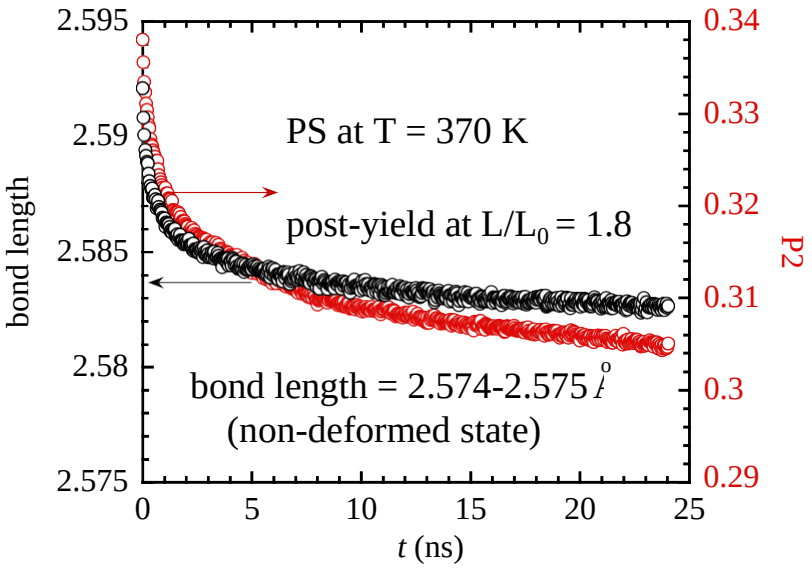

Figure 6.9 Bond length decrease and bond disorientation in terms of P_2 as a function of time during relaxation from post-yield drawing to $L/L_0 = 1.8$.

Mobilities in pre-yield and post-yield simulation are calculated based on the bond orientation auto-correlation of the backbone-bonds. The bond correlation calculation is performed following the work of Ediger [115], where the bond autocorrelation is defined

as:

$$C_b(t) = \frac{1}{2}(3\langle \cos^2 \theta_i(t) \rangle - 1)$$

Here, $\theta_i(t)$ is the angle between the i^{th} bond at time 0 and t, and the angular brackets indicate an average backbone bond in our sample.

Based on this definition, $C_b(t)$ would equal to 1 at time 0. With increasing time, the orientation of bonds varies from the initial condition and cause the function to decay. The higher the mobility of the system, the faster the decay of the function. The left two curves of Figure 6.10 show how the correlation decays during the relaxation process. Just as speculated, if the deformation stopped, the post-yield (circles) relaxation the sample clearly shows higher mobility than that the pre-yield relaxation, due to the high mobility introduced by the large deformation. As relaxation continues, the decaying slope of post-yield relaxation decreases and eventually becomes smaller than the pre-yield relaxation at the late stage of relaxation.

To clearly demonstrate mobility at late stage, we re-calculated $C_b(t)$ from 8 ns and 16 ns. As shown by the middle and right 2 sets of the curves in Figure 6.10, the functions of pre-yield relaxation decay faster, indicating that, at least from the 8 ns, the mobility of post-yield relaxations is slower than the pre-yield one.

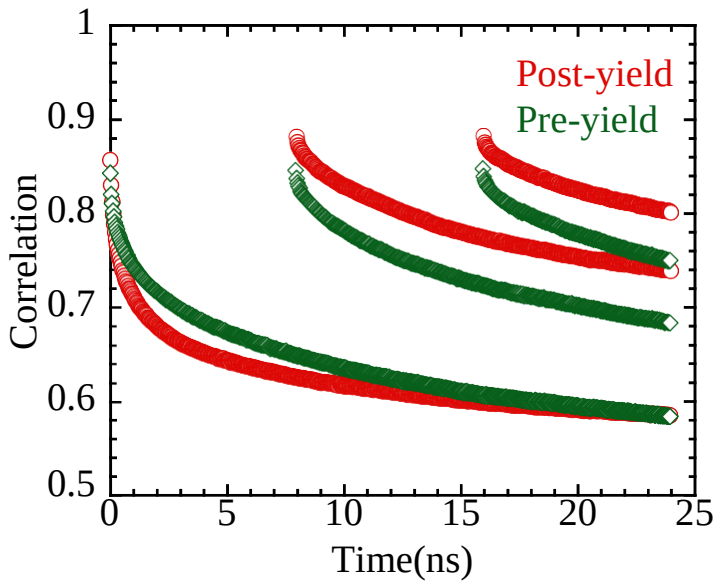

Figure 6.10 Bond orientation auto-correlation against relaxation time in post-yield relaxation and pre-yield relaxation. Starting time for correlation: t = 0 ns (left set), t = 8 ns (center set), t = 16 ns (right set).

To further investigate the origin of slow relaxation during post-yield relaxation, the mobility of the system is visualized with VMD tool[103], as shown in Figure 6.11.

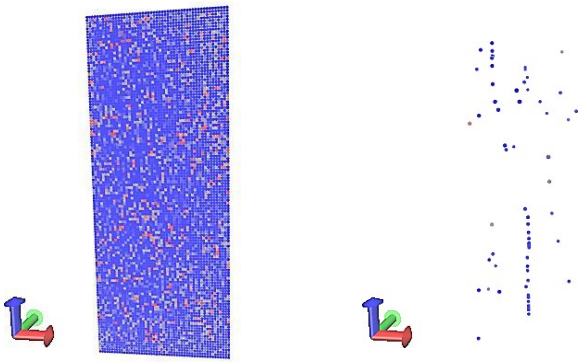

Figure 6.11 Visualization of sample mobility at post-yield relaxation. (left) whole piece of sample, (right) stretched part of the sample.

To perform the visualization, the simulation box is cut into cubic sub-boxes, each with the length around 5 Å. The mobility of each sub-box is calculated by averaging the mobility over backbone bonds (whose center-of-mass locating in the sub-box). Each sub-box is colored based on the correlation at the end of the relaxation, from red (high mobility) to blue (low mobility), shown as the left snapshot in Figure 6.11. To roughly estimate the mobility of the "chain network", the average bond length of each box at the end of deformation is calculated. The sub-boxes with average bond length more than 2.9 Å are selected and in the right snapshot of Figure 6.11, only the selected sub-boxes are shown with colored mobility. Despite the high variation of mobility over the whole sample, the part with high tension shows low mobility confirming that the slow relaxation of post-yield relaxation is caused by high-tension chain network.

To further explore the role of chain network during relaxation after large deformation, we perform additional analysis to visualize the buildup of chain tension during relaxation after cold drawing to $L/L_0 = 1.8$; in other words, we try to find out whether the chain network would stay stretched or not during the relaxation.

The bond length fluctuation of backbone due to random thermal motion can reach the order of 0.1 Å at 370 K. To determine whether a given backbone-bond is stretched at a single point time, the average bond length is calculated in a window of 0.4 ns. The bond is considered as stretched if its average bond length is longer than 2.6 Å (the equilibrium bond length is 2.56 Å). Based on this, the dynamic behavior of the stretched bonds, or more specifically, the following autocorrelation function:

$$C(t)=h(0)h(t)/h(0)$$

is studied to test the bonds stretch during the relaxation. h(t) is defined as 1 or 0 when the backbone-bond that is stretched at t=0 is also stretched at time t or not stretched, respectively. If C(t)=1 from time 0 to t, the bond is considered stretched till time t. Snapshots in Figure 6.12 (left and right) show those bonds that stayed stretched after 4 ns and 24 ns, respectively. The bonds are marked with color to indicate they are from different chains.

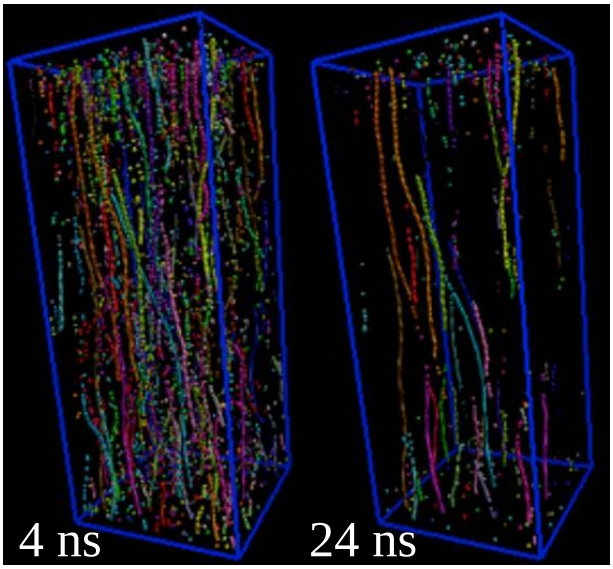

Figure 6.12 States of bond stretching after stress relaxation 4 (left) and 24 ns (right) respectively, after tensile extension to a draw ratio of $L/L_0 = 1.8$. All bonds longer than 2.6 Å are displayed with colors (online) representing different strands. At 4 ns, more load-bearing strands are observed than at 24 ns. These strands stem from one to the other end of the system. The equilibrium bond length is 2.574-2.575 Å.

Left snapshot in Figure 6.12 shows chains with bonds stretched more than 2.6 Å after 4 ns of the stress relaxation, where a clear chain network structure shows up with oriented and stretched strands. Global retractive stress remains because of these “force

chains" forming a network. The snapshot also Figure 6.12 indicates that some of these load-bearing strands survive after significant relaxation at $t = 24$ ns, providing the high level of stress in Figure 6.8.

In conclusion, we show that chain network makes a dominant contribution to the emergent tensile stress by experiment and MD simulation. The intra-segmental component of the stress can relax in longer time than the alpha relaxation. Consequently, the stress after post-yield extension relaxes much slower than that from pre-yield deformation. In addition, MD simulation confirms that the retractive tensile extension is from intra-segmental. At the beginning of post-yield relaxation, the intra-segmental stress drops rapidly due to accelerated mobility after large deformation, and after sufficient time of relaxation, the low mobility of the stretched, high-tension chain network locks and leaves longer relaxation time.

CHAPTER VII

ELASTIC YIELDING

7.1 Introduction

While the nature of glass remain an unsolved problem[116] in condensed matter physics, organic polymeric glass can be regarded as a good model because it possess additional controllable variables. Unlike other organic glasses with low molecular weight, such as non-crystalline sugar, glassy polymer can be ductile and undergo considerable external deformation without fracture.[37, 38, 117] Significant mechanical stress can be embedded in the glassy state after large ductile deformation at temperatures much lower than the glass transition temperature T_g. Conceptually analogous to deformation-induced crystallization in certain semi-crystalline polymers, the molecularly deformed polymer glasses differ from their undeformed isotropic state in at least one way: The stress-containing polymer glasses exhibit elastic yielding [118-120]. After ductile cold drawing (at room temperature) to a sufficient extent and unloading to permit stress relaxation in an unconstrained manner, the specimen attains an apparent stress-free state after days of storage at room temperature without mechanical constraint. However, when annealed at temperatures above the storage temperature (e.g., room temperature) yet still substantially

below T_g, considerable retractive stress may emerge after an induction period that depends on the annealing temperature and the condition of cold drawing. The elastic yielding may be viewed as a mechanically induced glass transition.

In this chapter, we will use molecular dynamics simulation to investigate the embedded stress after ductile deformation in glassy state and its elastic yielding phenomenon. This phenomenon will be interpreted based on our understanding of the origin of stress.

7.2 Simulation Protocol

Molecular dynamics simulation was conducted using the same copy as in chapter V. A system containing 500 PS chains (500-mers of each, 1000 beads per chain) was generated by randomly distributing the PS chains in a periodic box. This system was initially equilibrated at 550 K for 4.8 ns and cooled to 300 K at a rate of 10 K/ns.

To mimic an actual uniaxial extension experiment, we doubled the system size in deformation direction (z-direction). The periodicity was removed in this direction by cleaving chains across the periodic boundary at the top and bottom of the simulation box. Two different scenarios, pre-deformed and non-deformed, were examined using this system.

Pre-deformed case: Deformation was performed by pulling 3 layers of beads (about 7.7 Å thickness) at the top and bottom of the box in opposite directions at a constant rate at 300 K. A total deformation of $L/L_0=2.2$ was applied to the system at a rate of 0.5 /ns, followed by the constraint removed and the system allowed to retract freely 2.4 ns after the unloading. During the process, the stress in the deformation direction (z-

direction) decreases to zero. Holding the top and bottom layers and fixing their separation in the z-direction, the system was heated to 360 K in 0.16 ns to allow its lateral adjustment freely. The response of the system to the annealing is observed.

Non-deformed case: The non-deformed system was further equilibrated at 300 K for an additional 1 ns. During the process, the system was allowed to freely adjust in all directions. Then the temperature was elevated to 360 K in 0.16 ns. Subsequently, keeping the top and bottom layers fixing their separation in the z-direction, the dynamic behavior of the system was examined during the annealing at 360 K in the next 3.6 ns.

7.3 Result and discussion

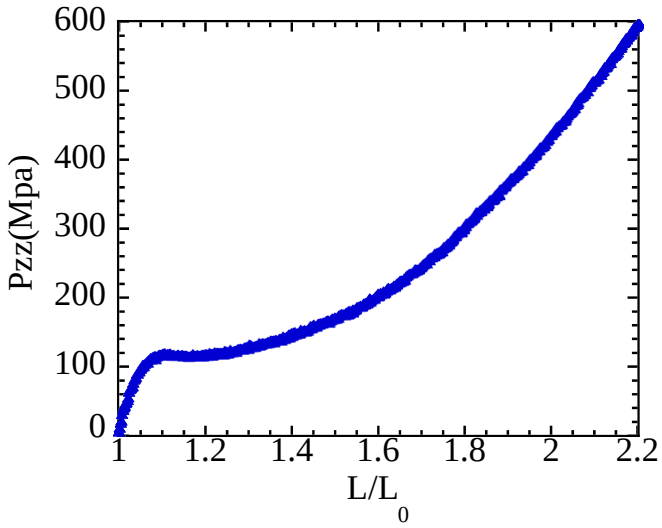

Figure 7.1 Stress-strain curve during the drawing of coarse-grained PS to a draw ratio L/L_0=2.2. Retractive stress value is defined as positive.

To elucidate the origin of retractive stress observed during annealing process, MD simulations is carried out based on a coarse-grained model for PS[98]. The system is

firstly uniaxially extended at 300 K to a draw ratio $L/L_0 = 2.2$. Stress response is shown in Figure 7.1. As detailed discussed in chapter V, the strong strain hardening stress at the end of deformation is produced by the oriented and stretched backbone bonds, as illustrated in Figure 7.4 regime 1.

Then the unloading is performed at the end of extension by setting the system constraint-free and letting the specimen shrink freely. As shown in Figure 2.4, a rapid drop of stress is observed with the rapid drop of specimen elongation shown as the insert. During this process, the backbone bonds, that are highly stretched and oriented after elongation, will rapidly shrink and disorient because of the stress imbalance. The recovery of bond length and disorientation (Figure 7.4 regime 2) leads to a rapid intra-segmental stress drop in Figure 7.2. In the meanwhile, the compressive inter-segmental stress decreases and approaches to its equilibrium state at a relatively slow rate. As a result, an apparent stress-free state is achieved, and the total stress reaches zero after 2.4 ns. The shrinkage of the specimen saturates and stops at $L/L_0 = 1.8$ after 2.4 ns, because the intra-segmental retractive forces are balanced by the inter-segmental compression. In addition, segmental relocation is needed if further shrinkage is to occur. However, at this point, within the time scale of our simulation, the potential barrier against relocation is too high to climb over and it is not possible to transfer to another energy minimum[121-123]. In other words, as discussed in chapter 6, the segmental relaxation time is too long at 300 K and forbidden further shrinkage.

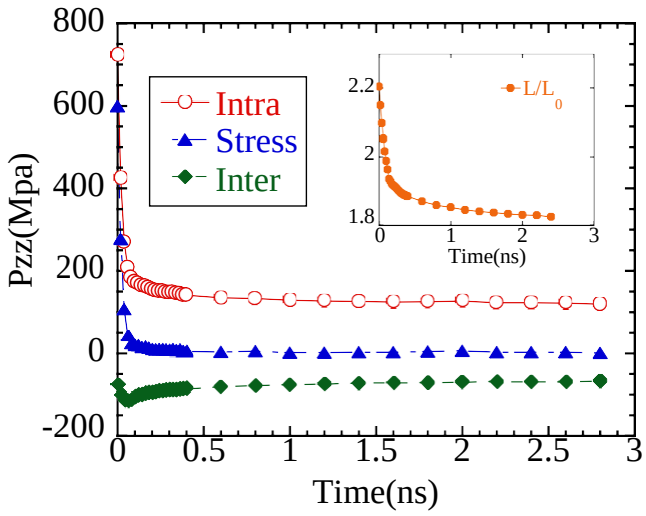

Figure 7.2 Stress decomposition during the unload of sample. Contribution of the stress is divided into intra-segmental, inter-segmental and kinetic components. Constant repulsive kinetic stress is not shown to clarify the relationship. Retractive stress value is defined as positive.

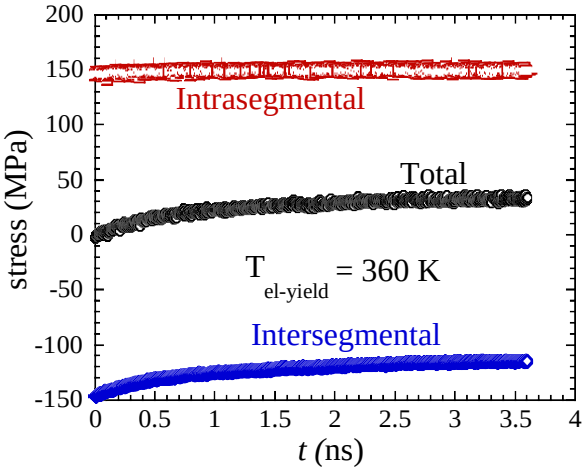

Figure 7.3. Emergent retractive stress (diamonds) during the annealing process at $T_{el\text{-}yield}$ (360 K) < T_g (380 K) of a pre-deformed PS. The result is based on MD simulation of a coarse-grained model, and the decomposition of the total stress is separated into intra-segmental (retractive-circles) and inter-segmental (compressive-squares) components.

Nevertheless, because of the mechanical rejuvenation (by the extension to L/L_0 = 2.2), the energy barrier between the present local energy minimum and a neighboring local minimum is expected to be lower than the energy barrier in an undeformed system. The reduced barrier height would allow the annealing to induce a more rapid inter-segmental re-packing. Specifically, upon annealing at 360 K, inter-segmental re-packing takes place, causing the force imbalance between the distorted load-bearing strands and the vitreous surroundings, while the bond length and orientation remain constant, as shown in Figure 7.4 regime 3. Consequently, as shown in Figure 5, intersegmental component of stress turns less compressive, resulting in a net retractive stress.

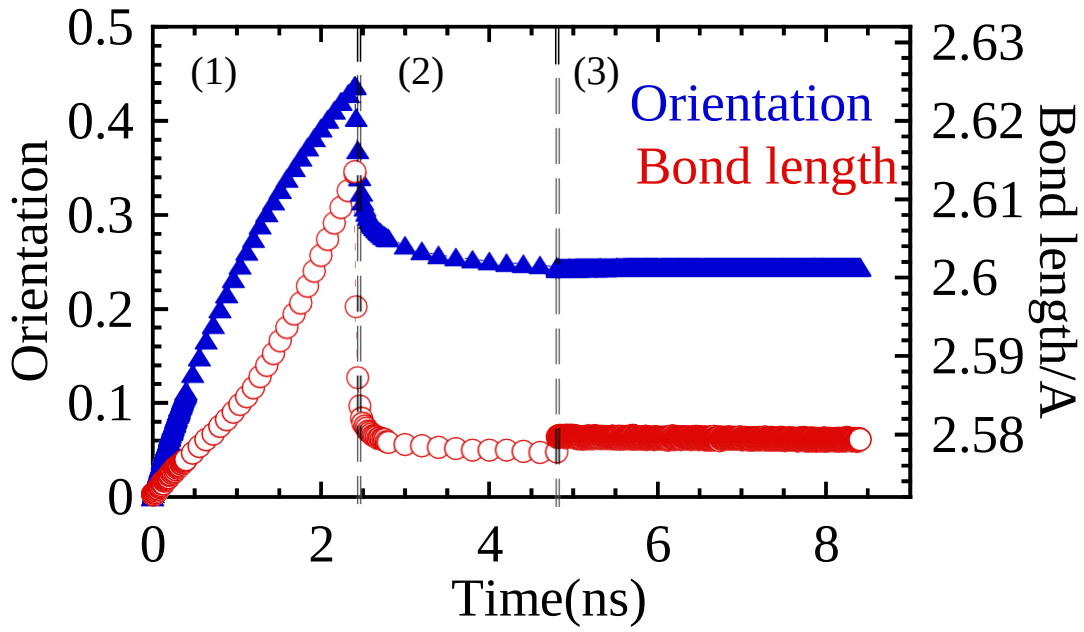

Figure 7.4 Orientation function (P_2) and average bond length of the backbone bond against time during the deformation at 300 K (regime (1)), upon releasing at 300 K (regime (2)) and during elastic yielding upon annealing at 360 K (regime (3)).

The lower energy barrier height in the rejuvenated state produced by the pre-deformation may imply a higher molecular mobility. We exam the mobility in terms of bond orientation autocorrelation. This bond orientation autocorrelation is defined according to Ref.[115]:

$$C_b(t) = \frac{1}{2}(3\langle \cos^2 \theta_i(t)\rangle - 1)$$

Here, $\theta_i(t)$ is the angle between the i^{th} bond at time 0 and t, and the angular brackets indicate an average backbone bonds in our sample. In addition, the bond orientation function $P_2(t)$ is calculated using the same preceding expression, where $\theta_i(t)$ is the angle formed between the i^{th} backbone bond at time t in the Z-direction.

Figure 7.5 shows that, compared to the non-deformed system, there is a significantly larger molecular mobility after the pre-deformation, shown by the fast decreasing of the autocorrelation function. Therefore, the MD simulation confirms that, upon annealing of a pre-deformed polymer, the emergence of retractive stress stems from the force imbalance arisen from their structural adjustment. The sufficient pre-deformation altered the energy landscape, making it possible for the thermal fluctuation to rearrange segmental packing.

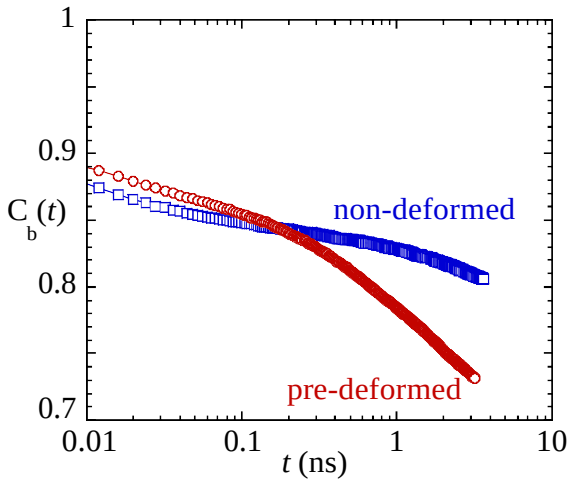

Figure 7.5 Orientational autocorrelation function against time in the pre-deformed and non-deformed systems at 360 K.

In summary, with the help of molecular simulation, we reveal the nature of emerging stress of elastic yielding phenomenon. After tensile deformation at glassy state, stretched and oriented bonds produces a high level of retractive stress. When the specimen is unloaded, bonds shrink and disorient and lead to a rapid drop of both intra-segmental stress and total stress. With time, the intra-segmental stress is balanced by the compressive inter-segmental stress, causing an apparent stress-free state and saturating shrinking of the specimen. Further shrinkage needs a segmental relocation, where the relaxation is too long to be reached within the experimental time at glassy state. But with the assistance of increasing temperature, segmental relocation is enabled and causes further relaxation of the inter-segmental stress. The force imbalance between the inter-segmental and intra-segmental stress leads to the emerging stress.

CHAPTER VIII

SUMMARY

Polymeric glasses can exhibit various mechanical responses under different conditions. Over decades, many efforts have been made to understand the physics behind. They are focusing on different aspects: the models from Haward[7], Boyce[8, 9] and Schweizer[11-14] were built to explain the response upon deformation; Ludwik[16]−Davidenov-Wittman[17]−Orowan[18] (LDWO) hypothesis and fracture mechanics theory focused on brittle-ductile response; and Kramer[44, 76-78] made a big progress on explanation of the form, propagation and failure of crazes.

However, we believe that the physics behind polymeric glass is unified and so as the physical theory. We proposed a coherent zero-order model to reveal all aspects of mechanical response in polymeric glass system[26]. Extending our understanding on chain network from polymer melt rheology[19-25], we propose a hybrid structure model that values the role of network and intra-chain interaction. With this model, we hope we can explain the various mechanical response exhibited by polymeric glass system.

In this work, both experimental and computer simulation study were performed to test this hybrid model and to understand the mechanical response of polymeric glasses.

In Chapter II, we firstly introduced polymer and polymeric glasses. Polymeric glasses are unique systems that can undergo various mechanic responses due to their

unique feature from connectivity and uncrossability. The method to detect the mechanical properties, which is deformation here, was described. After that, several different deformation modes and important related parameters, including stress and strain were demonstrated. Based on those knowledges, the common mechanical responses of polymeric glasses upon constant rate tensile deformation, including both ductile and brittle response, were discussed.

In Chapter III, we presented our recent proposed model to understand the mechanical response of polymeric glasses. In this model, polymeric glass is considered as a hybrid structure of chain network (intra-segmental) and vitreous (inter-segmental) primitive structure.[26] During the deformation, chain network and primitive structure, play active and passive roles, respectively. In addition, ductile response and plastic deformation can be only achieved in the condition that primitive structure fully mobilized by chain network before yield. The model also predicts that chain network is essential to stress buildup at large deformation.

In Chapter IV, we carried out a series of tensile extension tests on two most common polymer glasses (PMMA and PS) and describe their generic mechanical responses as a function of deformation rate at various temperatures. We found that PMMA and PS are brittle at the high applied rate, ductile at intermediate rate but become much less ductile as the rate further decreases. Intensive crazes were found on failure specimen at low rate. Based on the observations and further investigations, we made the reasonable speculation that, highly stretched fibrils inside the crazes would contain strands of chain network. When the specimen is deformed slowly enough, strands in the fibrils are given sufficient time to be pulled out, although the tension in the rest of chain

network is still low. This would cause the crazes to fail and pulled open into cavities. As cavities growing larger, they start to merge and connect to each other, finally form crack, leading to the failure of whole sample.

In Chapter V, we further tested the hybrid model by computer simulation and studied the origin of stress in both tensile and compression modes. Coarse-grained model for PS was used in molecular dynamics simulation. Results showed that specimen with low molecular weight were not capable of building high level of stress at large deformation, no matter in tensile or compression mode. However, the physics behind was different. In tensile mode, stress at large deformation is majorly contributed by deformed chain network; whereas in compression mode, chain network holds the structure in lateral direction, resulting in a denser packing and allowing the stress buildup.

In Chapter VI and Chapter VII, we further discussed our experimental results of stress relaxation and elastic yielding based on our understanding. In Chapter VI, we conducted relaxation experiment at near-T_g temperature. It was found that tensile stress vanished shortly after pre-yield deformation while the tensile stress from post-yield stayed high and is relaxed on much longer time scales. The experimental observation in this chapter is consistent with our simulation discovery in Chapter V. Molecular dynamics simulation based on the same coarse-grained PS proved that the high relaxation stress came from chain network. In Chapter VII, we studied the phenomenon of elastic yielding. After ductile drawing to a sufficient extension ratio and unloading to permit stress relaxation in an unconstrained manner at room temperature, the stress is still embedded in glassy state. When the sample annealed at temperature above the storage temperature yet still substantially below T_g, considerable retractive stress may emerge. Our model

speculates that this stress origins from chain network, with the support from molecular dynamics simulation.

BIBLIOGRAPHY

1. Haward, R.N., *The Physics of Glassy Polymers*. 2012: Springer Netherlands.
2. Ward, I.M. and J. Sweeney, *Mechanical properties of solid polymers*. 3rd ed. 2012, Chichester, UK: John Wiley & Sons, Ltd. Regarding the LDWO hypothesis on the brittle-ductile transition, the book states "As will be appreciated, this approach bepasses the relevance of fracture mechanics to brittle failure. If, hower, we consider fracture initiation as governed by fracture stress σ_B, this concept of regarding yield and fracture as competitive processes provides a useful starting point".
3. Williams, J.G., *Fracture mechanics of polymers*. 1984: E. Horwood.
4. Kinloch, A.J., *Fracture Behaviour of Polymers*. 2013: Springer Netherlands.
5. Struik, L.C.E., *Physical Aging in Amorphous Polymers and Other Materials*. 1978: Elsevier Scientific Publishing Company.
6. Flory, P.J. and J.G. Jackson, *Statistical Mechanics of Chain Molecules*. 1989: Hanser.
7. Haward, R. and G. Thackray. *The use of a mathematical model to describe isothermal stress-strain curves in glassy thermoplastics*. in *Proceedings of the Royal Society of London A: Mathematical, Physical and Engineering Sciences*. 1968. The Royal Society.
8. Arruda, E.M. and M.C. Boyce, *A three-dimensional constitutive model for the large stretch behavior of rubber elastic materials.* Journal of the Mechanics and Physics of Solids, 1993. **41**(2): p. 389-412.
9. Arruda, E.M. and M.C. Boyce, *Evolution of plastic anisotropy in amorphous polymers during finite straining.* International Journal of Plasticity, 1993. **9**(6): p. 697-720.
10. Kramer, E.J., *Open questions in the physics of deformation of polymer glasses.* Journal of Polymer Science Part B: Polymer Physics, 2005. **43**(23): p. 3369-3371.
11. Chen, K. and K.S. Schweizer, *Microscopic constitutive equation theory for the nonlinear mechanical response of polymer glasses.* Macromolecules, 2008. **41**(15): p. 5908-5918.
12. Chen, K. and K.S. Schweizer, *Theory of aging, rejuvenation, and the nonequilibrium steady state in deformed polymer glasses.* Physical Review E, 2010. **82**(4): p. 041804.
13. Chen, K. and K.S. Schweizer, *Theory of Yielding, Strain Softening, and Steady Plastic Flow in Polymer Glasses under Constant Strain Rate Deformation.* Macromolecules, 2011. **44**(10): p. 3988-4000.
14. Chen, K. and K.S. Schweizer, *Suppressed segmental relaxation as the origin of strain hardening in polymer glasses.* Physical Review Letters, 2009. **102**(3): p. 038301.
15. Eyring, H., *Viscosity, Plasticity, and Diffusion as Examples of Absolute Reaction Rates.* Journal of Chemical Physics, 1936. **4**(4): p. 283.
16. Ludwik, P.Z., Ver. Deut. Ing, 1927. **71**: p. 1532.

17. Davidenkov, N.N. and F. Wittman, Phys. Tech. Znst. (USSR), 1937. **4**: p. 300.
18. Orowan, E., Pept. Prog. Phys., 1949. **12**: p. 185.
19. Boukany, P.E., S.-Q. Wang, and X. Wang, *Step shear of entangled linear polymer melts: New experimental evidence for elastic yielding.* Macromolecules, 2009. **42**(16): p. 6261-6269.
20. Ravindranath, S. and S.-Q. Wang, *Large amplitude oscillatory shear behavior of entangled polymer solutions: Particle tracking velocimetric investigation.* Journal of Rheology, 2008. **52**(2): p. 341-358.
21. Wang, Y., et al., *Elastic breakup in uniaxial extension of entangled polymer melts.* Physical review letters, 2007. **99**(23): p. 237801.
22. Wang, Y. and S.-Q. Wang, *From elastic deformation to terminal flow of a monodisperse entangled melt in uniaxial extension.* Journal of Rheology, 2008. **52**(6): p. 1275-1290.
23. Wang, Y. and S.-Q. Wang, *Salient features in uniaxial extension of polymer melts and solutions: Progressive loss of entanglements, yielding, non-Gaussian stretching, and rupture.* Macromolecules, 2011. **44**(13): p. 5427-5435.
24. Wang, S.-Q., et al., *New experiments for improved theoretical description of nonlinear rheology of entangled polymers.* Macromolecules, 2013. **46**(8): p. 3147-3159.
25. Zhu, X. and S.-Q. Wang, *Mechanisms for different failure modes in startup uniaxial extension: Tensile (rupture-like) failure and necking.* Journal of Rheology, 2013. **57**(1): p. 223-248.
26. Wang, S.-Q., et al., *A phenomenological molecular model for yielding and brittle-ductile transition of polymer glasses.* The Journal of chemical physics, 2014. **141**(9): p. 094905.
27. Rubinstein, M. and R.H. Colby, *Polymer Physics*. 2003: OUP Oxford.
28. Odian, G., *Principles of Polymerization*. 2004: Wiley.
29. Ferry, J.D., *Viscoelastic Properties of Polymers*. 1980: Wiley.
30. Macosko, C.W., *Rheology: principles, measurements, and applications*. 1994: VCH.
31. Doi, M. and S.F. Edwards, *The Theory of Polymer Dynamics*. 1988: Clarendon Press.
32. Graessley, W.W., *The Entanglement Concept in Polymer Rheology*. 2014: Springer Berlin Heidelberg.
33. Roth, C.B., *Polymer Glasses*. 2016: CRC Press.
34. Fetters, L., et al., *Connection between polymer molecular weight, density, chain dimensions, and melt viscoelastic properties.* Macromolecules, 1994. **27**(17): p. 4639-4647.
35. Wang, S.-Q., *On chain statistics and entanglement of flexible linear polymer melts.* Macromolecules, 2007. **40**(24): p. 8684-8694.
36. Carlson, J.M. and J. Langer, *Properties of earthquakes generated by fault dynamics.* Physical Review Letters, 1989. **62**(22): p. 2632.
37. Argon, A.S., *The physics of deformation and fracture of polymers*. 2013: Cambridge University Press.
38. Haward, R.N. and R.J. Young, *The Physics of Glassy Polymers*. 1997: Springer Netherlands.

39. Aharoni, S.M., *Ductile and brittle behavior of amorphous polymers. Relationship with activation energy for glass transition and mechanical fracture.* Journal of Applied Polymer Science, 1972. **16**(12): p. 3275-3284.
40. Wu, S., *Secondary relaxation, brittle–ductile transition temperature, and chain structure.* Journal of applied polymer science, 1992. **46**(4): p. 619-624.
41. Chen, L.P., A.F. Yee, and E.J. Moskala, *The Molecular Basis for the Relationship between the Secondary Relaxation and Mechanical Properties of a Series of Polyester Copolymer Glasses.* Macromolecules, 1999. **32**(18): p. 5944-5955.
42. Kramer, E., *A molecular theory of the fracture toughness of low molecular weight polymers.* Journal of Materials Science, 1979. **14**(6): p. 1381-1388.
43. Donald, A.M. and E.J. Kramer, *EFFECT OF MOLECULAR ENTANGLEMENTS ON CRAZE MICROSTRUCTURE IN GLASSY-POLYMERS.* Journal of Polymer Science Part B-Polymer Physics, 1982. **20**(5): p. 899-909.
44. Kramer, E.J., *MICROSCOPIC AND MOLECULAR FUNDAMENTALS OF CRAZING.* Advances in Polymer Science, 1983. **52-3**: p. 1-56.
45. De Focatiis, D.S.A., C.P. Buckley, and L.R. Hutchings, *Roles of chain length, chain architecture, and time in the initiation of visible crazes in polystyrene.* Macromolecules, 2008. **41**(12): p. 4484-4491.
46. De Focatiis, D.S.A., J. Embery, and C.P. Buckley, *Large deformations in oriented polymer glasses: Experimental study and a new glass-melt constitutive model.* Journal of Polymer Science Part B: Polymer Physics, 2010. **48**(13): p. 1449-1463.
47. De Focatiis, D.S.A. and C.P. Buckley, *Craze initiation in glassy polymers: Quantifying the influence of molecular orientation.* Polymer, 2011. **52**(18): p. 4045-4053.
48. van Melick, H.G.H., L.E. Govaert, and H.E.H. Meijer, *On the origin of strain hardening in glassy polymers.* Polymer, 2003. **44**(8): p. 2493-2502.
49. Tervoort, T. and L. Govaert, *Strain-hardening behavior of polycarbonate in the glassy state.* Journal of Rheology, 2000. **44**: p. 1263.
50. Govaert, L.E. and T.A. Tervoort, *Strain hardening of polycarbonate in the glassy state: Influence of temperature and molecular weight.* Journal of Polymer Science Part B: Polymer Physics, 2004. **42**(11): p. 2041-2049.
51. Senden, D.J.A., J.A.W. van Dommelen, and L.E. Govaert, *Strain hardening and its relation to Bauschinger effects in oriented polymers.* Journal of Polymer Science Part B: Polymer Physics, 2010. **48**(13): p. 1483-1494.
52. Engels, T.T., L.L. Govaert, and H.H. Meijer, *Mechanical characterization of glassy polymers : quantitative prediction of their short- and long-term responses*, in *Polymer science : a comprehensive reference, Vol.2 / Ed. K. Matyjaszewski, M. Möller*. 2012, Elsevier: Amsterdam. p. 723 - null.
53. Senden, D.J.A., et al., *Rate- and temperature-dependent strain hardening of polycarbonate.* Journal of Polymer Science Part B: Polymer Physics, 2012. **50**(24): p. 1680-1693.
54. van Breemen, L.C.A., et al., *Rate- and temperature-dependent strain softening in solid polymers.* Journal of Polymer Science Part B: Polymer Physics, 2012. **50**(24): p. 1757-1771.
55. Williams, J.G., *Fracture mechanics of polymers*. 1987, New York: Halsted Press (Ellis Horwood Limited).

56. Kramer, E. and L. Berger, *Fundamental processes of craze growth and fracture*, in *Crazing in Polymers Vol. 2*, H. Kausch, Editor. 1990, Springer Berlin / Heidelberg. p. 1-68.
57. Lesser, A.J., *Fatigue Behavior of Polymers*, in *Encyclopedia of Polymer Science and Technology*. 2002, John Wiley & Sons, Inc.
58. Haward, R.N. and G. Thackray, *The Use of a Mathematical Model to Describe Isothermal Stress-Strain Curves in Glassy Thermoplastics.* Proceedings of the Royal Society of London. Series A. Mathematical and Physical Sciences, 1968. **302**(1471): p. 453-472.
59. Ender, D.H. and R.D. Andrews, *Cold Drawing of Glassy Polystyrene under Dead Load.* Journal of Applied Physics, 1965. **36**(10): p. 3057-&.
60. Zartman, G.D., et al., *How Melt-Stretching Affects Mechanical Behavior of Polymer Glasses.* Macromolecules, 2012. **45**(16): p. 6719-6732.
61. Matsushige, K., S.V. Radcliffe, and E. Baer, *The pressure and temperature effects on brittle-to-ductile transition in PS and PMMA.* Journal of Applied Polymer Science, 1976. **20**(7): p. 1853-1866.
62. Zhao, Y., X.X. Li, and S.Q. Wang, *unpublished*. 2015.
63. Zhao, J., et al., *Thermal and viscoelastic behavior of hydrogenated polystyrene.* Macromolecules, 2001. **34**(6): p. 1737-1741.
64. Roetling, J.A., *Yield stress behaviour of polymethylmethacrylate.* Polymer, 1965. **6**(6): p. 311-317.
65. Wu, S., *Effects of strain rate and comonomer on the brittle–ductile transition of polymers.* Journal of Applied Polymer Science, 1976. **20**(2): p. 327-333.
66. Vincent, P., *The tough-brittle transition in thermoplastics.* Polymer, 1960. **1**: p. 425-444.
67. Gersappe, D., *Molecular mechanisms of failure in polymer nanocomposites.* Physical review letters, 2002. **89**(5): p. 058301.
68. McKenna, G. and R. Penn, *Time-dependent failure in poly (methyl methacrylate) and polyethylene.* Polymer, 1980. **21**(2): p. 213-220.
69. Arad, S., J. Radon, and L. Culver, *Strain rate dependence of failure processes in polycarbonate and nylon.* Journal of Applied Polymer Science, 1973. **17**(5): p. 1467-1478.
70. Schirrer, R., *Optical interferometry: Running crack-tip morphologies and craze material properties*, in *Crazing in Polymers Vol. 2*. 1990, Springer. p. 215-261.
71. Döll, W. and L. Könczöl, *Micromechanics of fracture under static and fatigue loading: Optical interferometry of crack tip craze zones*, in *Crazing in Polymers Vol. 2*. 1990, Springer. p. 137-214.
72. Döll, W., *Optical interference measurements and fracture mechanics analysis of crack tip craze zones.* Crazing in Polymers, 1983: p. 105-168.
73. Kambour, R., *Structure and properties of crazes in polycarbonate and other glassy polymers.* Polymer, 1964. **5**: p. 143-155.
74. Kambour, R. and R. Kopp, *Cyclic stress–strain behavior of the dry polycarbonate craze.* Journal of Polymer Science Part B: Polymer Physics, 1969. **7**(1): p. 183-200.
75. Kambour, R. and R. Russell, *Electron microscopy of crazes in polystyrene and rubber modified polystyrene: use of iodine-sulphur eutectic as a craze reinforcing*

impregnant. Polymer, 1971. **12**(4): p. 237-246.
76. Donald, A.M. and E.J. Kramer, *Effect of molecular entanglements on craze microstructure in glassy polymers.* Journal of Polymer Science Part B: Polymer Physics, 1982. **20**(5): p. 899-909.
77. Kramer, E.J. and L.L. Berger, *Fundamental processes of craze growth and fracture*, in *Crazing in Polymers Vol. 2*. 1990, Springer. p. 1-68.
78. Lauterwasser, B.D. and E.J. Kramer, *Microscopic mechanisms and mechanics of craze growth and fracture*. Philosophical Magazine A, 1979. **39**(4): p. 469-495.
79. Cheng, S., L. Johnson, and S.-Q. Wang, *Crazing and strain localization of polycarbonate glass in creep.* Polymer, 2013. **54**(13): p. 3363-3369.
80. Plummer, C. and A. Donald, *Crazing mechanisms and craze healing in glassy polymers.* Journal of materials science, 1989. **24**(4): p. 1399-1405.
81. Nikolsky, B.P., *Guide-Book for Chemist*, ed. M. Khimia. Vol. 3. 1964.
82. Lin, P., et al., *Origin of mechanical stress and rising internal energy during fast uniaxial extension of SBR melts.* Polymer, 2017. **124**: p. 68-77.
83. Langer, J.S., *Shear-transformation-zone theory of plastic deformation near the glass transition.* Physical Review E, 2008. **77**(2): p. 021502.
84. Allen, M.P., *Introduction to molecular dynamics simulation.* Computational soft matter: from synthetic polymers to proteins, 2004. **23**: p. 1-28.
85. Kroese, D.P., et al., *Why the Monte Carlo method is so important today.* Wiley Interdisciplinary Reviews: Computational Statistics, 2014. **6**(6): p. 386-392.
86. Alder, B.J. and T.E. Wainwright, *Studies in molecular dynamics. I. General method.* The Journal of Chemical Physics, 1959. **31**(2): p. 459-466.
87. Fermi, E., et al., *Los Alamos Report No.* LA-1940, 1955: p. 978.
88. Rahman, A., *Correlations in the motion of atoms in liquid argon.* Physical Review, 1964. **136**(2A): p. A405.
89. Baschnagel, J., et al., *Bridging the gap between atomistic and coarse-grained models of polymers: status and perspectives*, in *Viscoelasticity, atomistic models, statistical chemistry*. 2000, Springer. p. 41-156.
90. Müller‐Plathe, F., *Coarse‐graining in polymer simulation: from the atomistic to the mesoscopic scale and back.* ChemPhysChem, 2002. **3**(9): p. 754-769.
91. Karimi‐Varzaneh, H.A., et al., *How good are coarse‐grained polymer models? A comparison for atactic polystyrene.* ChemPhysChem, 2012. **13**(15): p. 3428-3439.
92. Noid, W., *Perspective: Coarse-grained models for biomolecular systems.* The Journal of chemical physics, 2013. **139**(9): p. 09B201_1.
93. Padding, J. and W.J. Briels, *Time and length scales of polymer melts studied by coarse-grained molecular dynamics simulations.* The Journal of chemical physics, 2002. **117**(2): p. 925-943.
94. Li, Y., et al., *A predictive multiscale computational framework for viscoelastic properties of linear polymers.* Polymer, 2012. **53**(25): p. 5935-5952.
95. Harmandaris, V.A. and K. Kremer, *Dynamics of polystyrene melts through hierarchical multiscale simulations.* Macromolecules, 2009. **42**(3): p. 791-802.
96. Garrahan, J.P. and D. Chandler, *Coarse-grained microscopic model of glass formers.* Proceedings of the National Academy of Sciences, 2003. **100**(17): p. 9710-9714.

97. Kremer, K. and G.S. Grest, *Dynamics of entangled linear polymer melts: A molecular‐dynamics simulation.* The Journal of Chemical Physics, 1990. **92**(8): p. 5057-5086.
98. Hsu, D.D., et al., *Thermomechanically consistent and temperature transferable coarse-graining of atactic polystyrene.* Macromolecules, 2015. **48**(9): p. 3057-3068.
99. Reith, D., M. Pütz, and F. Müller‐Plathe, *Deriving effective mesoscale potentials from atomistic simulations.* Journal of computational chemistry, 2003. **24**(13): p. 1624-1636.
100. Dixon, W.J., *Efficient analysis of experimental observations.* Annual review of pharmacology and toxicology, 1980. **20**(1): p. 441-462.
101. Plimpton, S., *Fast parallel algorithms for short-range molecular dynamics.* Journal of computational physics, 1995. **117**(1): p. 1-19.
102. Everaers, R., et al., *Rheology and microscopic topology of entangled polymeric liquids.* Science, 2004. **303**(5659): p. 823-826.
103. Humphrey, W., A. Dalke, and K. Schulten, *VMD: visual molecular dynamics.* Journal of molecular graphics, 1996. **14**(1): p. 33-38.
104. Haward, R.N., *Strain-hardening of thermoplastics.* Macromolecules, 1993. **26**(22): p. 5860-5869.
105. Lyulin, A.V., et al., *Strain softening and hardening of amorphous polymers: Atomistic simulation of bulk mechanics and local dynamics.* Europhysics Letters, 2005. **71**(4): p. 618-624.
106. Hoy, R.S. and M.O. Robbins, *Strain hardening of polymer glasses: Effect of entanglement density, temperature, and rate.* Journal of Polymer Science Part B-Polymer Physics, 2006. **44**(24): p. 3487-3500.
107. Hoy, R.S. and M.O. Robbins, *Strain hardening in polymer glasses: Limitations of network models.* Physical Review Letters, 2007. **99**(11): p. 117801.
108. Hoy, R.S. and M.O. Robbins, *Strain hardening of polymer glasses: Entanglements, energetics, and plasticity.* Physical Review E, 2008. **77**(3): p. 031801.
109. Vorselaars, B., A.V. Lyulin, and M.A.J. Michels, *Deforming glassy polystyrene: Influence of pressure, thermal history, and deformation mode on yielding and hardening.* Journal of Chemical Physics, 2009. **130**(7): p. 074905.
110. Vorselaars, B., A.V. Lyulin, and M.A.J. Michels, *Microscopic Mechanisms of Strain Hardening in Glassy Polymers.* Macromolecules, 2009. **42**(15): p. 5829-5842.
111. Hoy, R.S., *Why is Understanding Glassy Polymer Mechanics So Difficult?* Journal of Polymer Science Part B-Polymer Physics, 2011. **49**(14): p. 979-984.
112. Bending, B., et al., *Measurement of segmental mobility during constant strain rate deformation of a poly (methyl methacrylate) glass.* Macromolecules, 2014. **47**(2): p. 800-806.
113. Liu, J.N., et al., *Nonlinear stress relaxation behavior of ductile polymer glasses from large extension and compression.* Polymer, 2015. **81**: p. 129-139.
114. Lin, P.P., J.N. Liu, and S.Q. Wang, *Delineating nature of stress responses during ductile uniaxial extension of polycarbonate glass.* Polymer, 2016. **89**: p. 143-153.
115. Lee, H.-N., et al., *Deformation-induced mobility in polymer glasses during*

multistep creep experiments and simulations. Macromolecules, 2009. **42**(12): p. 4328-4336.
116. Anderson, P.W., *Through the glass lightly.* Science, 1995. **267**(5204): p. 1615-1616.
117. Ward, I.M. and J. Sweeney, *Mechanical properties of solid polymers, 3rd*. 2012, Chichester, UK: John Wiley & Sons, Ltd.
118. Andrews, R.D., *Retraction of oriented polystyrene monofilaments.* Journal of Applied Physics, 1955. **26**(9): p. 1061-1067.
119. Legrand, D.G., *Yielding, crazing, and fracture of polymers. II. Studies of the retraction of crazed and drawn films.* Journal of Applied Polymer Science, 1972. **16**(6): p. 1367-1376.
120. Cheng, S. and S.-Q. Wang, *Elastic yielding in cold drawn polymer glasses well below the glass transition temperature.* Physical review letters, 2013. **110**(6): p. 065506.
121. Debenedetti, P.G. and F.H. Stillinger, *Supercooled liquids and the glass transition.* Nature, 2001. **410**(6825): p. 259-267.
122. Lacks, D.J. and M.J. Osborne, *Energy landscape picture of overaging and rejuvenation in a sheared glass.* Physical Review Letters, 2004. **93**(25): p. 4.
123. Malandro, D.L. and D.J. Lacks, *Relationships of shear-induced changes in the potential energy landscape to the mechanical properties of ductile glasses.* Journal of Chemical Physics, 1999. **110**(9): p. 4593-4601.